CHAPTER 6

COMPUTER IMPLEMENTATION

6.1 Introduction

The development of an effective computer program for axisymmetric shell analysis requires a knowledge of three scientific disciplines - structural mechanics, numerical analysis and computer application. A most important aspect of a computer program is, however, the ease with which it can be modified and extended.

In the preceding chapter, the characteristic equations of the simple truncated cone element was described and established, together with the overall system matrices required to solve both the static and dynamic problems. Gaussian quadrature was adopted because of its accuracy and economical saving. More economical saving is achieved by adopting a single point numerical integration.

In this chapter, we describe the implementation of the information presented in Chapter 5 in the form of a structural computer program. The top down approach is applied, both in the documentation and structure of the program. By this it is implied that the problem will be studied from a global to a particular point of view. The

package may be classified into two main sections: static analysis and dynamic analysis. The formation of the structure matrices is carried out in the same way in a static or dynamic analysis. The static analysis is continued by solving the equations of equilibrium followed by the computation of element stresses. In a dynamic analysis, natural frequencies and vibration mode shapes are obtained by solving the eigen problem. The programs were designed to be modified or extended easily by the user.

6.2 Computer System Configuration

Desk top computers are becoming increasingly popular for engineers and scientists to use. Their memory capacity and computational speed has improved considerably over the last decade or so.

The computer system used is the Hewlett-Packard 9845B desk top computer option 204. This incorporates 120k byte of system ROM and 187k byte of available read/write memory for program and data, and an enhanced language processor which permits execution speed of three times that of the standard model. Integral to the basic system is a graphics display with a 560 × 455 dot resolution, two cartirdge mass-storage units of 0.2 m byte each, a thermal printer and QWERTY keyboard. The external peripherals supported were a BENSON drum plotter, an HP9885M flexible

disk drive of 0.5 m byte storage capacity and an HP9872A flat-bed plotter.

6.3 Datafile and Storage Types

On the HP9845B system enhanced BASIC there are available two file types and four data types. The available file types are sequential and random. The data types are full precision, short precision, integer precision and string.

A sequential file type is one where data is stored or acquired from the mass-storage device, one data item at a time. In contrast, the random file is one where data can be written to, or read from file in a random sequence of a pre-defined group of data items, called a record. The data type relates to the type and required precision of the data to be stored. For numerical data, it can be stored in full, short or integer precision. Besides numeric variables there are string variables; these are for storage of ASCII characters.

Storage requirements are different for the various types of data. For full precision 8 bytes of storage are required due to the higher degree of accuracy required. Short and integer precision requires 4 byes of storage per variable. A string character requires 1 byte per character. Where large arrays are involved, it is

especially important that a lower precision data type should be defined if the higher precision is not required. This saves both mass-storage space and read/write memory.

Due to the high accuracy required in the present analysis, it was found necessary to store data in a full precision type. The file type used is sequential.

6.4 Static Analysis (ASSNAL)

The stress analysis process can be understood to consist of essentially three phases:

1. Calculation of structure matrices.
2. Solution of equilibrium equations
3. Evaluation of element stresses.

In a static analysis the computer program needs to calculate the structure stiffness matrix and load vector. In the implementation to be described here, the program ASSNAl can be subdivided into five main sections:

(1) **Specification of the structure idealisation. Data is input to the program in the following order:**

(i) Number of elements, number of nodes and nodal coordinates. The radial and axial coordinates of

the nodes are input in global directions. The program accepts shells with branched members.

(ii) Number of terms in Fourier Series representation. The user should be able to specify the number of terms in the Fourier Series which generates convergence to the exact solution.

(iii) Element properties: Young's Modulus and Poisson's Ratio. The program accepts different properties to be specified to the elements.

(iv) Element thickness. The program accepts different thicknesses to be specified to the elements.

(v) Load components expanded into Fourier Series. The coefficients of the Fourier Series expansion are only needed to be input. The load vector can be input in local or global coordinates. The load vector is subdivided into forces and moments acting on nodal rings or distributed on elements. There are two categories of load configuration with respect to the circumferential direction θ :

(a) axisymmetric loads which do not vary in the θ direction so that the number of terms required in the solution is one ($n=0$).

(b) non-axisymmetric loads. In this case the user should decide the number of terms required in the solution. In case of point loads acting at $\theta = 0$, the load is represented by a superposition of axisymmetric terms and harmonic patterns using half range cosine series.

(vi) Boundary conditions. At a nodal point any degree of freedom (u, v, w, β, α) of boundary may be specified as "0" or "1". If the concerned freedom is constrained then 1 is the option while 0 is specified for non-constrained degrees of freedom.

(2) **Generation and compliation of the element stiffness matrices.**

The element stiffness matrices of nth harmonic ${}_n[K]^e$, ${}_n[K_1]^e$ and ${}_n[K_2]^e$ were given in equations (5.27) (5.44) and (5.45) respectively. As was stated in section 5.6, a single point integration is applied to evaluate those matrices. The evaluation of $\int_{-1}^{1} f(\eta)d\eta$, by a single point integration, is equivalent to the evaluation of $f(\eta)$ at the midpoint of the element (i.e., at $\eta=0$ and $r=r_m$ where $r_m = \frac{r_i+r_j}{2}$) and then multiplying that by the length of the element which is simply 2. Therefore, for example, the element stiffness matrix ${}_n[K]^e$ can be

written in the form

$$ {}_n[K]^e = \pi L \, r_m [\bar{B}_{\eta=0}]^T [D] [\bar{B}_{\eta=0}] $$

(See section 5.7 for explicit form of the element stiffness matrices.)

The element stiffness matrices, which are of dimension 10 × 10, were partitioned into sub-matrices as follows:

$$ {}_n[K]^e = \begin{bmatrix} K_{ii} & K_{ij} \\ K_{ji} & K_{jj} \end{bmatrix} $$

the submatrices ${}_n[K_{ij}]^e$ is a 5×5; i and j correspond to the two nodes of an element. The aim of this subdivision was to save time and memory of the computing.

After transformation from local to global coordinates the structure stiffness matrix is assembled in an assembly process.

(3) **Load vector calculation and compilation.**

The distributed load on an element was given as

$$ {}_n\{P_d\}_o^e = \pi \, L \, r \begin{Bmatrix} \{P_{di}\}_o^e \\ \{P_{dj}\}_o^e \end{Bmatrix} $$

If there is any applied ring load, say at node i, which

can be written as

$$ {}_n\{P_r\}_o^e = \pi\, r_i \begin{Bmatrix} \{P_{ri}\}_o^e \\ \{\ 0\ \} \end{Bmatrix} $$

then the overall force vector of an element is given as

$$ {}_n\{P\}_o^e = {}_n\{P_r\}_o^e + {}_n\{P_d\}_o^e $$

To remind the reader of the fact that at node i of an element, for example, ${}_n\{P_{di}\}_o^e$ and ${}_n\{P_{ri}\}_o^e$ has five components each. These Fourier coefficients could be input in local or global coordinates.

(4) Solution of equilibrium equations.

The local vector ${}_n\{P\}$ has been assembled at the same time as the structure stiffness matrix was formed. After assembly, a static analysis involves the solution of M_1+1 set of equations

$$ \sum_{n=0}^{n=M_1} {}_n[K]\ {}_n\{q\}_o = \sum_{n=0}^{n=M_1} {}_n\{P\}_o . $$

These equations are solved using the compact Gauss elimination method on the positive definite symmetrical system of equations [74]. It must be mentioned here that before solving these equations the boundary conditions must be imposed.

(5) **Evaluation of the element stresses.**

After the nodal point displacements have been evaluated sequentially, the stress resultants, at the centre of the elements, are calculated in the final phase of the analysis. The user can choose the element, or elements, in which the stress resultants to be calculated for. The other option is the calculation of stress resultants for all the elements.

6.5 Dynamic Analysis (FVASS)

In a dynamic analysis, the program must also establish the system mass matrix. The program "FAVSS" may be classified into the following main sections:

(1) **Specification of the structure idealisation.**

Data is input to the program in the following order:

(i) number of elements, number of nodes and the nodal coordinates.

(ii) circumferential wave number in the case of shells, or the number of nodal diameters in the case of circular or annular plates. In view of the axisymmetric nature of the problem each Fourier component is considered separately as it was

pointed out in Chapter 5.

(iii) Element properties. The program accepts different properties to be specified to the elements. In the case of orthotropic shells, the properties required to be specified are: E_{ϕ}, Young's Modulus in the meridional direction; E_{θ}, Young's Modulus in the circumferential direction; $\nu_{\phi\theta}$, Poisson's Ratio (ratio of contraction in θ direction to elongation in ϕ direction when loaded in ϕ direction; $\nu_{\theta\phi}$, and ρ_a, the average mass density. The other properties ($G_{\phi\theta}$, $G_{\zeta\phi}$, $G_{\zeta\theta}$) are calculated automatically in the program.

(iv) Element thickness. The program accepts different thicknesses to be specified to the elements.

(v) Boundary conditions. Boundary conditions are input as before but care should be taken to prevent rigid body motion. As when, for example, the axial displacement u is unconstrained at both ends of a simply supported circular shell, the shell will have rigid body motion. To overcome this problem, a method was devised to add a fictitious flexible element, fully clamped at one end. In the program there is a question mark to remind the user of the fictitious element when it is needed.

(2) **Generation and compilation of the element stiffness matrices.**

(3) **Generation and compilation of the element mass matrices.**

The consistent element mass matrix was given in equation (5.58) and explicitly in equation (5.66). A single point integration is applied to evaluate the element mass matrices. The element mass matrix which is of dimension 10 × 10 was partitioned into submatrices as follows:

$$[M]^e = \left[\begin{array}{c|c} M_{ii} & M_{ij} \\ \hline M_{ji} & M_{jj} \end{array}\right],$$

The submatrix $[M_{ij}]$ is a 5 × 5.

After transformation from local to global coordinates the structure mass matrix is assembled in an assembly procedure.

(4) **Solving the eigen problem.**

As pointed out in section 3.6, the Householder-QR-Inverse iteration method (HQRI) is the one which is

adopted in solving the eigen problem. In using this method the generalised eigen problem (equationn 3.18) must first be transformed into the standard form (equation 3.32) before the HQRI solution technique can be used.

The treatment of the eigenvalue problem in this thesis is based on the standard procedures, TRANS, QL, Evl and EvlVec which are available at the Mechanical and Production Engineering Department of Aston University. The overall stiffness and mass matrix are assembled in full (square matrices). The use of these procedures yield the eigenvalues and eigenvectors which can be output in six options:

(1) All natural frequencies and vibration mode shapes;

(2) A certain sequence of frequencies with mode shapes;

(3) Frequencies, with mode shapes, in a certain interval;

(4) All natural frequencies;

(5) A certain sequence of frequencies;

(6) Frequencies in a certain interval.

6.6 Flow Charts of the Programs and Sub-Programs

The general flow charts of the programs and sub-programs are covered in the pages that follow. The variables used in the flow charts are:

Ne	=	Number of elements
N2	=	Number of nodes
M1	=	Total number of harmonics used in static problems
R(I)	=	Radial coordinate of node I
Z(I)	=	Axial coordinate of node I
Ee(I,1)	=	Node number at beginning of element I in branched shells
Ee(I,2)	=	Node number at end of element I in branched shells
E(I)	=	Young's Modulus of element I
Nu(I)	=	Poisson's Ratio of element I
Tm(I)	=	Thickness of element I
C3	=	The coordinate system selected for input loads
C6	=	Number of separate portions of the shell subjected to distributed loads
C66	=	Number of separate portions of the shell subjected to nodal ring loads
C7, C8	=	Element numbers at the beginning and end of portion I which is subjected to a distributed load
C77,C88	=	Element numbers at the beginning and end of portion I which is subjected to a nodal ring load
C10(Mm) throught C14(Mm)	=	The five components of distributed loads for harmonic Mm

C15(Mm) through C19(Mm)	=	The five components of nodal ring loads for harmonic Mm
M	=	The harmonic to be considered in free vibration problems
E1(I) E2(I)	=	Young's Modulus in direction 1 and 2 of element I
Nu1(I), Nu_2(I)	=	Poisson's ratio in direction 1 and 2 of element I
P(I)	=	Mass density of element I
T(I)	=	Thickness of element I.

Fig. 6.1 Flow diagram for program ASSNAL

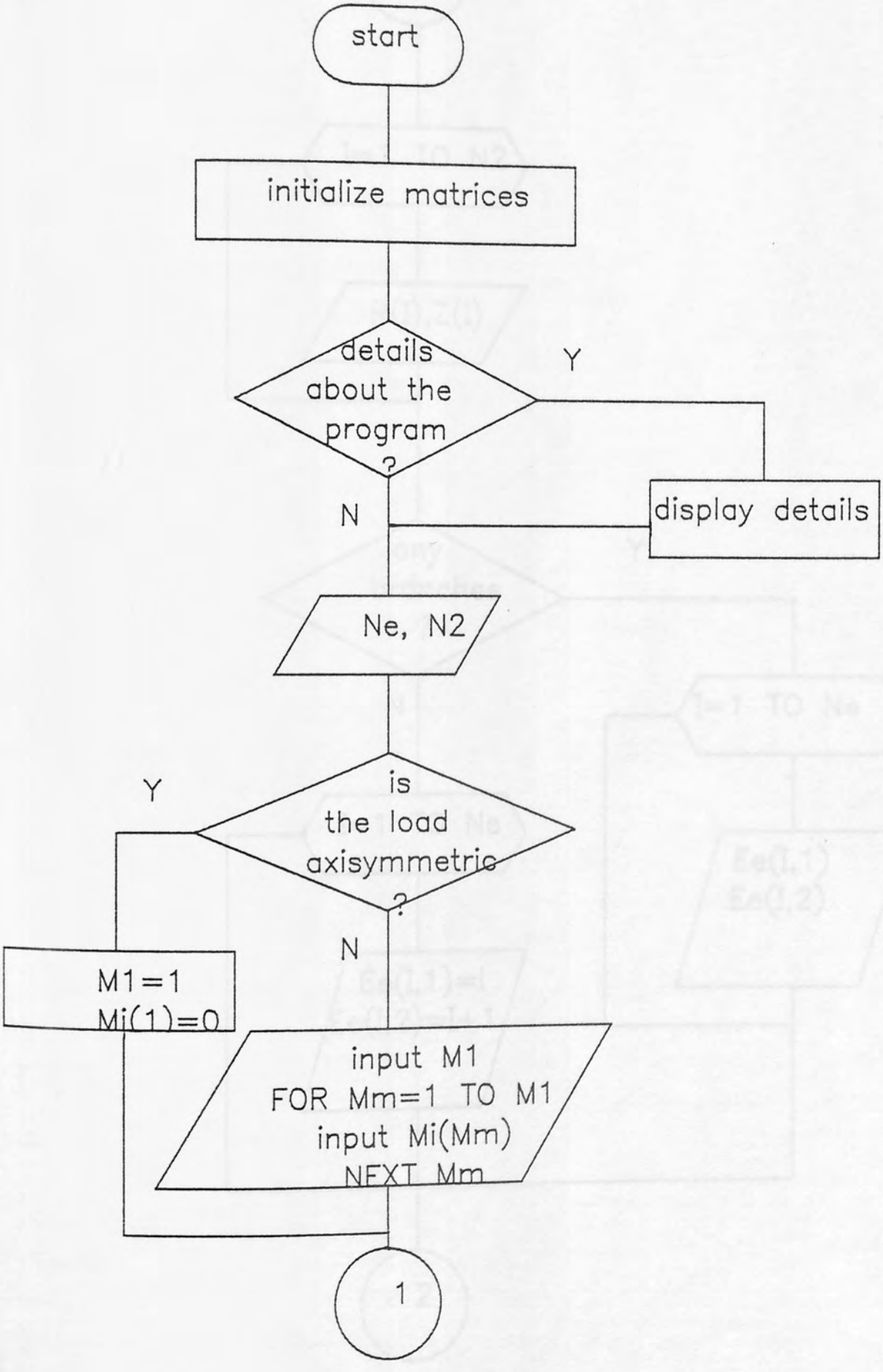

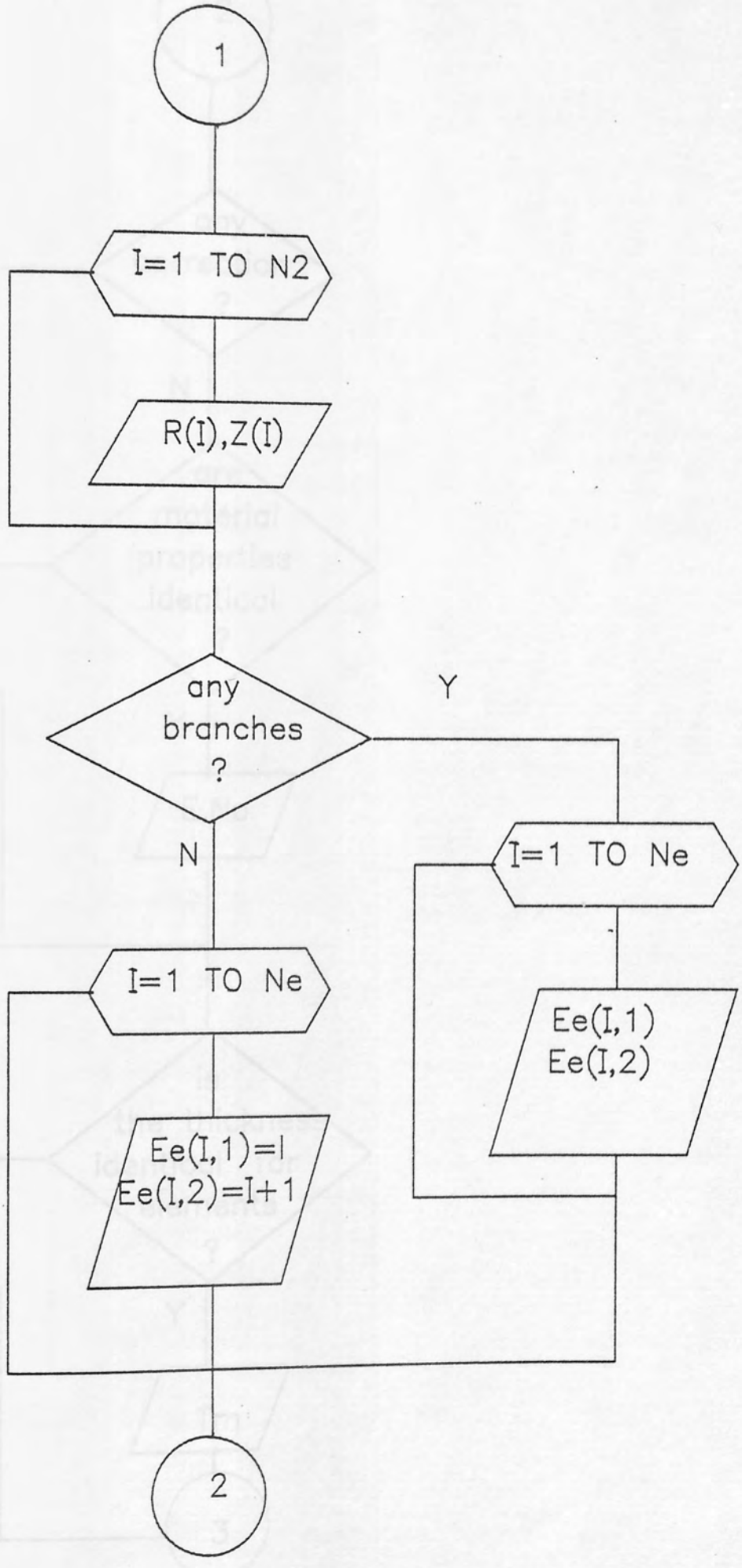
1
I=1 TO N2
R(I),Z(I)
any branches ?
Y
N
I=1 TO Ne
Ee(I,1)
Ee(I,2)
I=1 TO Ne
Ee(I,1)=I
Ee(I,2)=I+1
2

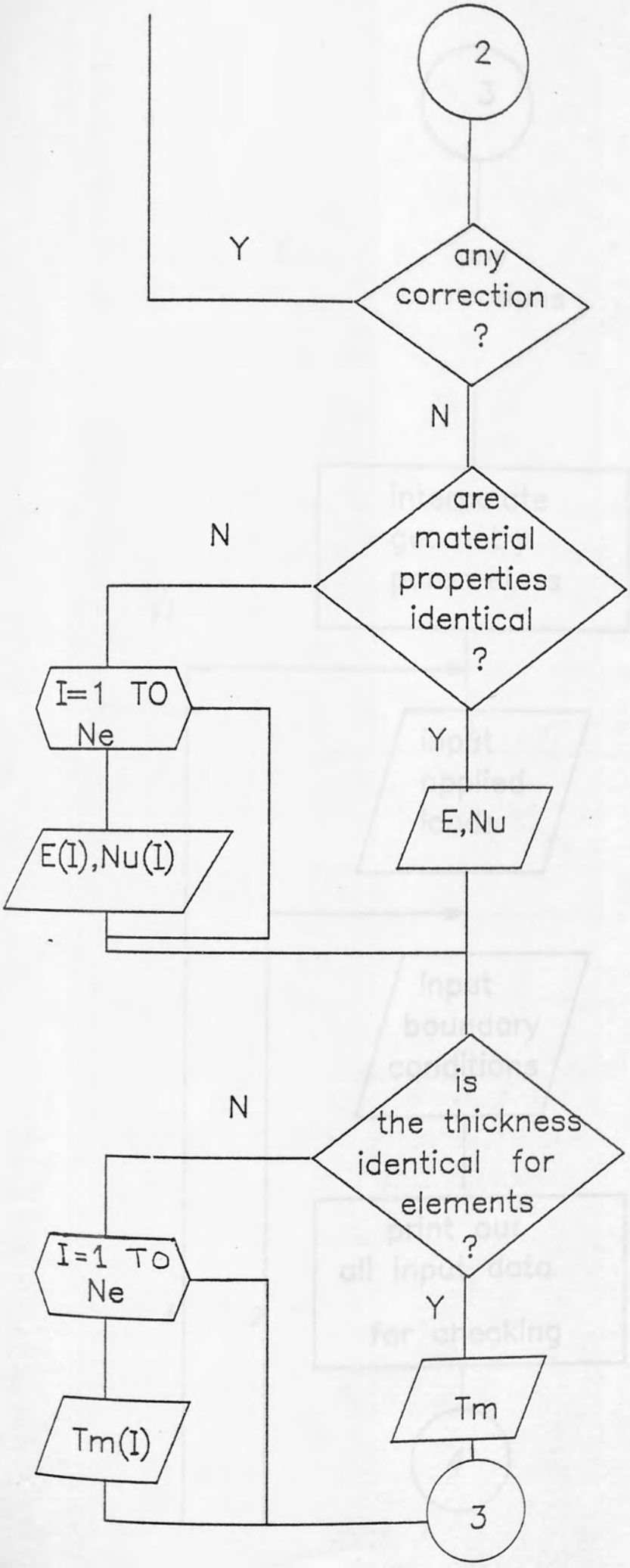
2
any correction ?
Y
N
are material properties identical ?
N
I=1 TO Ne
E(I),Nu(I)
Y
E,Nu
is the thickness identical for elements ?
N
I=1 TO Ne
Tm(I)
Y
Tm
3

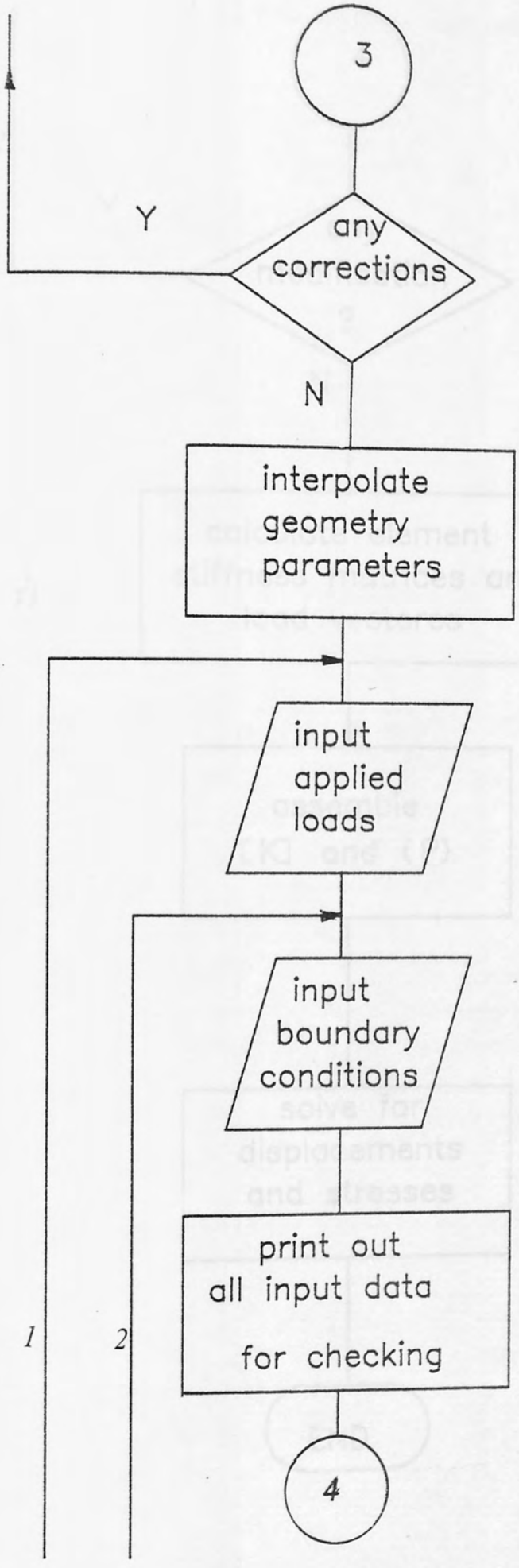
3
Y
any corrections
N
interpolate geometry parameters
input applied loads
input boundary conditions
print out all input data for checking
4
1
2

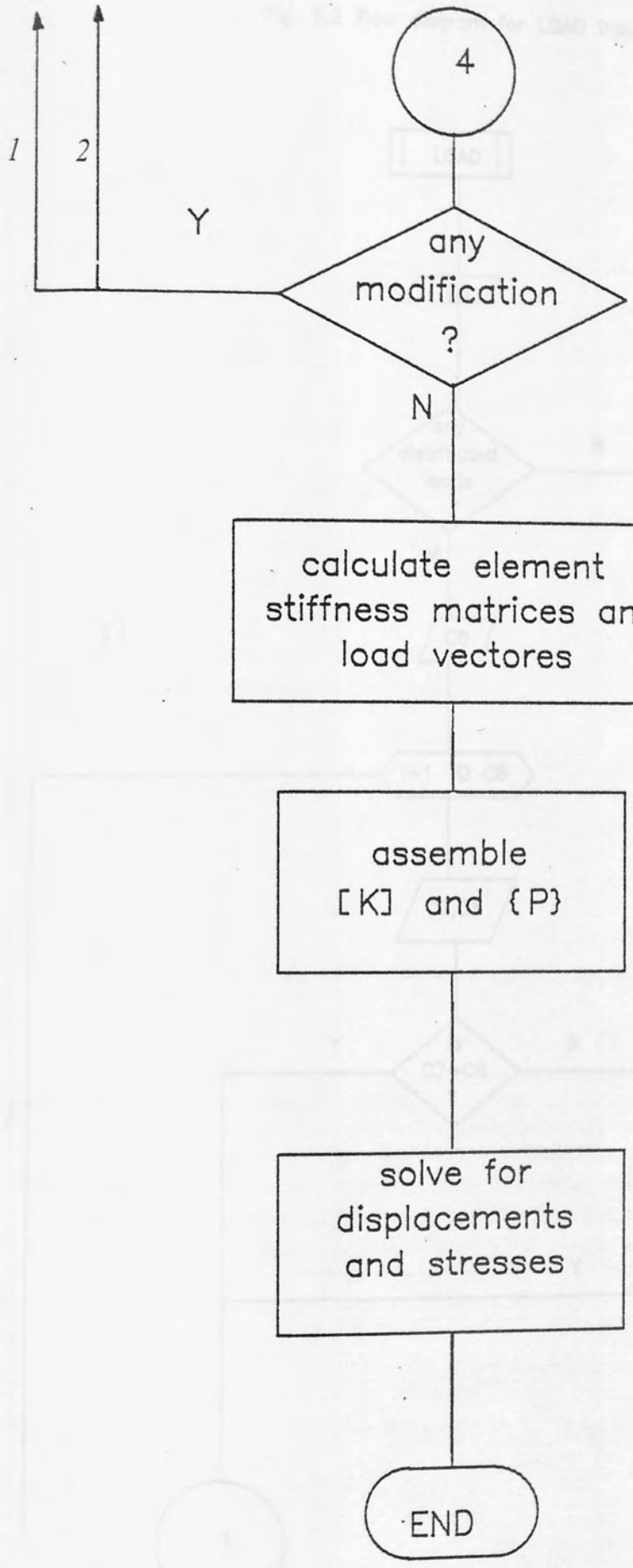
4
1
2
Y
any modification ?
N
calculate element stiffness matrices and load vectores
assemble [K] and {P}
solve for displacements and stresses
END

Fig. 6.2 Flow diagram for LOAD input

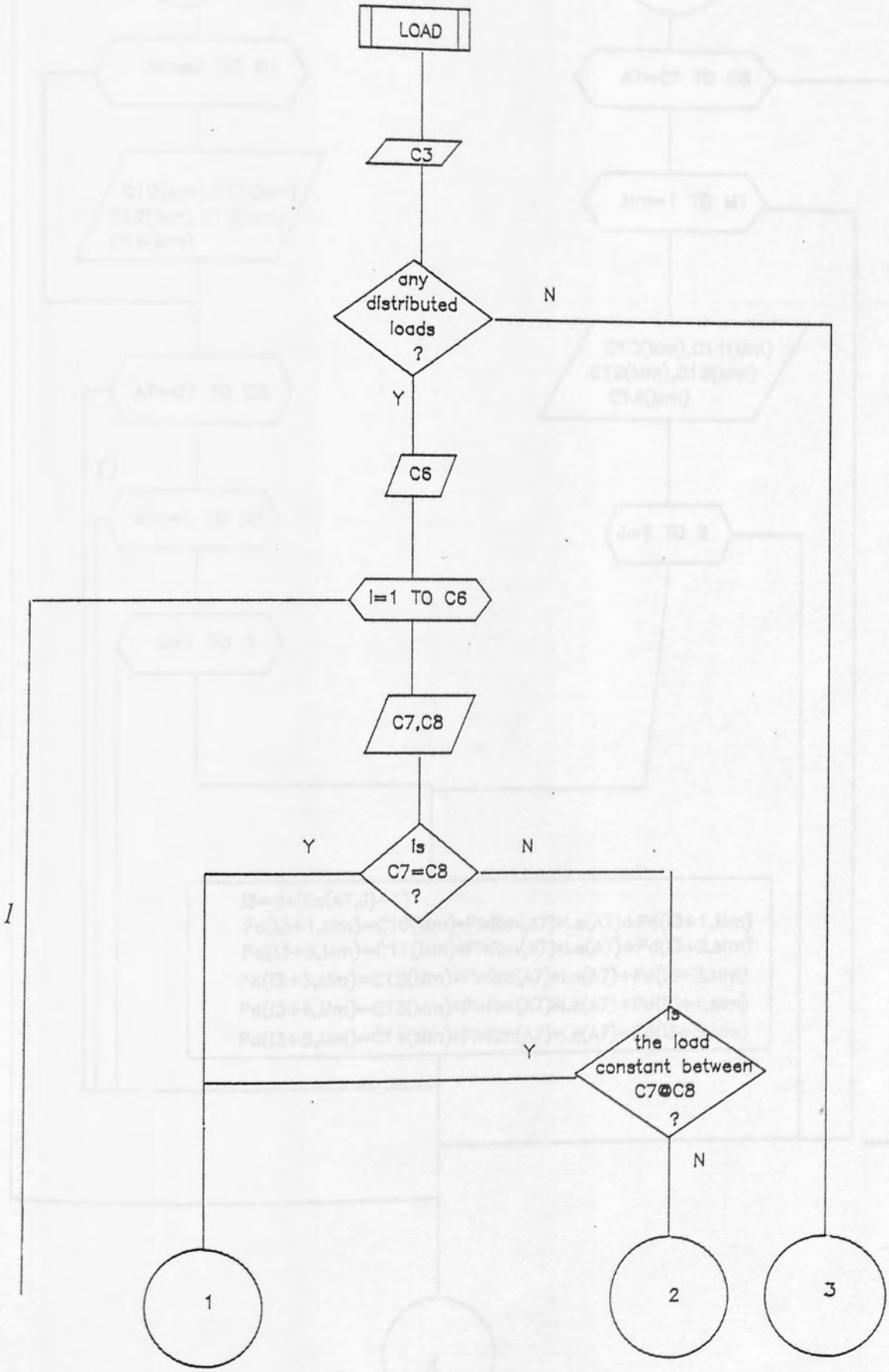

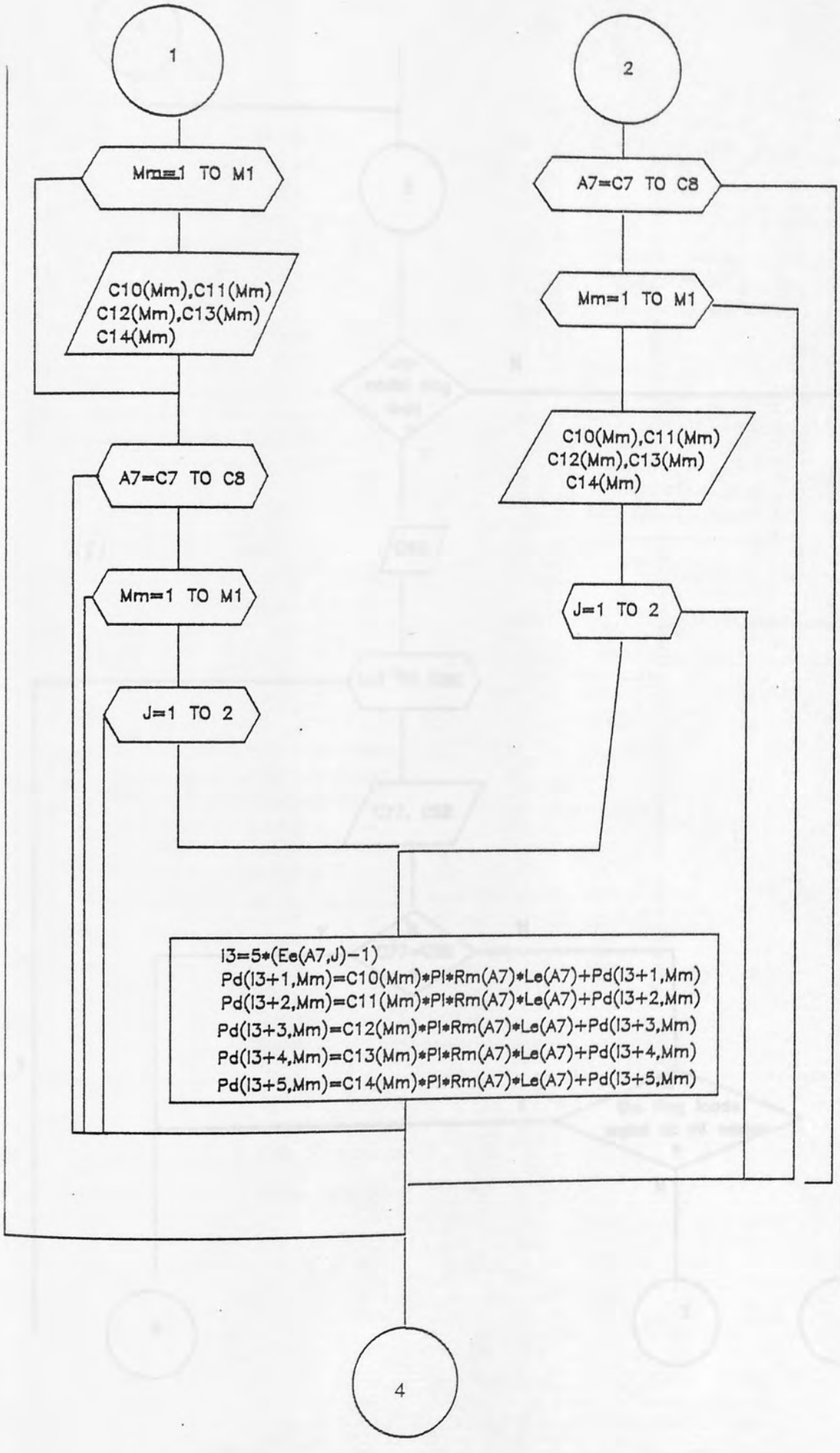
1
Mm=1 TO M1
C10(Mm),C11(Mm)
C12(Mm),C13(Mm)
C14(Mm)
A7=C7 TO C8
Mm=1 TO M1
J=1 TO 2
2
A7=C7 TO C8
Mm=1 TO M1
C10(Mm),C11(Mm)
C12(Mm),C13(Mm)
C14(Mm)
J=1 TO 2
I3=5*(Ee(A7,J)-1)
Pd(I3+1,Mm)=C10(Mm)*PI*Rm(A7)*Le(A7)+Pd(I3+1,Mm)
Pd(I3+2,Mm)=C11(Mm)*PI*Rm(A7)*Le(A7)+Pd(I3+2,Mm)
Pd(I3+3,Mm)=C12(Mm)*PI*Rm(A7)*Le(A7)+Pd(I3+3,Mm)
Pd(I3+4,Mm)=C13(Mm)*PI*Rm(A7)*Le(A7)+Pd(I3+4,Mm)
Pd(I3+5,Mm)=C14(Mm)*PI*Rm(A7)*Le(A7)+Pd(I3+5,Mm)
4

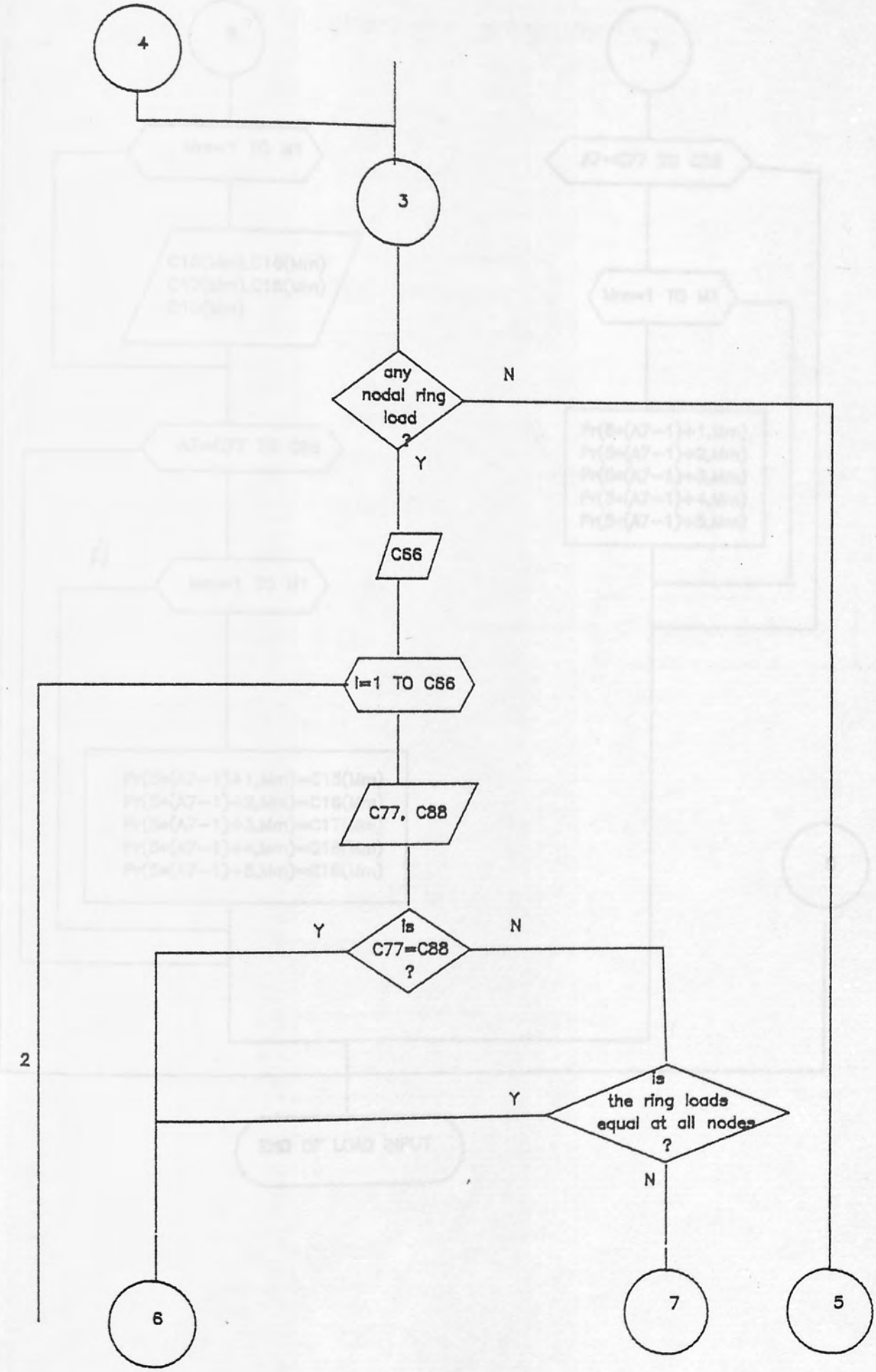
4
3
any nodal ring load ?
N
Y
C66
I=1 TO C66
C77, C88
Is C77=C88 ?
Y
N
2
Is the ring loads equal at all nodes ?
Y
N
6
7
5

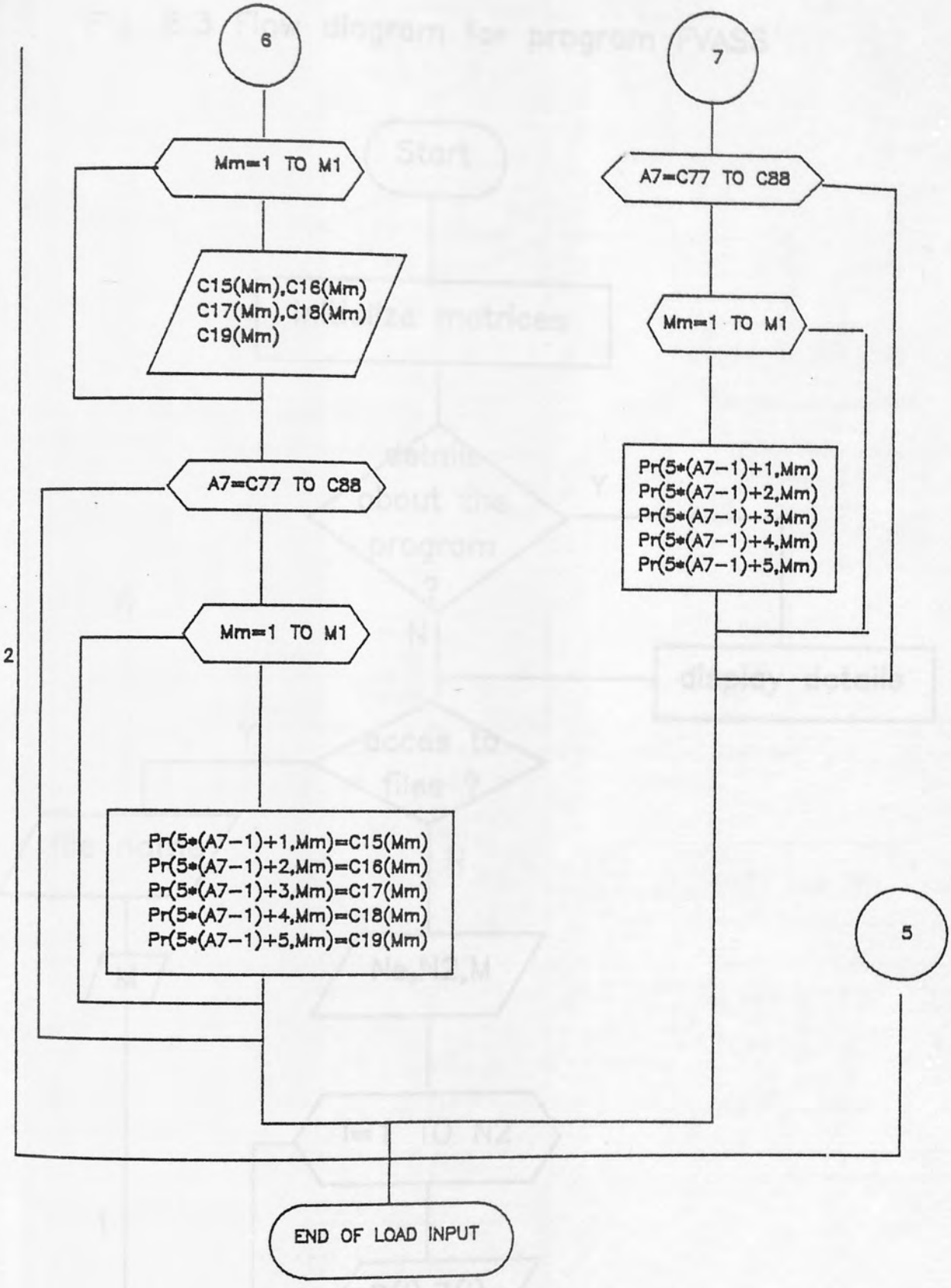
6
7
Mm=1 TO M1
C15(Mm),C16(Mm)
C17(Mm),C18(Mm)
C19(Mm)
A7=C77 TO C88
Mm=1 TO M1
Pr(5*(A7-1)+1,Mm)
Pr(5*(A7-1)+2,Mm)
Pr(5*(A7-1)+3,Mm)
Pr(5*(A7-1)+4,Mm)
Pr(5*(A7-1)+5,Mm)
A7=C77 TO C88
Mm=1 TO M1
2
Pr(5*(A7-1)+1,Mm)=C15(Mm)
Pr(5*(A7-1)+2,Mm)=C16(Mm)
Pr(5*(A7-1)+3,Mm)=C17(Mm)
Pr(5*(A7-1)+4,Mm)=C18(Mm)
Pr(5*(A7-1)+5,Mm)=C19(Mm)
5
END OF LOAD INPUT

Fig. 6.3 Flow diagram for program FVASS

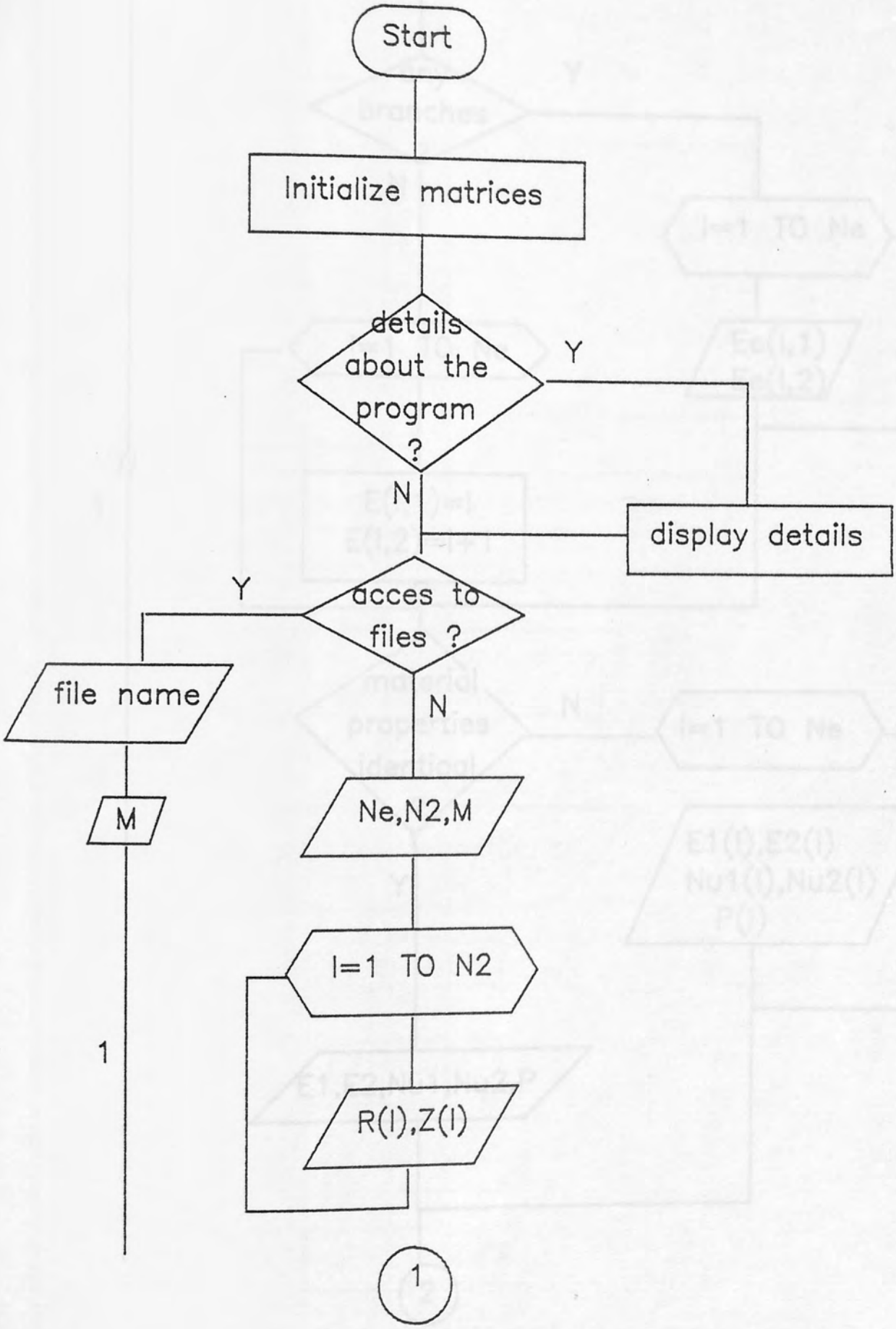

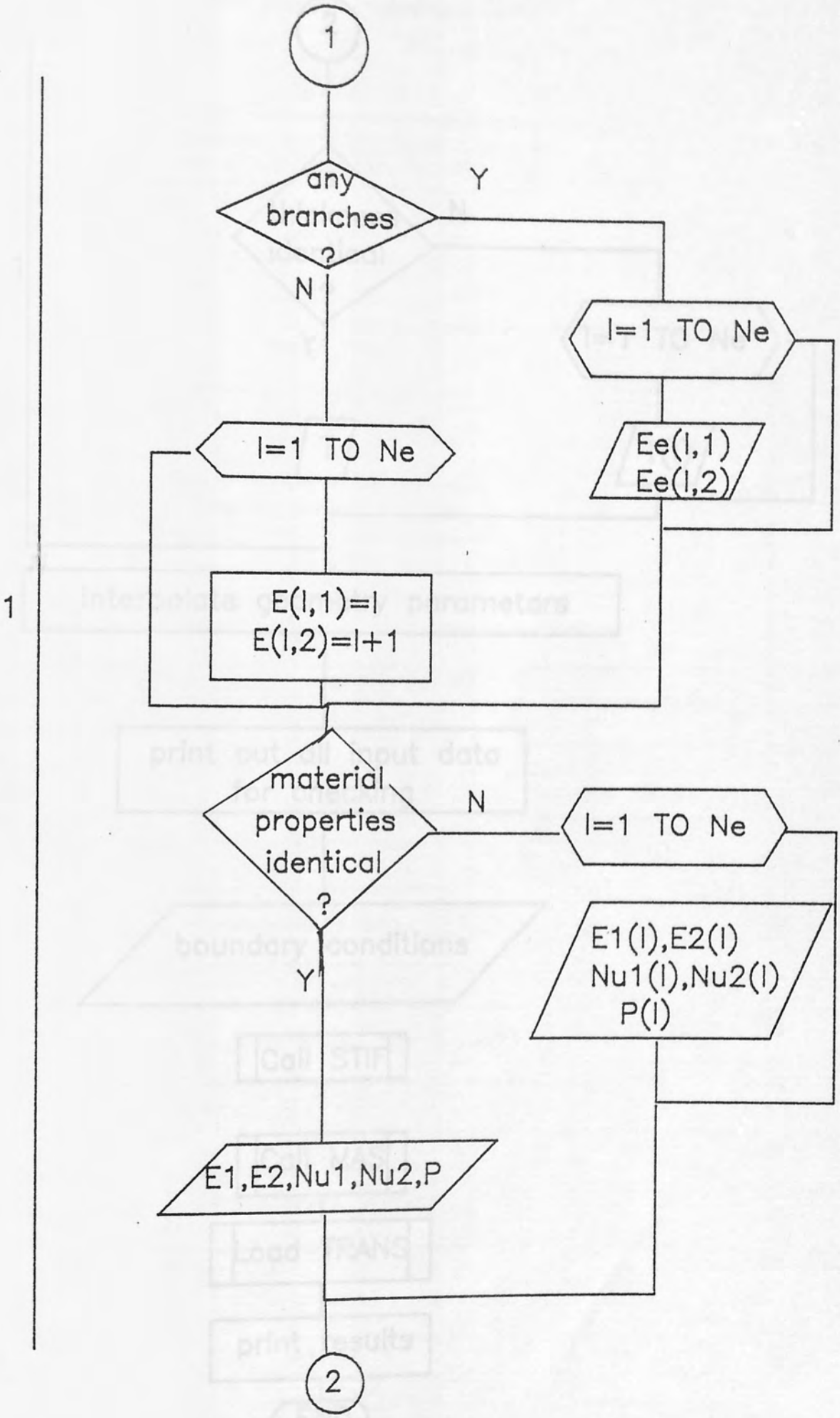
1
any branches ?
Y
N
I=1 TO Ne
Ee(I,1)
Ee(I,2)
I=1 TO Ne
E(I,1)=I
E(I,2)=I+1
material properties identical ?
N
Y
I=1 TO Ne
E1(I),E2(I)
Nu1(I),Nu2(I)
P(I)
E1,E2,Nu1,Nu2,P
2
1

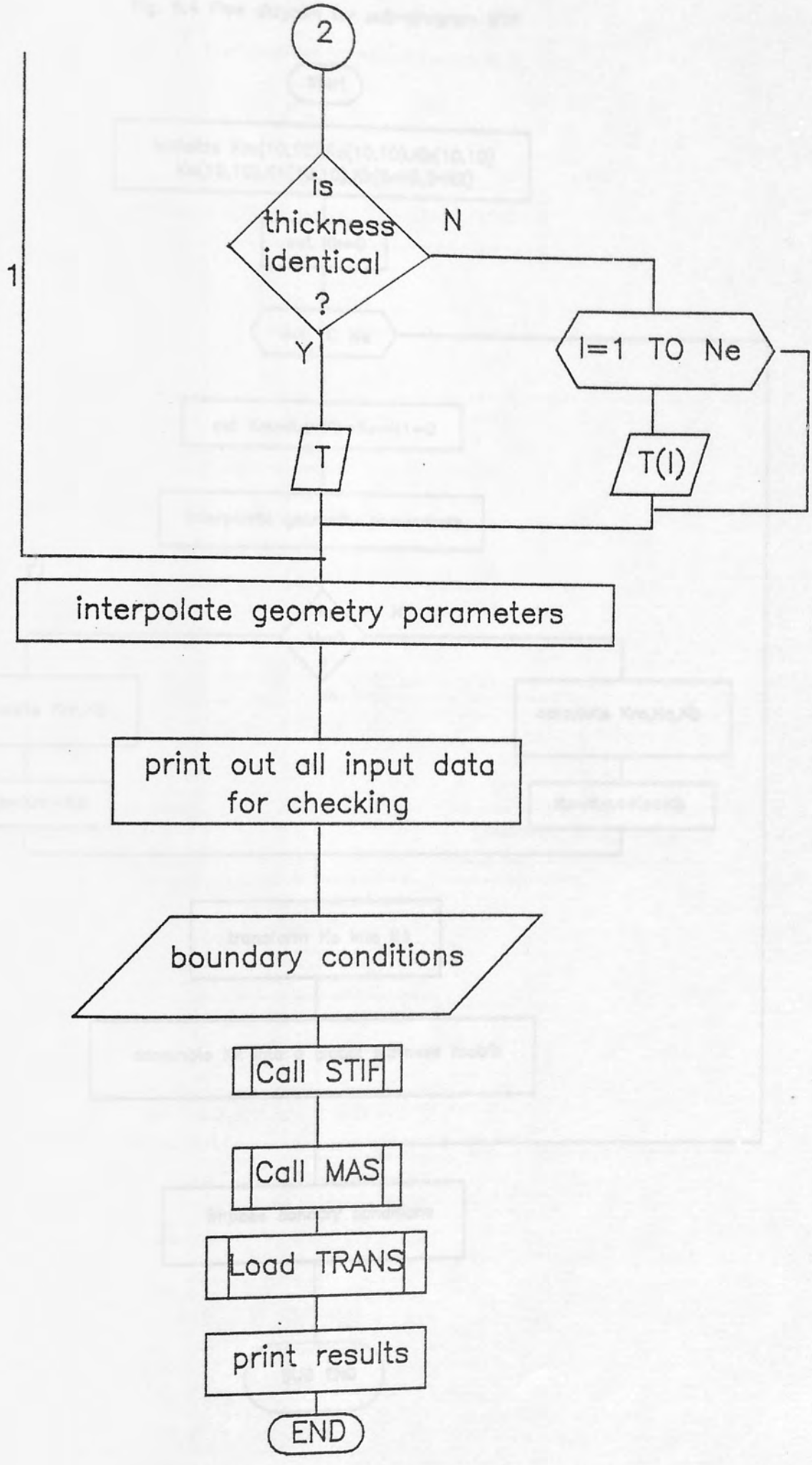
2
is thickness identical ?
N
Y
1
I=1 TO Ne
T
T(I)
interpolate geometry parameters
print out all input data for checking
boundary conditions
Call STIF
Call MAS
Load TRANS
print results
END

Fig. 6.4 Flow diagram for sub-program STIF

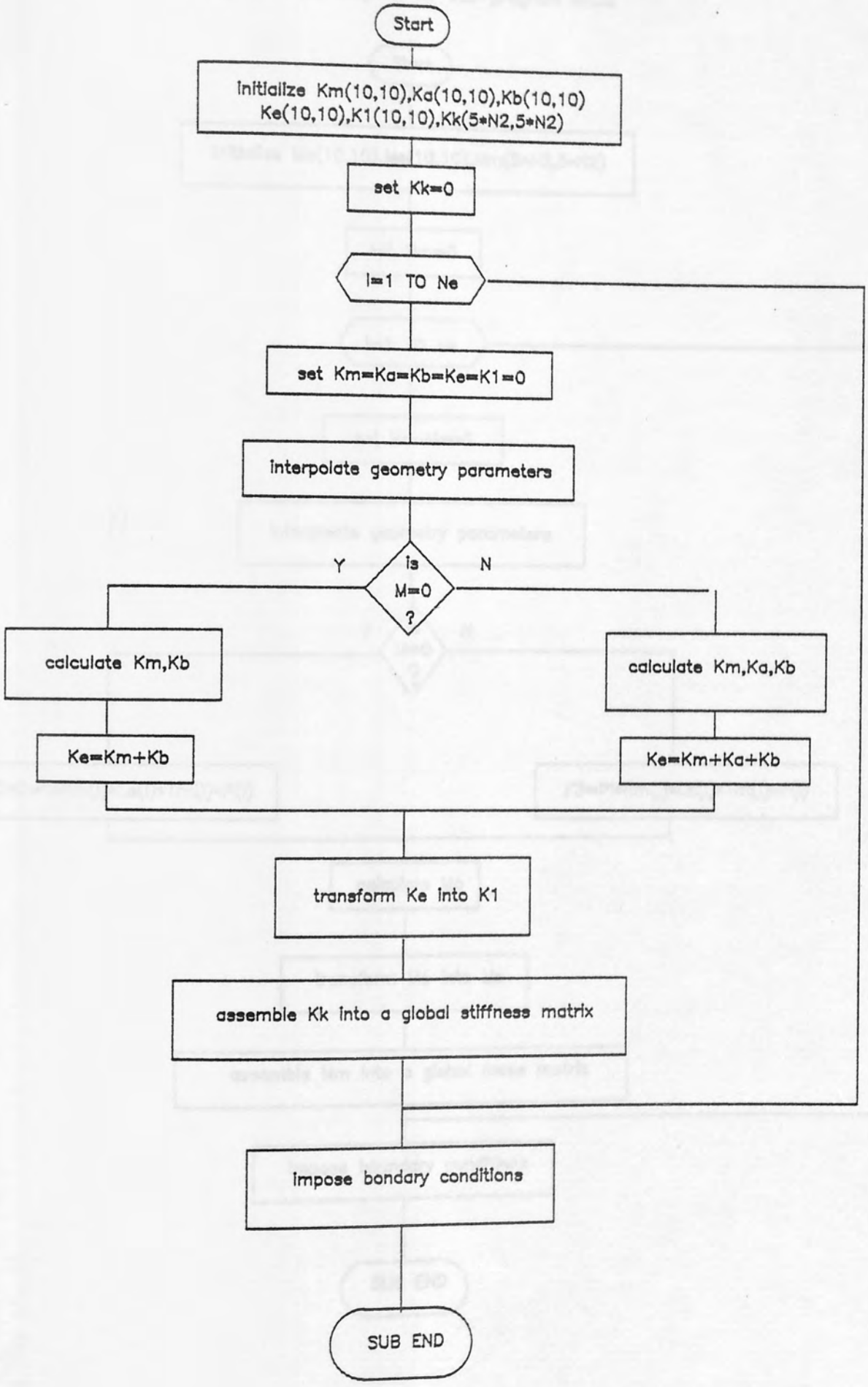

Fig. 6.5 Flow diagram for sub-program MASS

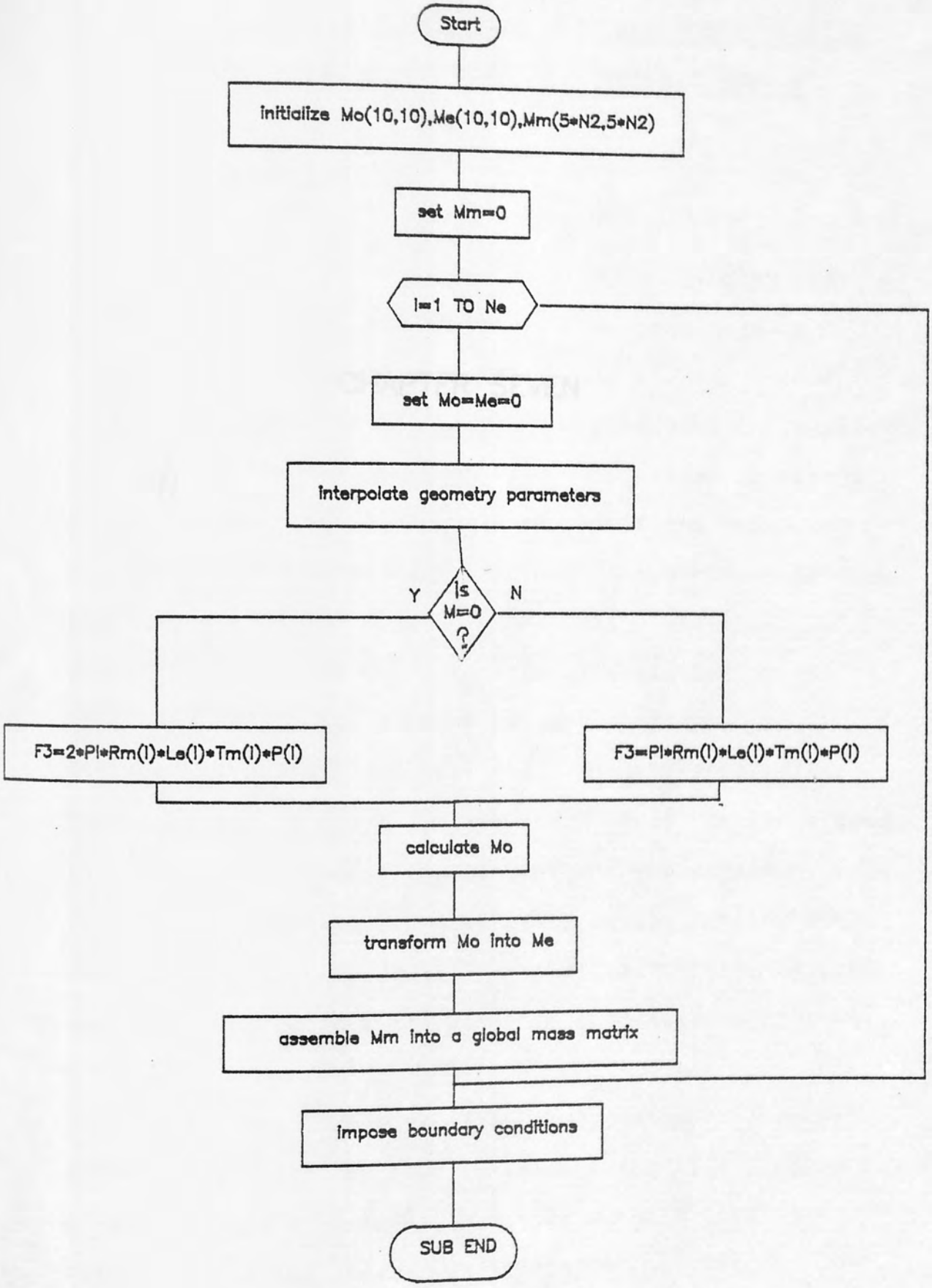

CHAPTER SEVEN

CHAPTER 7

APPLICATION OF THE TRUNCATED CONE ELEMENT IN STATIC AND DYNAMIC ANALYSES OF AXISYMMETRIC SHELLS

7.1 Introduction

In this chapter a series of examples ranging from thin to thick shell situations will be presented to demonstrate the accuracy of the finite element method based on the truncated cone element presented in Chapter 5. The results are compared with theoretical solutions and with some other finite element solutions based on different types of elements. Examples are chosen to show the adequacy of the element representing the shell geometry, i.e., the generator shape, variation in thickness, etc.; the element ability to respond to different types of loadings; the element's ability in solving thin and thick shells; the adequacy of the element in determining natural frequencies and corresponding mode shapes for different types of axisymmetric shells, e.g., circular and annular plates, cylindrical shells, conical shells, spherical shells, and some combinations of these.

Within the framework of an application, the actual number of elements employed to solve a specific problem is usually chosen arbitrarily and then altered until the displacements and stress resultants, or natural

frequencies and mode shapes, exhibit convergence for successively refined element idealisation. The corresponding spatial distribution of the elements along the shell meridian is often determined and adjusted by means of heuristic reasoning, such as specifying a relatively close element spacing in regions of rapid variations of displacements, stress resultants and changes in geometry. A few examples will be presented to study the above mentioned aspects, namely the convergence and element distributions along the shell meridian.

7.2 Static Analysis

In this section the stresses and displacements, in axisymmetric shells subjected to different types of loads, are determined. The effectiveness of the element in tackling both thin and thick shell problems is examined by comparing the results with those obtained by different finite element formulations and/or with exact solutions.

7.2.1 Bending of a Uniformly Loaded, Clamped Circular Plate

This example has become more or less a standard one for evaluating plate elements [5,6,71]. The data for this example consists of the following: $E = 10.92 \times 10^5$ lb/in^2, $\nu = 0.3$, R=5 in and the plate thickness h is considered for two cases:

Thin Plate h = 0.1 in; (R/h = 50),

Thick Plate h = 2 in; (R/h = 2.5).

The deflection of the plate, subjected to a uniform distributed load, is studied with different coarse meshes of 2, 4, 5, 10 and 16 elements. The centre displacement of the plate, for the different meshes, is shown in Table 7.1 while the normalised deflections of the plate solved with a five elements coarse mesh is shown in Fig. 7.1(a). The results are plotted against those obtained in reference [71] and the exact solution taken from reference [78]. For thin plates, very accurate results are obtained; for thick plates, the results are a very good approximation to the exact solution with the same accuracy as those obtained by Hughes et al [71] with 48 plate elements (four node quadrilateral) of the same order as the present element. Figure 7.1(b) shows the different idealisation techniques used in the present analysis and used in reference [71].

7.2.2 Clamped circular plate under an eccentric concentrated load

A finer subdivision is needed for a concentrated load. Ten elements and six terms are found to be adequate to give good agreement with the exact solution [79]. It is assumed that the load P is applied at point A, distance b from the centre 0 of the plate as shown in Fig. 7.2. The point load P is represented, using the usual rules of

Fourier series expansion, by

$$P = \frac{P}{2\pi b} + \sum_{n=1}^{\infty} \frac{P}{\pi b} \cos n\theta \ ,$$

the first term represents the axisymmetric contribution whilst the remainder represents a superposition of harmonic patterns. In the computer program Fourier coefficients need to be input while the remaining operations are done automatically. Results are shown in Fig. 7.2.

7.2.3 Annular Plate Clamped at the Inner Edge and Supporting a Point Load at the Outer Edge

The point load is represented in a similar manner to that described in the previous problem. To study the influence of the number of elements used and number of terms employed in the Fourier expansion, computational experiments were carried out. Table 7.2 shows the improvement in the results according to the number of elements and terms used. Ten elements and 21 terms were adopted for comparison with those obtained by Richards and Delves [80]. With the same number of elements and terms used there; the comparison is made in Fig. 7.3(a,b). An exact solution is available in reference [12].

7.2.4 Circular Plate of Varying Thickness Subjected to Non-Uniform Pressure

The annulus considered in this example has a linear variation in thickness along the radius. The plate is clamped at the edges and subjected to a cubic distribution of lateral pressure of the following type (Fig. 7.4(a)):

$$P = \frac{1}{9}\left\{430\left(\frac{r}{100}\right)^3 - 970\left(\frac{r}{100}\right)^2 + 585\left(\frac{r}{100}\right) - 85\right\}$$

where $100 \leq r \leq 200$.

The original finite element solution to this problem was from reference [81] where a 20 curved element approximation was used. To apply the present element, the plate was divided into a series of five, ten and sixteen elements; for each element, the pressure was assumed to be constant, and equal to the pressure at the centroid of that element. The good agreement of the present element approximation (16 elements mesh) with the theoretical values [81] is shown in Fig. 7.4 (b,c).

7.2.5 Thin Cylinder Under Radial, Edge Ring Load

A circular cylinder fixed at one end carrying a radial ring load at the other is treated here. Due to the decaying nature of the edge effect, the radial displacements and meridional moment in the loaded edge

zone of the cylinder are obtained by using different numbers of elements for the 1 in length next to the loaded end; the idealisation procedure is shown in Fig. 7.5(a) while the radial displacements and meridional moment are shown in Fig. 7.5(b),(c). A theoretical solution is available, which has been used extensively as a test for other finite element solutions [3,4,37]. Input data was: $E = 10^7$ lb/in^2, $\nu = 0.3$, $P = 1$ lb/in, $h = 0.01$ in, $R = 5$ in, $L = 6$ in. In spite of the extreme thickness ($R/h = 500$) the agreement with exact solution is excellent: exact end deflection equal to 2.872×10^{-3} in; end deflection obtained by the present finite element = 2.875×10^{-3} in.

7.2.6 Pressurised Cone

A thin cone with half apex angle of 45° is shown in Fig. 7.6(a). The structure was subjected to a uniform internal pressure and was fixed rigidly round its rim. The cone was divided into 10 elements and the results are compared with the analytical solution which was taken from reference [82]. The details of geometry and the variation in various stress resultants are given in Fig. 7.6(a-e). The input data was: $E = 200$ KN/mm^2, $\nu = 0.3$, $P = 1$N/mm^2, $z = 70.77$ mm, $R = 70.71$ mm, $h = 2$mm.

7.2.7 Cylindrical Shell with Branching Members

Figure 7.7(a) shows a typical joint in a missile in

which the shells are pressurised and also carry thrust loads. The main aim of introducing this example is to show the technique used in node numbering, which is illustrated in the computer code, for branched shells; note, for example, that element number six has started with node six and ended with node ten, while element nine started with node nine and ended with node ten; so two nonsequence elements have shared one node. One more point should be mentioned here, that is, the branched members have different thicknesses.

A total of sixteen elements are used to represent the branched shell. The number of elements in the original representation [3] is unclear but it appears that there were 29 sampling points on the cylindrical portion alone. The good agreement between the analytical [18] and the present results is shown in Fig. 7.7(b). The interest here is to determine the cylinder radial displacement in the joint area with the spherical shell.

7.2.8 Spherical Cap with Uniform Pressure

A spherical cap with its dimensions, manner of loading and support conditions is shown in Fig. 7.8. A comparison is made of the distributions of meridional bending moment and circumferential tensile stress with an exact solution obtained by a hypergeometrical series solution [12] for a clamped-edge spherical shell of 35°

half angle and R/h = 30 subjected to uniform external pressure. It is seen that, for the present finite element idealization which consists of 16 conical elements, the error introduced by a straight line approximation to the curved shapes appears insignificant. The accuracy of the solution increases when the elements are reduced in size.

TABLE 7.1 Centre displacement (in) for a clamped circular plate subjected to a uniform pressure

Ne	Displacement h = 0.1 in	Percentage Error	Displacement h = 2 in	Percentage Error
2	1.4498×10^{-1}	48.45	2.9997×10^{-5}	28.37
4	1.1044×10^{-1}	13.00	2.3367×10^{-5}	0.0
5	1.0233×10^{-1}	4.78	2.2335×10^{-5}	-4.4
10	0.9885×10^{-1}	1.22	2.1453×10^{-5}	-8.19
16	0.9822×10^{-1}	0.57	2.1267×10^{-5}	-8.99
exact [78]	0.9766×10^{-1}	-	2.3368×10^{-5}	-

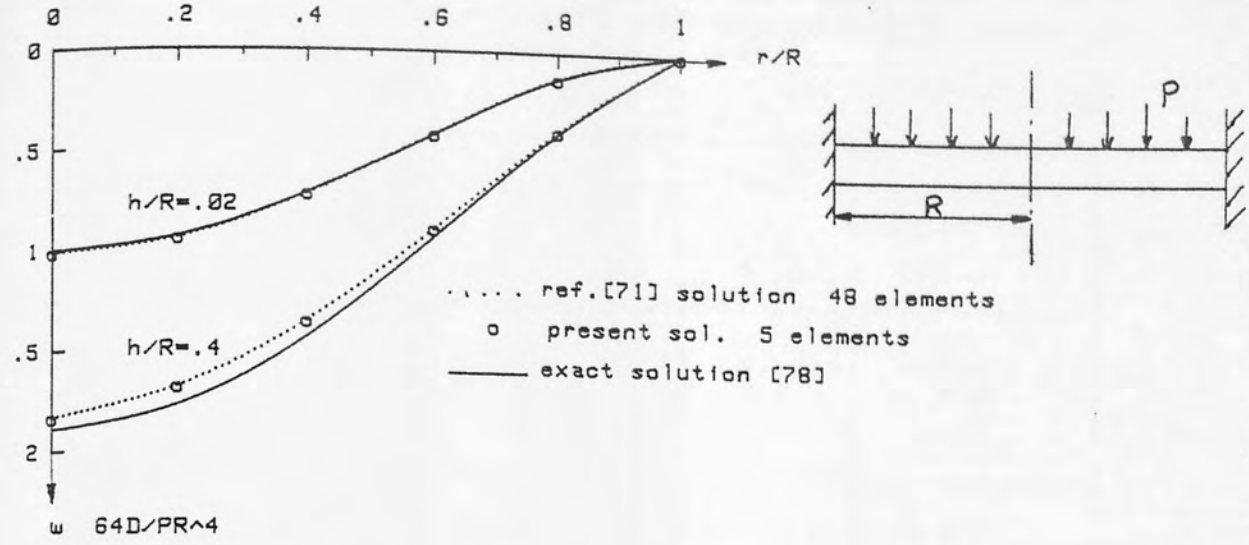

Fig. 7.1(a) deflections of a clamped circular plate under uniformload

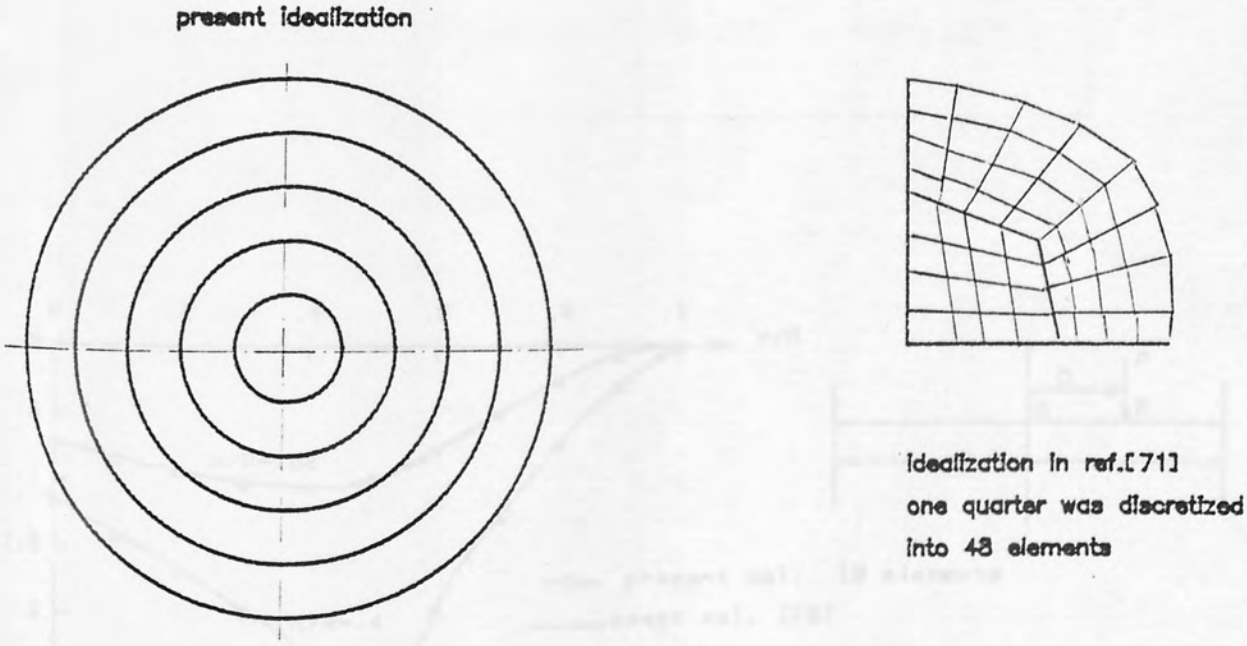

Fig. 7.1(b) finite element meshes for the clamped circular plate

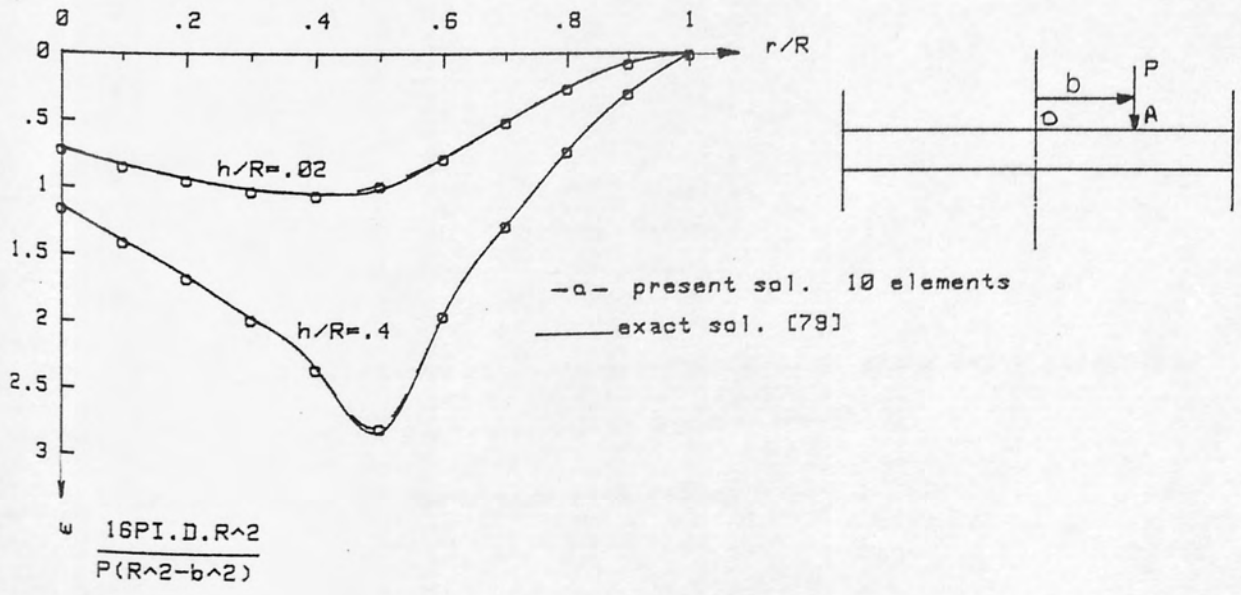

Fig. 7.2 deflections of clamped circular plate under eccentric point load

TABLE 7.2 Clamped-free annular plate under point load at outer edge. Comparison of results according to number of elements and terms used.

Deflections ($mm \times 10^{-3}$) at free edge r = 0.225 m				Deflections at r=0.220
Angle θ°	Ne = 5 Nt = 6	Ne = 10 Nt = 6	Ne = 10 Nt = 21	Ne = 10 Nt = 21
0	8.4987	8.5535	8.9529	8.4870
30	4.8472	4.8850	4.7127	4.5225
60	0.6664	0.7015	0.8113	0.7898
90	-0.4432	-0.4125	-0.4998	-0.4751
120	-0.5170	-0.5096	-0.4303	-0.4125
150	-0.0247	-0.0293	-0.1072	-0.1039
180	-0.0392	-0.0511	+0.0271	+0.0245

Ne = number of elements used

Nt = number of terms used

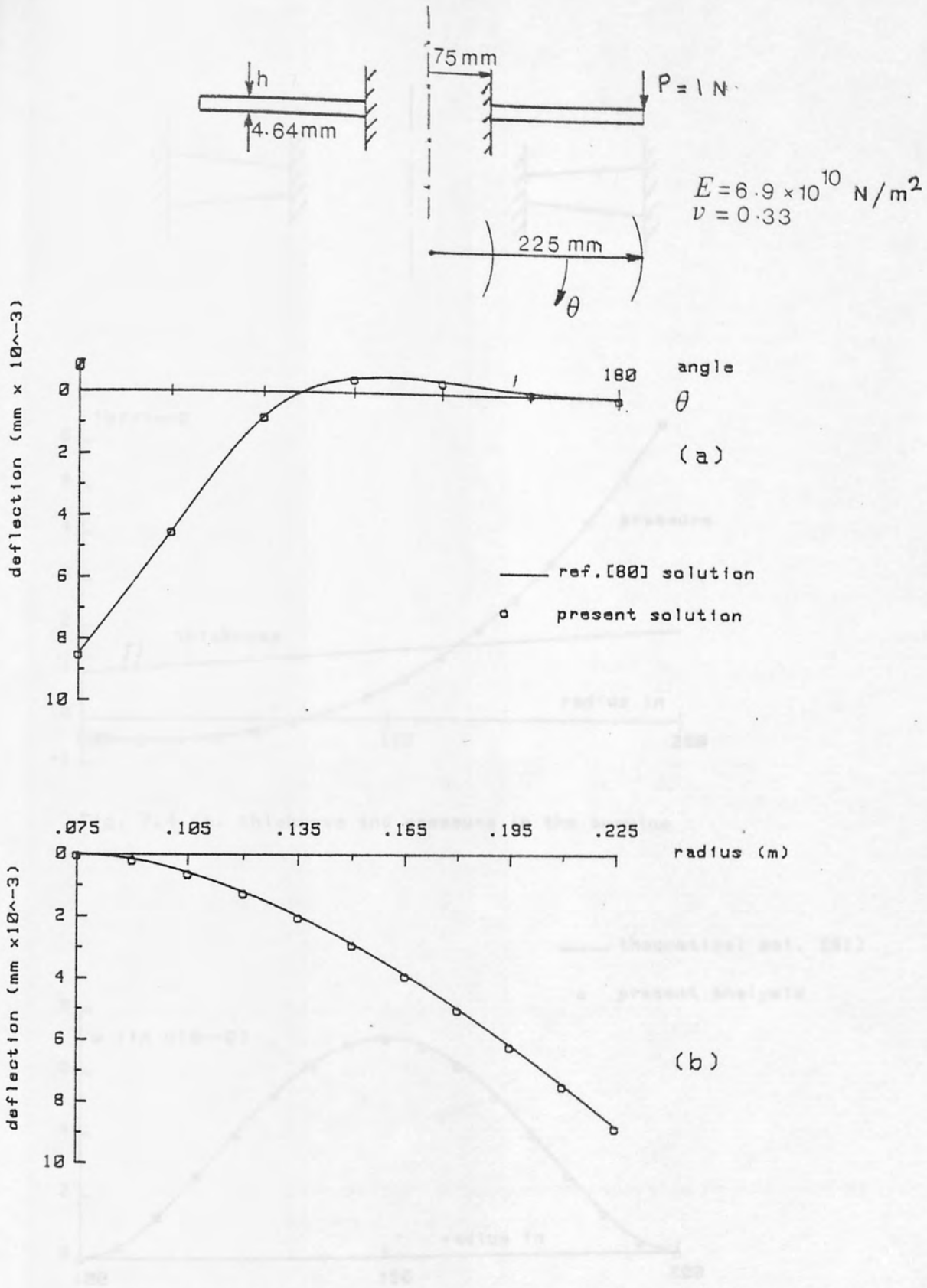

Fig. 7.3 deflections of a clamped-free annular plate under point load

(a) variation of deflection with angle θ (r=.220 m)

(b) variation of deflection with radius r (θ=0)

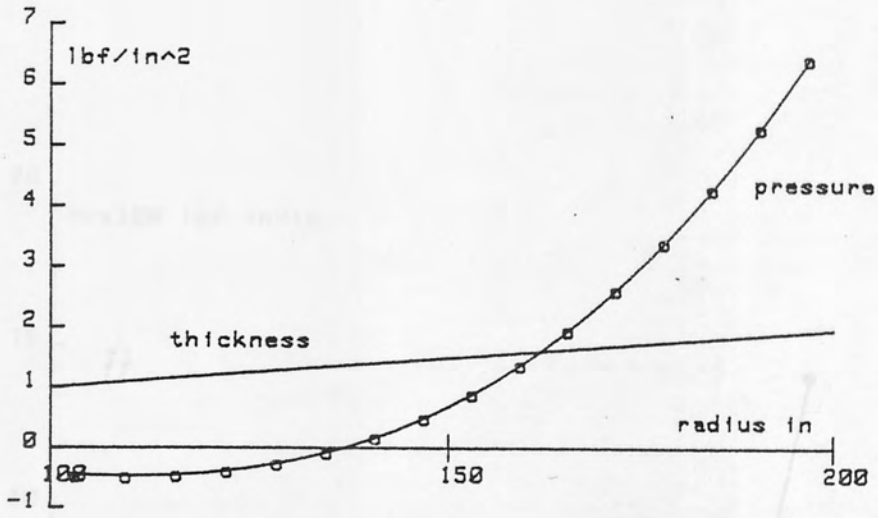

Fig. 7.4 (a) thickness and pressure in the annulus

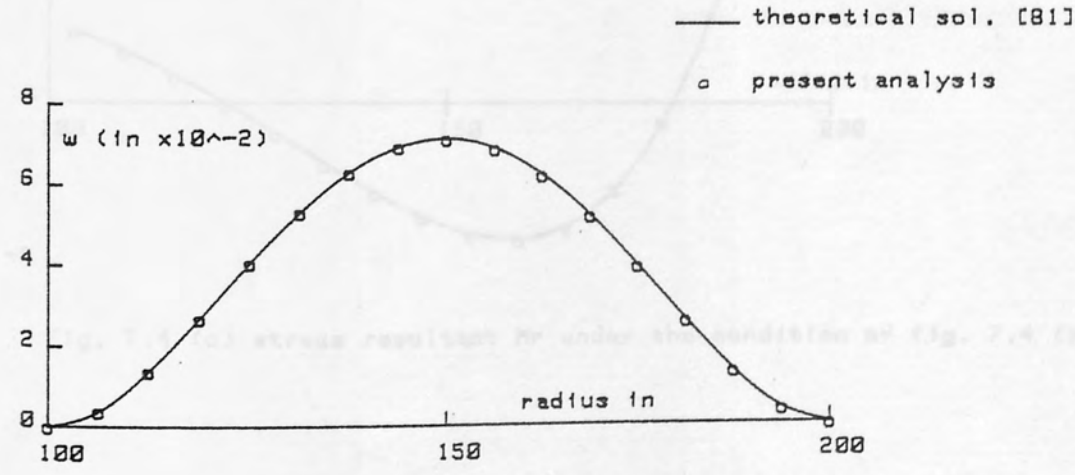

Fig. 7.4 (b) axial displacement w against radial distance r for the annulus of fig. 7.4 (a)

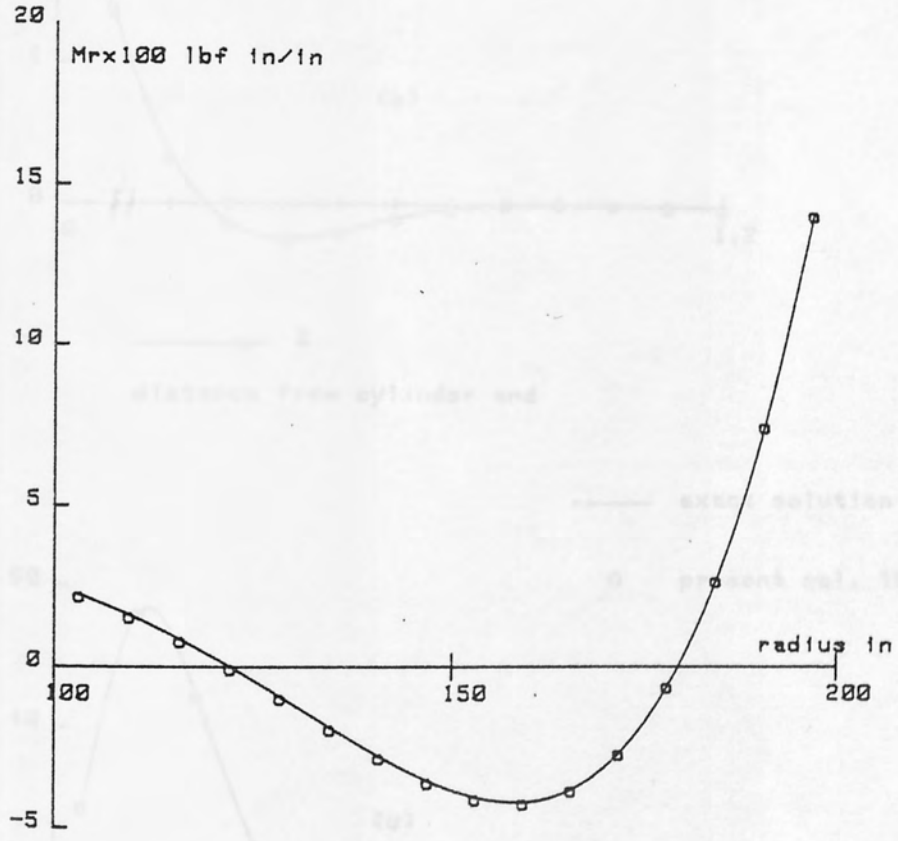

Fig. 7.4 (c) stress resultant Mr under the condition of fig. 7.4 (a)

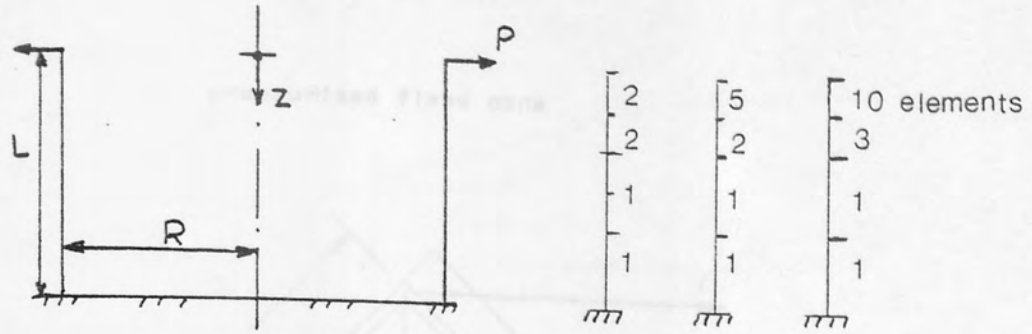

(a) different subdivisions of the 1-in length next to the loaded end

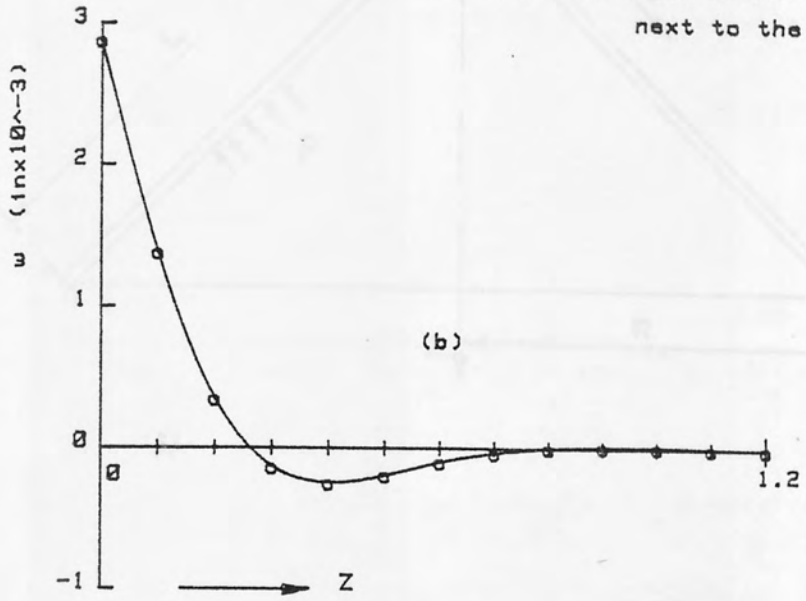

distance from cylinder end

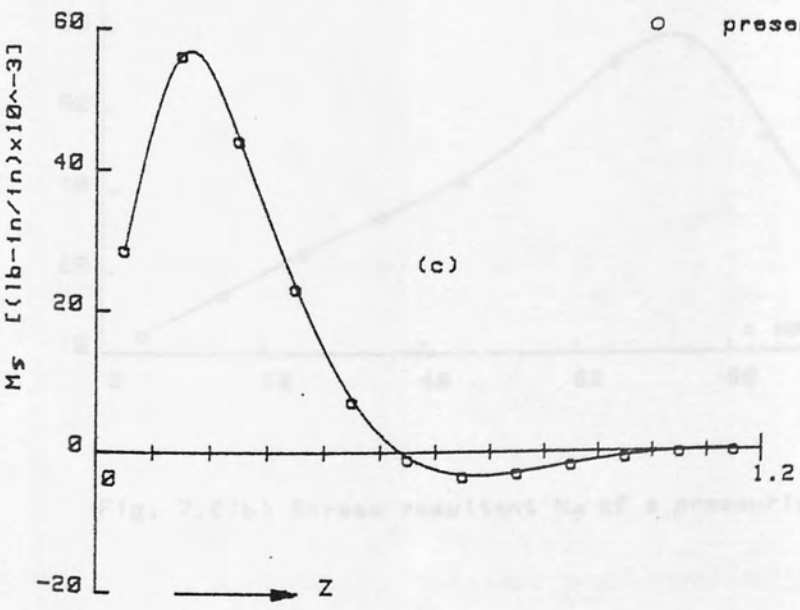

Fig. 7.5 thin cylinder under radial edge load

(b) radial diceplacement (inx10^-3), (c) meridional moment (lb-in/in x10^-3)

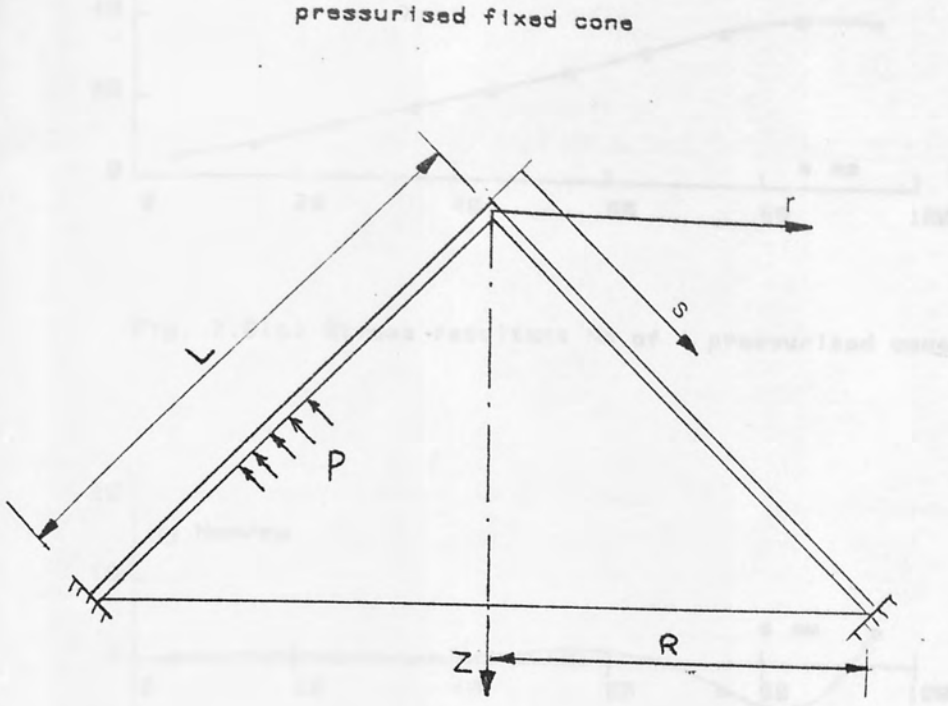

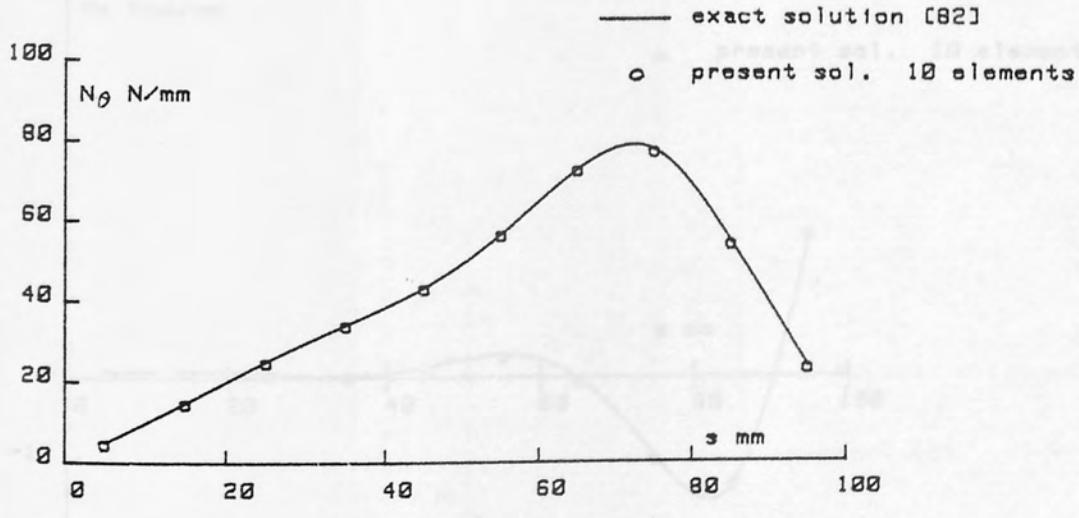

Fig. 7.6(b) Stress resultant N_θ of a pressurized cone

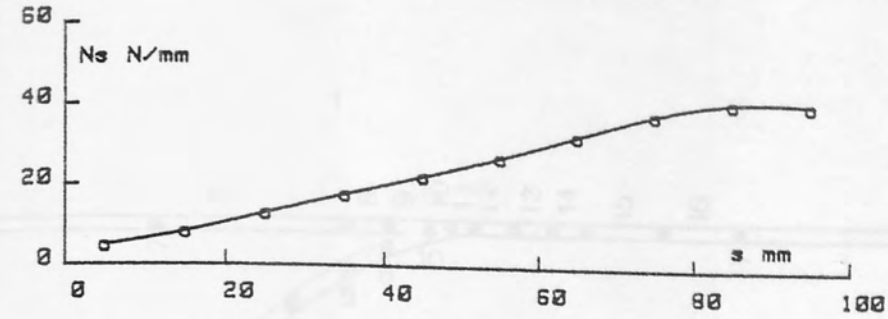

Fig. 7.6(c) Stress resultant Ns of a pressurized cone

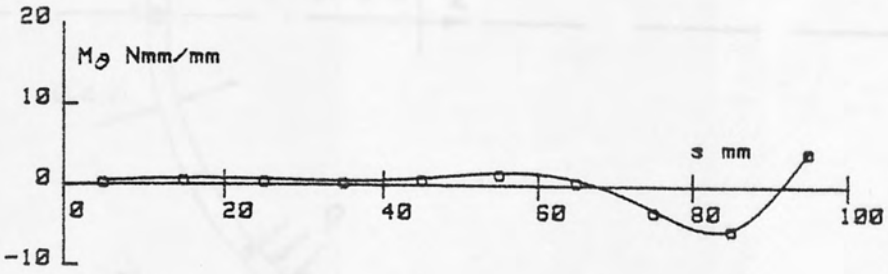

Fig. 7.6(d) Stress resultant M_θ of a pressurized cone

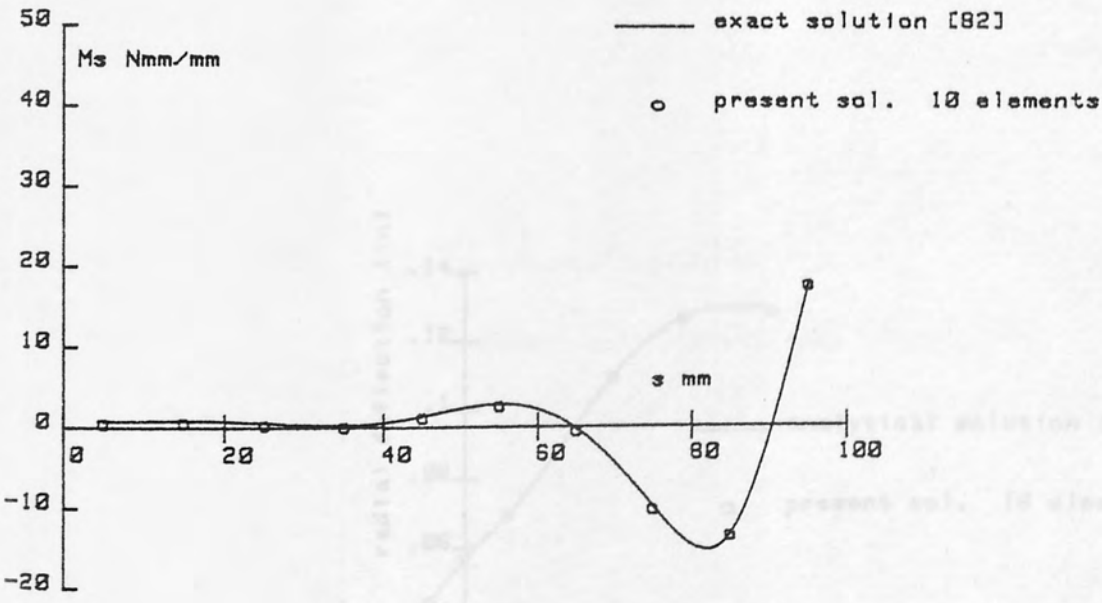

Fig. 7.6(e) Stress resultant Ms of a pressurized cone

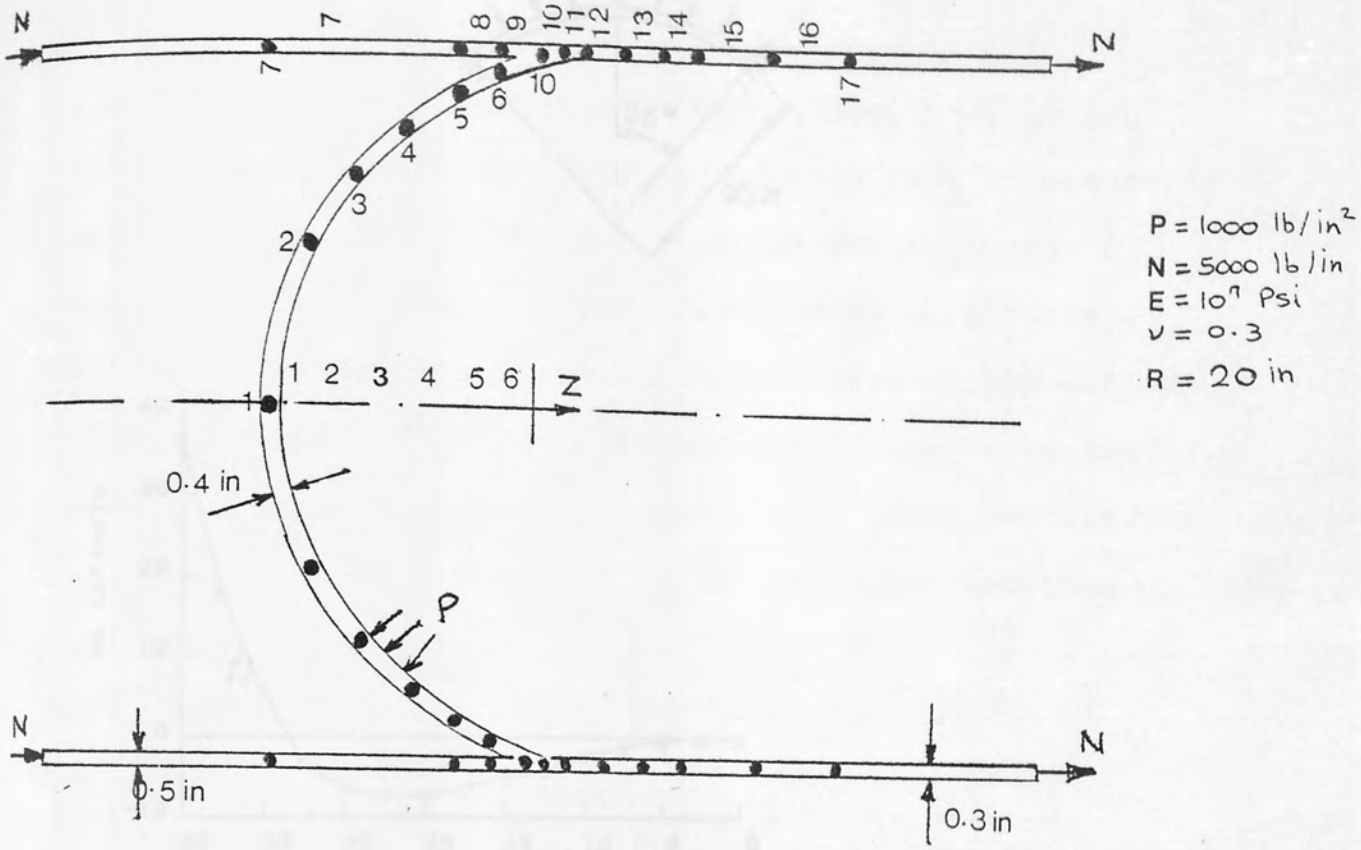

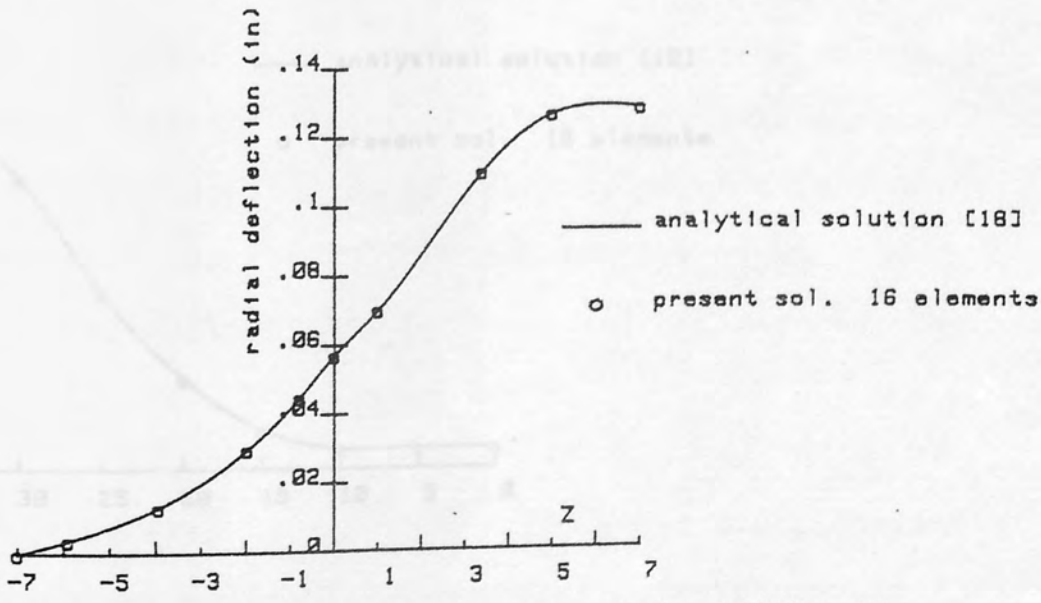

Fig.7.7 Radial deflection along direction of the cylinder axis near junction point

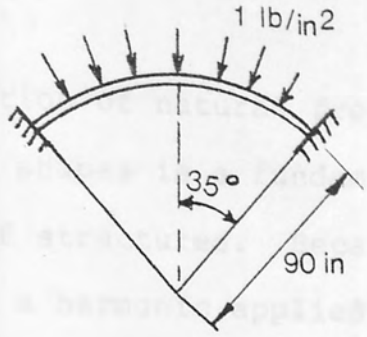

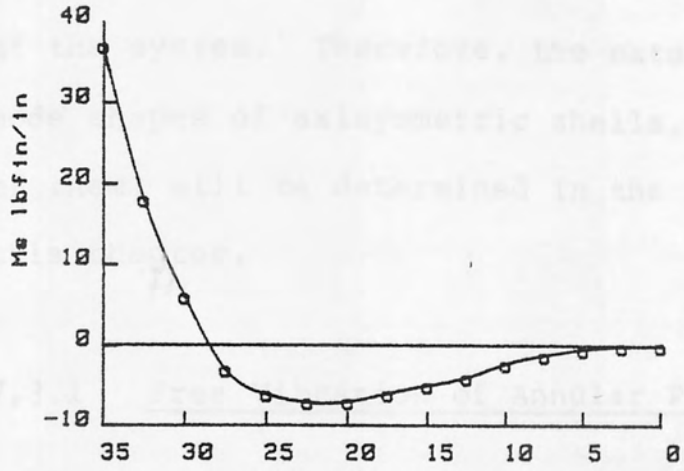

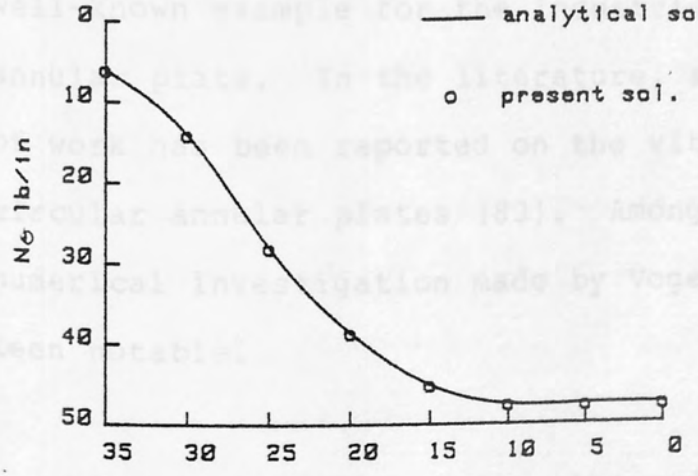

Fig. 7.8 spherical dome under uniform pressure

7.3 Dynamic Analysis - Free Vibration

The determination of natural frequencies and corresponding mode shapes is a fundamental step in the dynamic analysis of structures. Because if a structure is subjected to, say, a harmonic applied force, large amplitudes will occur if the frequency of this force is equal, or nearly equal, to one of the natural frequencies of the system. Therefore, the natural frequencies and mode shapes of axisymmetric shells, and some combinations of them, will be determined in the following sections of this chapter.

7.3.1 Free Vibration of Annular Plates

As structural elements, circular annular plates are extensively used in the construction of aircraft, ships, automobiles and other vehicles. The turbine disc is a well-known example for the industrial application of the annular plate. In the literature, a considerable amount of work has been reported on the vibrations of thin circular annular plates [83]. Among all the works, the numerical investigation made by Vogel and Skinner [84] has been notable.

Throughout this section the radii a and b will define the outer and concentric inner boundaries, respectively. Seven combinations of the boundary conditions - clamped,

simply supported and free - on the outer and inner edges are to be considered in this section. The natural frequencies and mode shapes of each of the seven combinations are presented for specified values of b/a (between 0.1 and 0.7) and Poisson's ratio of 1/3. The presentations cover those modes which can be characterised as having up to three uniformly spaced nodal diameters and two concentric nodal circles; it should be mentioned here that only those nodal circles are considered which exist away from either boundary.

The following seven sets of boundary conditions are considered in this section:

(1) C-C, clamped at both the inner and outer edge.

(2) C-SS, clamped at the outer edge and simply supported at the inner edge.

(3) C-F, clamped at the outer edge and free at the inner edge.

(4) SS-C, simply supported at the outer edge and clamped at the inner edge.

(5) SS-SS, simply supported at both edges.

(6) SS-F, simply supported at the outer edge and free at the inner edge.

(7) F-C, free at the outer edge and clamped at the inner edge.

A clamped, simply supported or free boundary should satisfy the following conditions:

$u=v=w=\beta=\alpha=0$; or $w=v=\alpha=0$, $u\neq0$, $\beta\neq0$, or $u\neq0$, $v\neq0$, $w\neq0$, $\beta\neq0$, $\alpha\neq0$ respectively.

It should be noted here that in all cases the first specified boundary represents the outer edge while the second represents the inner edge.

The theory underlying the analysis in reference [83] assumed small deflections and neglected the effects of rotary inertia and of the additional deflection caused by shear forces. The frequencies, for b/a = 0.1, 0.3, 0.5, 0.7 and $\nu = 1/3$, compared with those in reference [83] are shown in Table 7.3 through to Table 7.9. Adjacent to each table there is a graph relating to that table. The curves on these plots indicate the relationship between a non-dimensional quantity, $\lambda = a[\rho\omega^2 h/D]^{1/4}$, which is proportional to the frequency and the ratio of radii for the different modes. As b/a approaches zero, each of the curves tends to a finite limit in all but one case. This limit for these curves can be determined approximately by extending the curve until it intersects with the ordinate. The one exception to the foregoing cases is for the modes characterised by one nodal diameter for the case of a plate with a free outside edge and a clamped inner edge. The limiting frequency for each of these modes is

zero since the motion is simply a rigid body rotation of the disc about a diameter. For the seven cases , the ratio a/h is taken equal to 100/3. No significant error is recorded in the results.

Mota-Soares and Petyt [85] developed a curved annular semi-analytic element for the dynamic analysis of practical discs; it had 2 nodes and 12 degrees-of-freedom and was based on the Mindlin thick plate theory. The shape functions used were cubic in n (radial direction). A comparison is made here with the results published in reference [85] of a centrally clamped thin disc and b/a = 0.3. The number of elements used in reference [85] was eight while the number of elements used in this investigation is fourteen. The comparison is shown in Table 7.10.

The results agree very closely indeed. However, when the number of nodal circles and nodal diameters are small the present element representation gives slightly lower frequencies than those in reference [85] while when the number of nodal circles and diameters increases the results obtained in reference [85] are slightly lower than the present results.

In Tables 7.3 through to 7.10 the non-dimensional frequency parameter λ^2 is given; to transform this into frequencies the following formula was used

$$\text{Natural frequency (Hz)} = \frac{\lambda^2}{2\pi a^2}\sqrt{\frac{Eh^2}{12\rho(1-\nu^2)}} \quad .$$

As the plates used in actual practice may have large thickness, it is important to include the effects of rotary inertia and shear deformation in order to predict their dynamic behaviour with a fair amount of accuracy. It is well known that both effects serve to decrease the computed frequencies because of increased inertia and flexibility of the system.

Although some amount of work has been reported on the vibrations of thick circular plates [83], no work which gives the natural frequencies of thick annular plates was reported there. Rao and Prasad [86] have derived the frequency equations, by including the effects of transverse shear deformation and rotary inertia. The quantity $\bar{\delta}_o$ was determined for specified values of b/a (between 0.1 and 0.7) and a/h (between 2 and 7) for nine sets of simple boundary conditions. The calculations covered those modes which can be characterised as having up to two concentric nodal circles and two uniformly spaced nodal diameters.

When both the effects of transverse shear and rotary inertia are neglected, the frequency parameter was given as

$$\delta_o^2 = [\rho\ \omega^2 h/D]^{\frac{1}{2}} = \lambda^2/a^2$$

where λ^2 has been used, in this work, for the foregoing examples.

When the effects of rotary inertia and shear deformation are considered, the frequency parameter was given as

$$\bar{\delta}_o^4 = \delta_0^4\ R^2 = \frac{\lambda^4}{144(\frac{a}{h})^4}$$

where $R = \frac{h^2}{12}$.

To test the performance of the present finite element, in thick shell problems, we have chosen two thick annular plates: these are (a) clamped-clamped and (b) simply supported-clamped annular plates. In the computations the quantity $\bar{\delta}_o$ is determined for two values of b/a, 0.1 and 0.3, and for a/h = 7.

Both plates were discretised into 6 or 9 elements when b/a = 0.1 and 5 or 7 elements when b/a = 0.3; the reason behind this discretisation was to investigate the behaviour of the present finite element in relation to the thickness-to-length ratio $\frac{h}{L_e}$ of the element. The results show that in all cases, for both plates, the present element gave, as it was expected, lower frequencies than those obtained by a classical means (neglecting shear

deformation and rotary inertia). Compared with the results obtained by the exact method, where both transverse shear and rotary inertia were included, the present analysis gave higher results in axisymmetric modes, while it gave lower results as the number of nodal diameters and nodal circles increases. When $\frac{h}{L_e}$ exceeded unity, the difference could be as high as 15%, because the element becomes very flexible. However, if $\frac{L_e}{h}$ was kept over unity no difference higher than 5% was recorded.

Table 7.3 Frequency parameters λ^2
for a clamped-clamped annular plate

mode shape Nd	Nc	λ^2 for values of b/a of 0.1 exact [83]	0.1 P.F.E Ne=16	0.3 exact [83]	0.3 P.F.E Ne=15	0.5 exact [83]	0.5 P.F.E Ne=13	0.7 exact [83]	0.7 P.F.E Ne=10
0	0	27.3	27.3	45.2	45.4	89.2	88.6	248	236
0	1	75.3	76.8	125	127	246	245.4	686	623
0	2	-	154	-	255	-	487	-	-
1	0	28.4	28.8	46.6	46.6	90	89.5	249	239
1	1	78.6	79.8	127	129	248	246.6	686	641
1	2	-	159	-	257	-	488	-	-
2	0	36.7	36.5	51	51	93.3	92.3	251	242
2	1	90.5	91.2	134	134.8	253	250.3	689	678
2	2	-	172.6	-	263.5	-	492	-	-
3	0	51.2	51	60	59.54	99	97.7	256	245
3	1	112	112.6	145	145.2	259	256.6	694	680
3	2	-	198.5	-	274	-	498	-	-

P.F.E = present finite element
Nd =number of nodal diameters
Nc =number of nodal circles

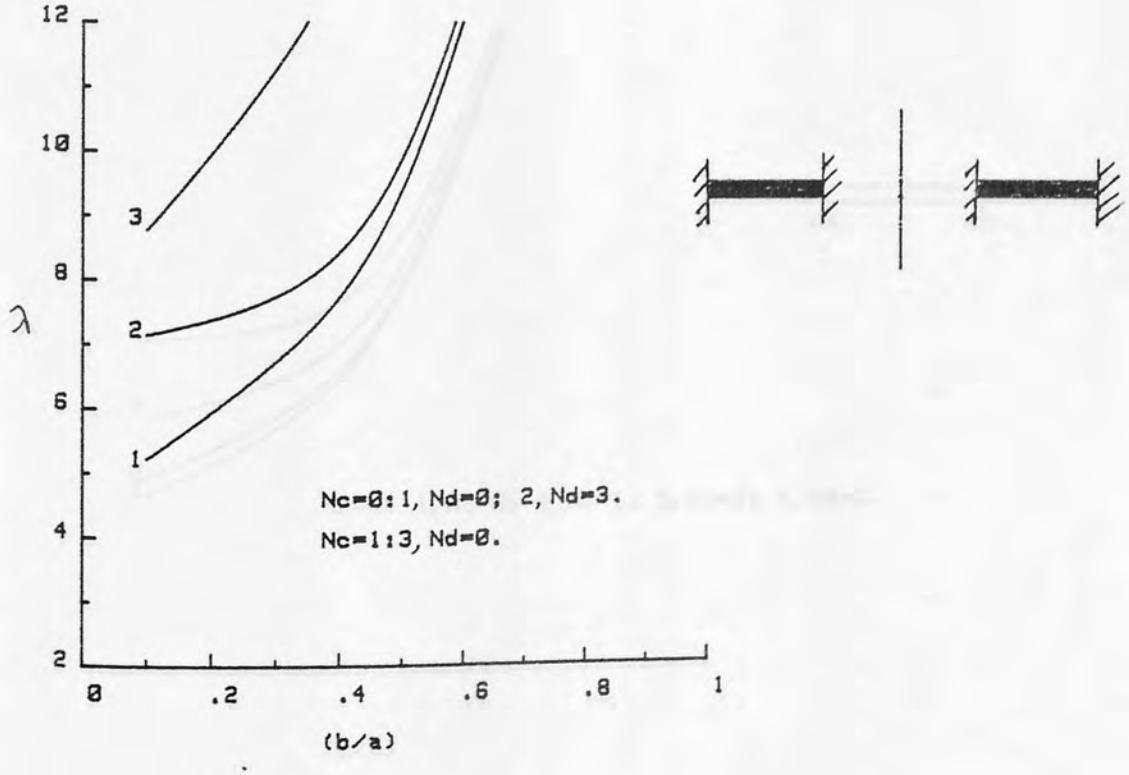

Table 7.4 Frequency parameters λ^2
for a clamped-simply supported annular plate

mode shape Nd	Nc	λ^2 for values of b/a of 0.1 exact [83]	0.1 P.F.E Ne=15	0.3 exact [83]	0.3 P.F.E Ne=14	0.5 exact [83]	0.5 P.F.E Ne=10	0.7 exact [83]	0.7 P.F.E Ne=10
0	0	22.6	22.5	33.7	33.7	64	63.7	175	170
0	1	65.6	65.8	104	105	202	203	558	538
0	2	-	135	-	224	-	417	-	-
1	0	25.1	25.2	35.8	35.8	65.4	65.2	175	172
1	1	70.5	71.7	107	108.5	203	204.7	560	540
1	2	-	145	-	226	-	427	-	-
2	0	35.4	35.4	42.8	42.6	70	70	178	175
2	1	86.7	87	116	116.7	210	209.6	563	543
2	2	-	165	-	235	-	434	-	-
3	0	51	50.9	54.7	54.3	78.1	77.5	185	180
3	1	111	112	130	130.6	218	217.8	570	548
3	2	-	196	-	249	-	442	-	-

P.F.E = present finite element
Nd = number of nodal diameters
Nc = number of nodal circles

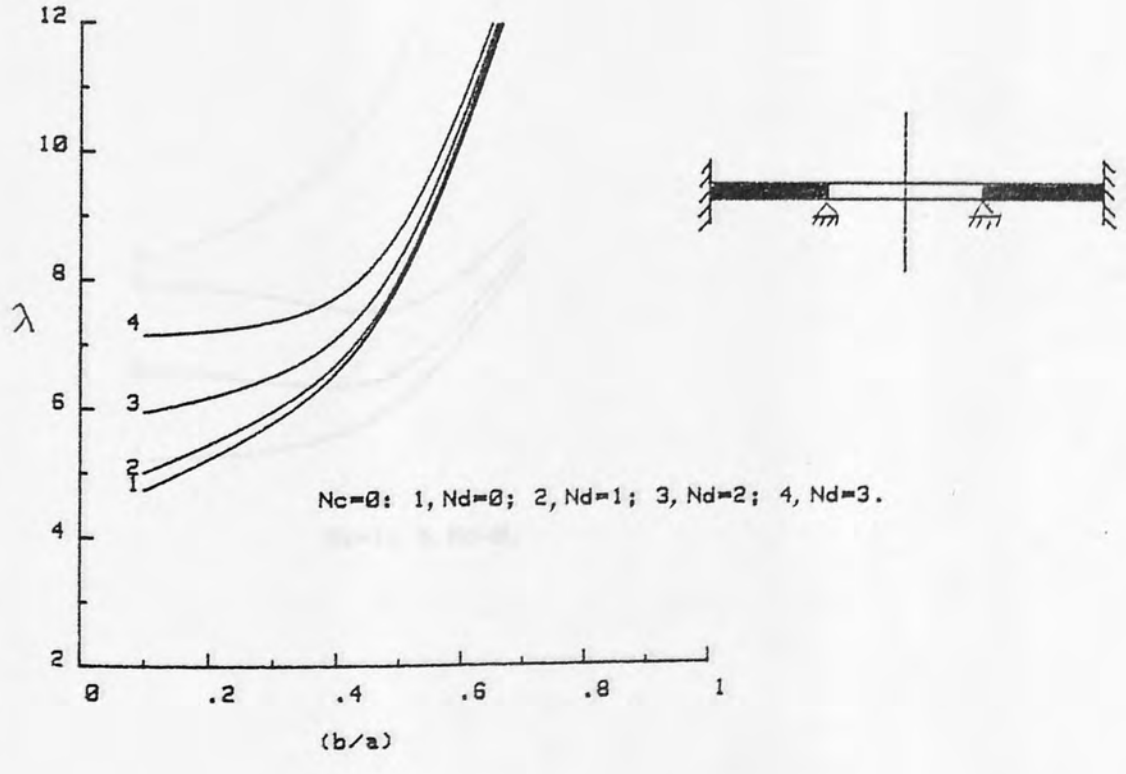

Table 7.5 Frequency parameters λ^2
for a clamped-free annular plate

mode shape Nd	Nc	λ^2 for values of b/a of 0.1 exact [83]	0.1 P.F.E Ne=15	0.3 exact [83]	0.3 P.F.E Ne=14	0.5 exact [83]	0.5 P.F.E Ne=10	0.7 exact [83]	0.7 P.F.E Ne=10
0	0	10.2	10.1	11.4	11.3	17.7	17.5	43.1	42.1
0	1	39.5	39.5	51.7	51.7	93.8	93.5	253	245
0	2	90.4	91.7	132	134	253	254	692	665
1	0	21.1	21.1	19.5	19	22	21.4	45.3	44.4
1	1	60	59.8	59.8	58.8	97.3	97.5	254	246
1	2	-	116	-	139	-	265	-	667
2	0	34.5	34.43	32.5	32.3	32	31	51.5	49.6
2	1	83.4	84	79	76.5	108	105.5	259	251
2	2	-	155	-	154	-	272	-	670
3	0	51	50.8	49.1	48.8	45.8	44.4	61.3	58.2
3	1	-	111	-	101.8	-	119.2	259	258
3	2	-	193.8	-	178.4	-	282.7	-	676

P.F.E = present finite element
Nd = number of nodal diameters
Nc = number of nodal circles

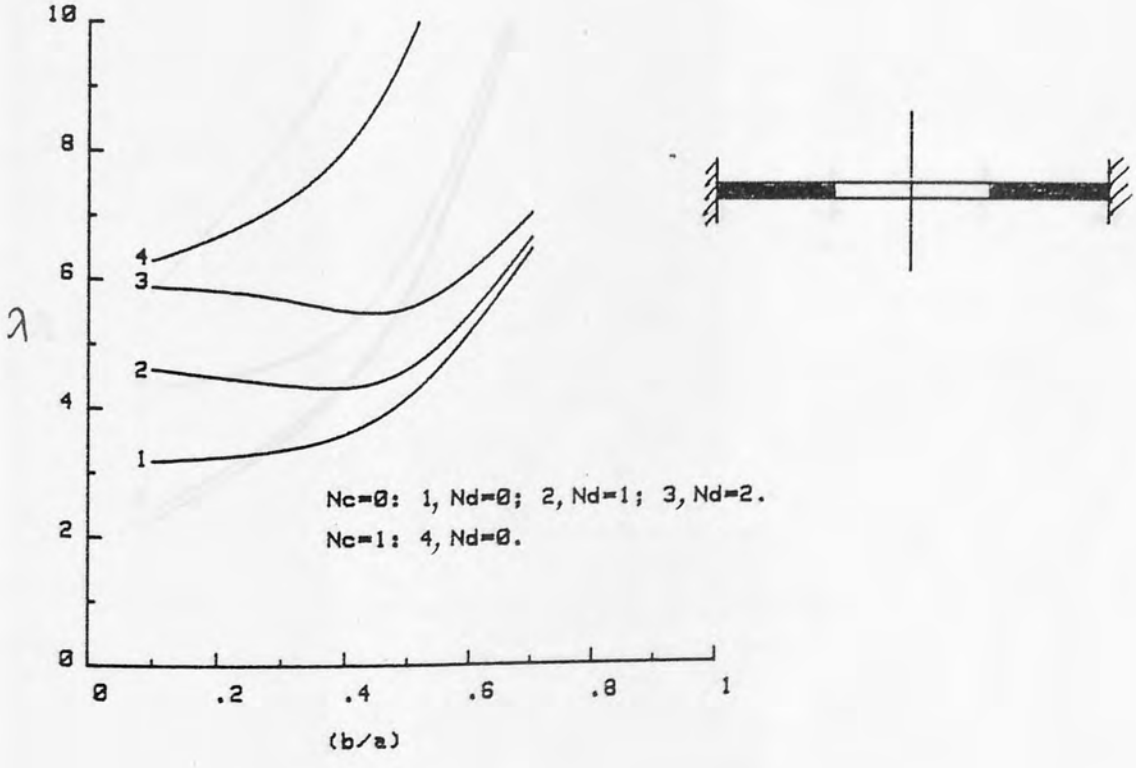

Table 7.6 Frequency parameters λ^2
for a simply supported-clamped annular plate

mode shape Nd	Nc	λ^2 for values of b/a of							
		0.1		0.3		0.5		0.7	
		exact [83]	P.F.E Ne=15	exact [83]	P.F.E Ne=14	exact [83]	P.F.E Ne=13	exact [83]	P.F.E Ne=10
0	0	17.8	17.9	29.9	30.1	59.8	59.8	168	165
0	1	60.1	61	100	102	198	198	552	533
0	2	-	125	-	218	-	320	-	718
1	0	19	19.4	31.4	31.5	61	61	170	166.2
1	1	62.8	65	102	104	200	200.7	553	534
1	2	-	135	-	223	-	425	-	734
2	0	26.8	26.7	36.2	36.2	64.6	64.5	172	168
2	1	74.7	75.4	109	110	205	204.8	557	537
2	2	-	150	-	229	-	429	-	794
3	0	40	40	45.4	45.3	71	70.7	177	173
3	1	95.3	95.9	120	121	211	211.7	563	542
3	2	-	176	-	253	-	436	-	868

P.F.E = present finite element
Nd = number of nodal diameters
Nc = number of nodal circles

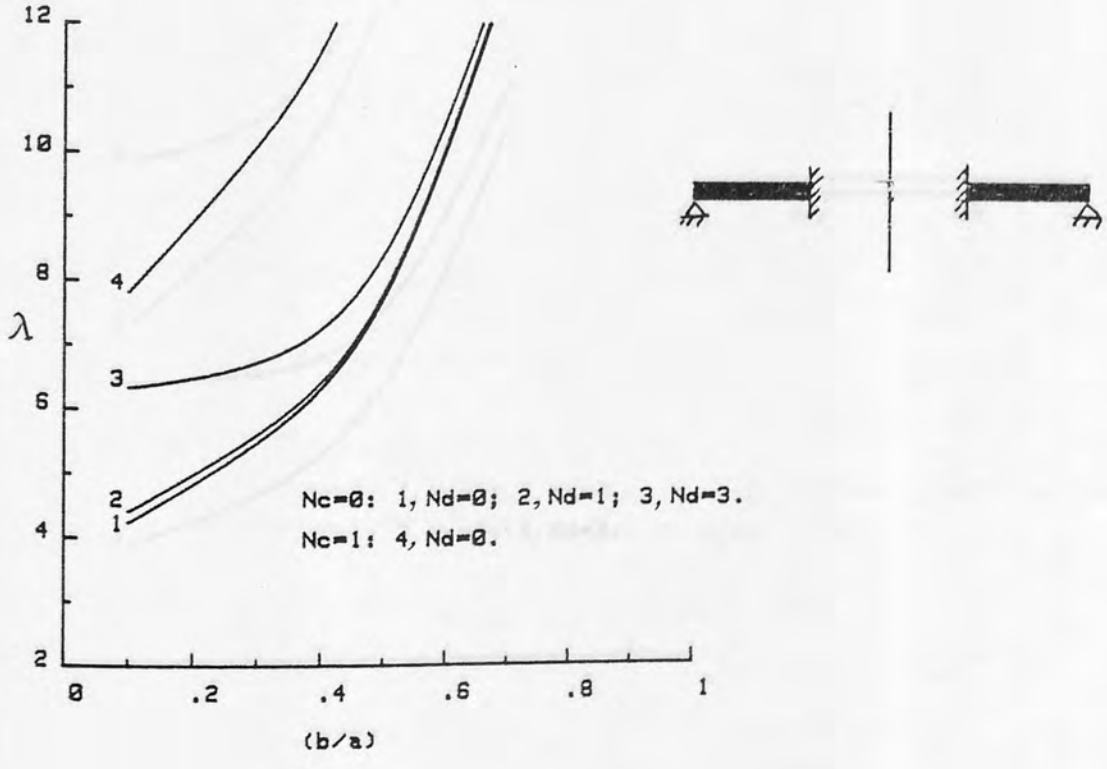

Table 7.7 Frequency parameters λ^2
for a simply supported-simply supported annular plate

mode shape Nd	Nc	λ^2 for values of b/a of 0.1 exact [83]	0.1 P.F.E Ne=15	0.3 exact [83]	0.3 P.F.E Ne=14	0.5 exact [83]	0.5 P.F.E Ne=10	0.7 exact [83]	0.7 P.F.E Ne=10
0	0	14.5	14.6	21.1	21.12	40	40.1	110	108
0	1	51.7	52.1	81.8	82.1	159	159.8	439	435
0	2	-	111	-	185	-	386	-	700
1	0	16.7	16.8	23.3	23.33	41.8	42	112	110.9
1	1	56.5	57.3	84.6	85.9	161	162	441	437
1	2	-	124	-	193	-	390	-	712
2	0	25.9	25.9	30.2	30.2	47.1	47.1	116	114.9
2	1	71.7	72.5	93.3	94.4	167	171	444	440
2	2	-	143	-	202	-	395	-	727
3	0	40	39.95	42	41.8	56	56	122	121
3	1	94.7	95.4	108	108.8	177	179	453	446
3	2	-	174	-	241	-	400	-	753

P.F.E = present finite element
Nd = number of nodal diameters
Nc = number of nodal circles

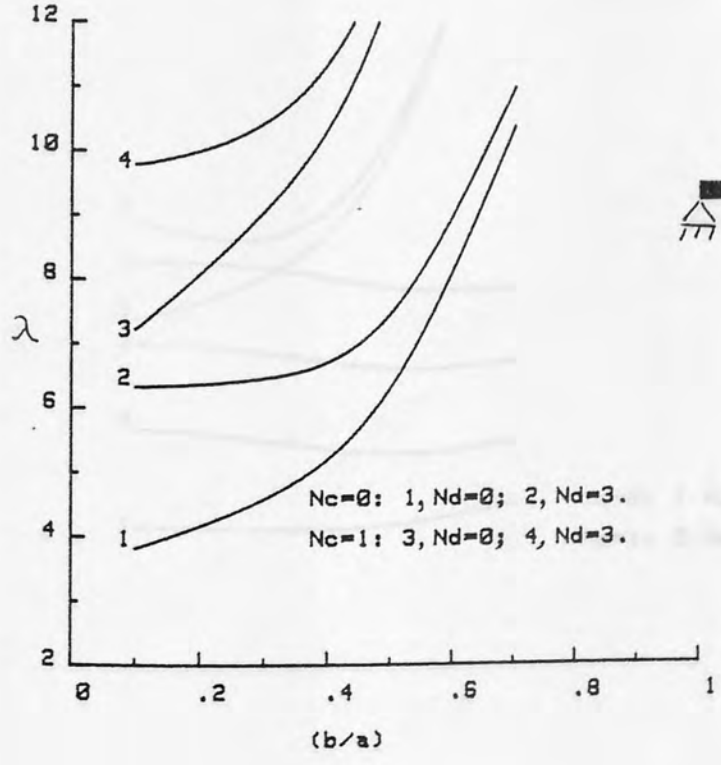

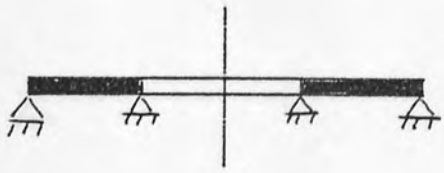

Table 7.8 Frequency parameters λ^2
for a simply supported-free annular plate

mode shape Nd	Nc	λ^2 for values of b/a of 0.1 exact [83]	0.1 P.F.E Ne=15	0.3 exact [83]	0.3 P.F.E Ne=14	0.5 exact [83]	0.5 P.F.E Ne=10	0.7 exact [83]	0.7 P.F.E Ne=10
0	0	4.86	4.86	4.66	4.66	5.07	5	6.93	6.65
0	1	29.4	29.42	37	37.1	65.8	65.7	175	172
0	2	74.8	75	107	108	203	203	558	555
1	0	13.9	13.9	12.8	12.5	11.6	11.12	13.3	12.6
1	1	48	48	45.8	44.6	69.9	69.84	178	176
1	2	-	77.5	-	114	-	215	-	556
2	0	25.4	25.4	24.1	24.1	23.3	21.7	24.3	23
2	1	69.2	69.8	65.1	63.33	81.1	79	185	182
2	2	-	135.6	-	131	-	222	-	560
3	0	40	39.89	38.8	38.7	35.7	35	37.2	35.1
3	1	-	95	-	88	-	94.5	-	191
3	2	-	172	-	-	-	234	-	566

P.F.E = present finite element
Nd = number of nodal diameters
Nc = number of nodal circles

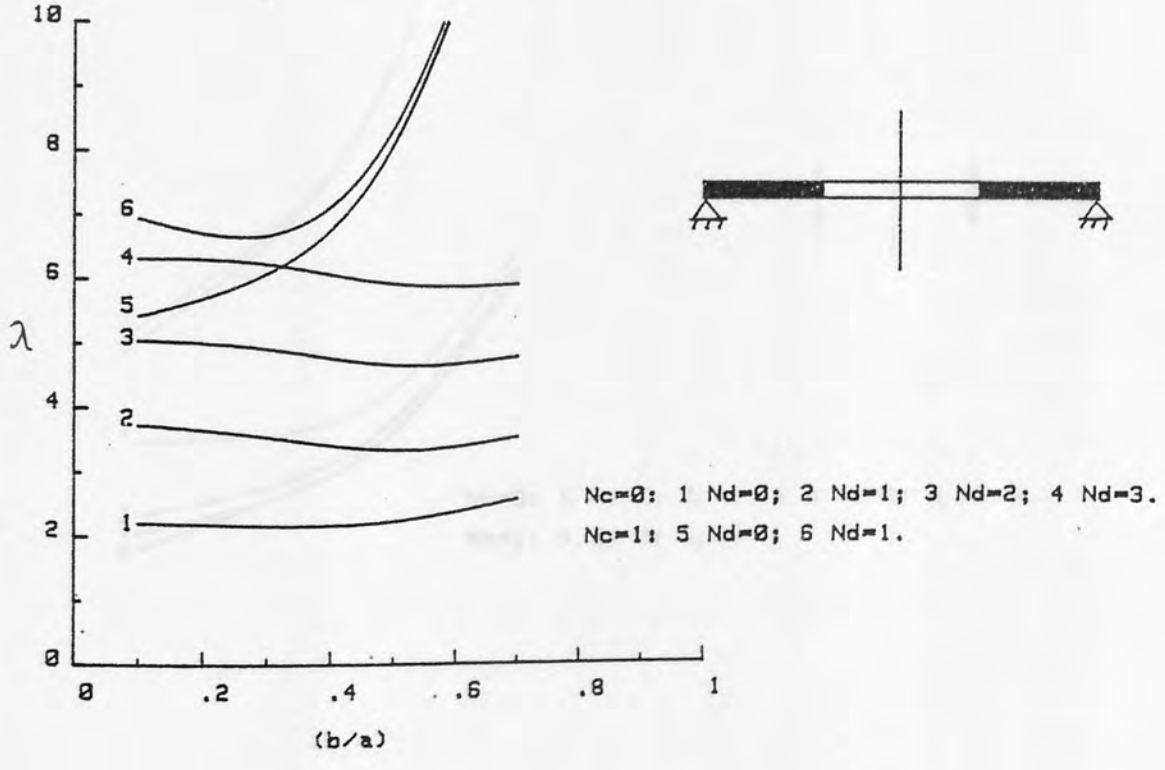

Table 7.9 Frequency parameters λ^2 for a free-clamped annular plate

mode shape Nd	Nc	λ^2 for values of b/a of 0.1 exact [83]	0.1 P.F.E Ne=15	0.3 exact [83]	0.3 P.F.E Ne=14	0.5 exact [83]	0.5 P.F.E Ne=10	0.7 exact [83]	0.7 P.F.E Ne=10
0	0	4.23	4.25	6.66	6.7	13	13.1	37	36.8
0	1	25.3	25.4	42.6	43	85.1	86.6	239	234.7
0	2	-	75	-	126	-	256	-	609
1	0	3.14	3.3	6.33	6.52	13.3	13.3	37.5	3
1	1	27.3	27.7	44.6	44.9	86.7	88	241	237
1	2	-	79.4	-	128	-	258	-	613
2	0	5.62	5.44	7.96	7.77	14.7	14.6	39.3	38.8
2	1	37	36.7	51	50.85	91.7	92	246	240
2	2	-	91	-	135	-	263	-	621
3	0	12.4	12.2	13.27	12.9	18.5	18.5	42.6	41.7
3	1	53.2	52.6	62.1	61.4	100	101	253	246
3	2	-	113	-	147	-	270	-	635

P.F.E = present finite element
Nd = number of nodal diameters
Nc = number of nodal circles

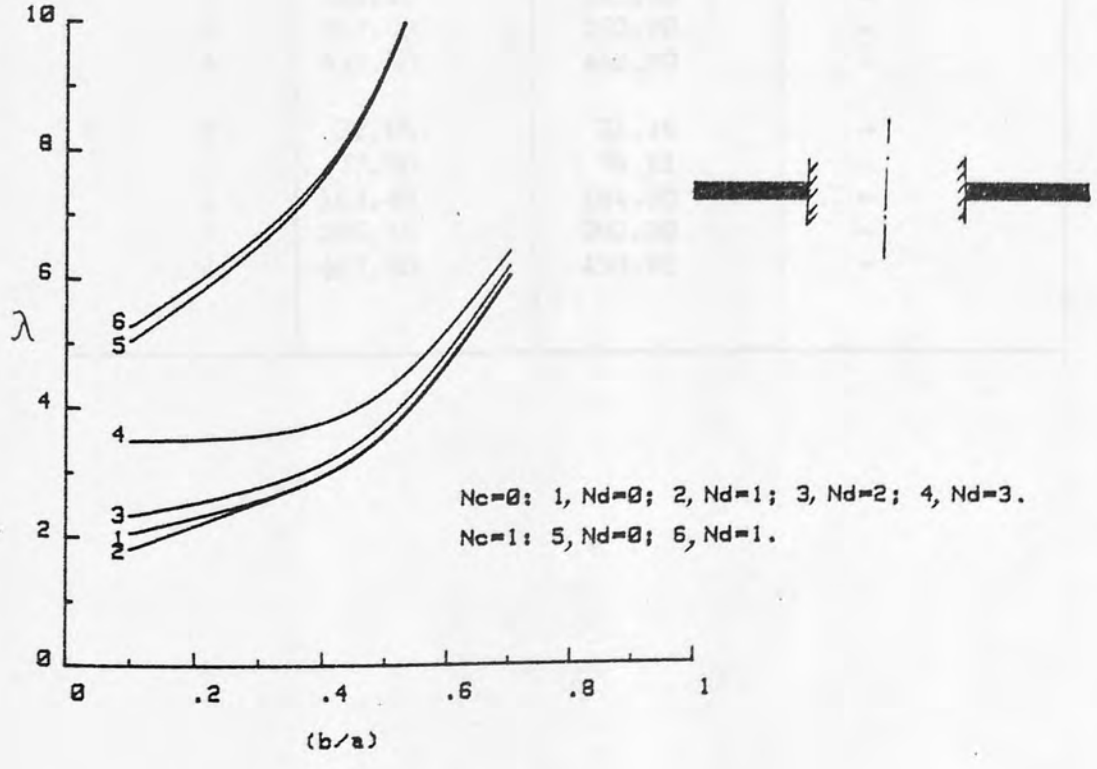

TABLE 7.10 Frequency parameters of centrally clamped thin disc (b/a = 0.3)

$$\lambda^2 = \omega \sqrt{12\rho(1-\nu^2)a^4/Eh^2}$$

Nd	Nc	[84] Ne = 8	Present Ne = 14	Exact [83]
0	0	6.66	6.66	6.66
	1	42.60	42.90	42.60
	2	123.2	126.00	-
	3	243.8	257.00	-
	4	405.9	444.00	-
1	0	6.54	6.52	6.33
	1	44.60	44.85	44.60
	2	125.50	128.60	-
	3	245.90	250.00	-
	4	406.10	416.20	-
2	0	7.95	7.77	7.96
	1	50.90	50.85	50.90
	2	132.70	135.00	-
	3	254.10	259.00	-
	4	416.00	447.00	-
3	0	13.26	12.90	13.27
	1	61.90	61.40	62.10
	2	145.20	145.00	-
	3	267.00	270.00	-
	4	430.00	460.00	-
4	0	22.05	21.46	-
	1	77.90	76.81	-
	2	163.40	164.00	-
	3	286.10	290.00	-
	4	447.60	450.80	-

TABLE 7.11 Frequency parameters $\bar{\delta}_o$ of a clamped-clamped thick annular plate of a/h = 7.

Mode Shape		$\bar{\delta}_o$ for values of b/a of -							
		0.1				0.3			
		Exact [86]		Present Work		Exact [86]		Present Work	
Nd	Nc	classical	$S_d + R_i$	Ne = 6	Ne = 9	classical	$S_d + R_i$	Ne = 5	Ne = 7
0	0	0.2155	-	0.2048	0.2000	0.2773	-	0.2582	0.2516
0	1	0.3579	-	0.3370	0.3177	0.4611	-	0.4219	0.3948
0	2	0.5020	-	0.4827	0.4318	0.6471	-	0.6165	0.5386
1	0	0.2198	0.1779	0.2116	0.2069	0.2785	0.2351	0.2615	0.2551
1	1	0.3656	0.3406	0.3447	0.3258	0.4647	0.4447	0.4244	0.3976
1	2	0.5081	0.4630	0.4881	0.4384	0.6522	0.6370	0.6177	0.5403
2	0	0.2498	0.2398	0.2366	0.2328	0.2945	0.2895	0.2725	0.2667
2	1	0.3923	0.3673	0.3667	0.3619	0.4774	0.4474	0.4320	0.4062
2	2	0.5315	0.4765	0.5404	0.4570	0.6615	0.6515	0.6214	0.5455

$S_d + R_i$ = Shear deformation and rotary inertia are included in the analysis.

TABLE 7.12 Frequency parameters $\bar{\delta}_o$ of a simply supported-clamped thick annular plate of a/h = 7.

Mode Shape		$\bar{\delta}_o$ for values of b/a of -							
		0.1				0.3			
		Exact [86]		Present Work		Exact [86]		Present work	
Nd	Nc	Classical	$S_d + R_i$	Ne = 6	Ne = 9	classical	$S_d + R_i$	Ne = 5	Ne = 7
0	0	0.1741	0.1513	0.1691	0.1656	0.2255	0.2104	0.2175	0.2125
0	1	0.3197	0.3696	0.3110	0.2940	0.4124	0.3822	0.3960	0.3713
0	2	-	-	0.4641	0.4153	-	-	0.6033	0.5249
1	0	0.1798	0.1689	0.1775	0.1740	0.2311	0.2290	0.2223	0.2175
1	1	0.3268	0.3097	0.3193	0.3029	0.4165	0.4062	0.3879	0.3746
1	2	-	-	0.4703	0.4225	-	-	0.5035	0.3870
2	0	0.2103	0.1982	0.2072	0.2046	0.2481	0.2310	0.2375	0.2333
2	1	0.3564	0.3515	0.3439	0.3283	0.4306	0.4220	0.4100	0.3845
2	2	-	-	0.4885	0.4429	-	-	0.5056	0.4375

7.3.2 Free Vibration of Circular Cylindrical Shells

The vibration of circular cylindrical shells is of practical importance in many branches of engineering, including nuclear engineering and the aerospace industry, where the structural response to dynamic loads must be predicted with extreme accuracy. A comprehensive survey of shell theories, their application to cylindrical shells and their accuracy in determining natural frequencies has been summarised by Leissa [27].

Methods of solution for cylindrical shell vibration have ranged from the approximate energy methods used by Arnold and Warburton [88], Sharma and Johns [89-90] and Johns and Allwood [91] to the exact solution studied by Forsberg [92,93] and Warburton [94]. In the study of circular cylindrical shells several physical parameters can be varied, including:

(1) Number of circumferential waves
(2) Thickness-to-radius ratio (R/h)
(3) Length-to-radius ratio (L/R)
(4) Poisson's ratio.

In contrast to plates the lowest frequencies for finite cylindrical shells decrease to a minimum before they increase as the number of circumferential waves is increased. This seemingly anomalous behaviour was first

observed by Arnold and Warburton [88], who concluded that it is caused by the division of the strain energy between bending deformation and stretching of the middle surface.

The number of axial half waves cannot be specified in advance, but one can select a circumferential nodal pattern, the length and radius of the shell, the boundary conditions and then solve to determine the frequencies and mode shapes.

7.3.2.1 Simply Supported Cylindrical Shells

Simply supported boundaries should satisfy the following conditions: radial displacement, tangential displacement and circumferential rotation are zero at the supports, i.e. $v = w = \alpha = 0$, $u \neq 0$, $\beta \neq 0$. This type of boundary condition at both ends create problems for the present element as when, for example, the axial displacement u is unconstrained at both ends the shell will have rigid body motion and the program fails to give results. To overcome this problem, a method was devised to add a fictitious flexible element, fully clamped at one end. This in turn creates the problem of determining the appropriate rigidity E_f and length L_f of the fictitious element. To determine E_f and L_f, a wide range of computation tests were carried out: the results of some of these test are presented here.

Determining the Rigidity of the Fictitious Element

Test No. 1

E_f	2×10^{11}	2×10^{9}	2×10^{6}	2×10^{3}
L_f	0.1	0.1	0.1	0.1
m				
1	47.29	45.47	43.77	43.77
2	99.74	99.53	99.50	99.50
3	116.66	108.92	99.60	99.58
4	133.97	133.45	133.40	133.40
5	151.78	150.66	150.04	150.62

The actual shell material properties and dimensions were: $E = 2 \times 10^{11}$ N/m^2, $\nu = 0.3$, $\rho = 7850$ Kg/m^3, L = 20m, R = 5m, h = 0.25m. The number of elements was ten, the frequencies are in Hz, n=1.

Test No. 2

E_f	2×10^{6}	2×10^{3}
L_f	0.075	0.075
m		
1	68.398	68.395
2	191.108	191.107
3	306.778	306.778
4	396.030	396.030
5	466.560	466.560

The material properties and dimensions of the actual shell were: $E = 2 \times 10^{11}$ N/m^2, $\nu = 0.3$, $\rho = 7850$ Kg/m^3, L = 6m, R = 1.5m, h = 0.075m. The number of elements, the actual shell was divided into, was fifteen, frequencies in Hz, n=2.

Determining the length of the fictitious element

Test No. 1

E_f	2×10^6	2×10^6	2×10^6	2×10^6	2×10^6	2×10^6
L_f m	0.01	0.05	0.1	0.2	0.4	0.6
1	43.81	43.78	43.77	43.77	43.76	43.76
2	99.51	99.50	99.50	99.49	99.39	99.26
3	99.81	99.65	99.60	99.53	99.51	99.51
4	133.40	133.40	133.40	133.40	133.40	133.40
5	150.36	150.14	150.04	149.88	149.56	149.24

actual shell: $E = 2 \times 10^{11}$ N/m^2, $\nu = 0.3$, $\rho = 7850$ Kg/m^3, $L = 20m$, $R = 5m$, $h = 0.25m$, $Ne = 10$, $n=1$.

Test No. 2

E_f	2×10^6	2×10^6	2×10^6	2×10^6	2×10^6	2×10^6
L_f m	0.003	0.015	0.03	0.06	0.12	0.18
1	146.03	145.93	145.91	145.90	145.88	145.86
2	331.69	331.68	331.68	331.66	331.30	330.87
3	332.71	332.16	331.99	331.77	331.70	331.69
4	444.68	444.67	444.67	444.67	444.67	444.67
5	501.20	500.47	500.14	499.59	498.52	497.48

Test No. 3

E_f	2×10^6	2×10^6
L_f	0.075	0.15
m		
1	68.398	68.393
2	191.108	191.098
3	306.778	306.772
4	396.030	396.026
5	466.560	466.553

Actual shell: $E = 2 \times 10^{11}$ N/m^2, $\nu = 0.3$, $\rho = 7850$ Kg/m^3, L = 6m, R = 1.5m, h = 0.075, Ne= 15. For test No.2, n = 1, and n =2 for test No. 3.

Test No. 4

E_f	1×10^6	1×10^6	1×10^6
L_f	h/2	h	2h
m			
1	4.266	4.269	4.262
2	11.452	11.450	11.447
3	24.398	24.396	24.394
4	41.962	41.960	41.959
5	63.400	63.399	63.398

actual shell: $E = 2 \times 10^{11}$ N/m^2, $\nu = 0.3$, $\rho = 7850$ Kg/m^3, L = 30m, R = 3m, h = 0.015625m, Ne = 15 and n = 3.

It was found, from the computation tests, that the length of the fictitious element could be taken as the thickness or half the thickness of the actual shell whilst its rigidity should be 10^{-5} times the rigidity of the actual shell. The other properties of the fictitious element could be taken as those of the actual shell.

To complete the test, three circular cylindrical shells simply supported at both ends were examined. The shells had the same length/radius and radius/thickness ratios but were chosed to have different lengths and thicknesses. The natural frequencies were compared with the exact solution obtained by Warburton [94] and the finite element solution obtained by Webster [58]. It should be mentioned here that the element used by Webster was a curved ring element where the displacements of the middle surface were represented by truncated power series in the meridional coordinate. The simplest displacement functions for the tangential and meridional displacements contained two terms and there were four terms in the simplest normal displacement function; this is the minimum number of terms required to specify continuity of tangential, meridional and normal displacement and meridional rotation at the junctions between Webster shell elements. For each value of n (the circumferential wave number) the lowest six natural frequencies were tabulated in order of increasing magnitude.

The results show that the natural frequencies of the lower four frequency modes were predicted more accurately by the present element representation than by Webster whilst for the high two frequency modes, the Webster element representation gave more accurate approximations to the natural frequencies.

However, the disagreement between the two elements does not exceed 1% in any frequency.

Finally, as can be seen from Table 7.13 through to Table 7.15, the present element representation, not only gives very accurate results but converges monotonically to the exact solution.

The fundamental natural frequencies, for various shell configuration, i.e. different L/R and R/h ratios, are predicted next. The computations were carried out for three different circumferential wave numbers for every specified L/R, R/h ratio and the minimum frequencies were checked against those by Forsberg [92, Fig. 3] and by Johns and Allwood [91]. The present element representation gave excellent agreement with the exact solution in reference [92] whilst the minimum natural frequencies obtained here are always lower than those reported in reference [91]. There are two reasons for that:

(1) Johns and Allwood did neglect some terms of the frequency determinant equation, and

(2) the present element formulations include shear deformation and rotary inertia which decrease the frequencies as it is well known.

The non-dimensional frequency parameters are given in Table 7.16 where

$$\Delta = \rho R^2(1-\nu^2)\omega^2/E$$

So that to determine the natural frequencies the following formula could be used:

$$\omega \text{ (Hz)} = \frac{\Delta^{\frac{1}{2}}}{2\pi} [E/(\rho R^2(1-\nu^2))]^{\frac{1}{2}}$$

The number of elements used for this specific problem is 15.

7.3.2.2 Clamped-free Cyclindrical Shells

A clamped boundary should satisfy the following conditions: axial displacement, tangential displacement, radial displacement, meridian and circumferential rotation are zero at the support, i.e. $u = v = w = \beta = \alpha = 0$. For a free end, none of the displacements or rotations should be restrained.

As an example of a thin clamped-free cylindrical shell we consider the thermal liner of an American Fast Test Reactor (F.T.R.) which is situated concentrically inside the main reactor vessel. The experimental model of the thermal liner was approximately 1/14 scale of the prototype, giving the following dimensions and material properties: length, L = 51.12 cm; radius, R = 21.62 cm, thickness, h = 0.15cm; density, ρ = 7492 Kg/m^3; Young's Modulus, E = 1.83 x 10^{11} N/m^2; Poisson's ratio, ν = 0.3. Chung [95] obtained the analytical solution, to this problem, through a direct solution procedure in which Sander's shell equations were used; the modal displacement functions were expanded in Fourier Series in the circumferential direction and with the axial modal displacements represented as simple Fourier Series expressions. Chung [95] also solved the problem using two computer codes [96-97]. The finite element grid used in both codes was the same and consists of ten divisions vertically and nine divisions over a quarter of the shell circumferentially. The element used in reference [96] was a quadrilateral one. The present finite element solution was obtained by dividing the shell into two grids, one consisting of 12 elements and the other of 15 elements. In Table 7.17 the solutions of the present element are compared with the exact, SAPIV and NASTRAN results for the thermal liner with clamped-free boundary conditions. The present solution almost always gives closer values to the exact solution even with only a 12-element grid whilst

with 15 elements, the present solution is superior to both the other two computer codes and has excellent agreement with the exact solution. Figure 7.9 shows, in a graphical form, a comparison between the present solution and those obtained in reference [95].

It was mentioned in reference [95] that a probable casues for disagreement between the experimental resutls (no experimental results were given) and the analytical predictions of natural frequencies is the insufficient clamping ($\beta \neq 0$) and imperfect axial constraints ($u \neq 0$) at the bottom of the thermal liner. Therefore, the sensitivity of the natural frequencies to changes in the bottom-boundary conditions was investigated using the present element. The boundary conditions considered were as follows:

(1) C-F: clamped-free;

(2) SSAC-F: simply supported with axial constraint-free;

(3) CNAC-F: clamped with no axial constraint-free;

(4) SSNAC-F: simply supported with no axial constraint-free; i.e. at the bottom boundary

(1) $u = v = w = \beta = \alpha = 0$

(2) $u = v = w = \alpha = 0, \quad \beta \neq 0$

(3) $v = w = \beta = \alpha = 0, \quad u \neq 0$

(4) $v = w = \alpha = 0, \quad \beta \neq 0, \; u \neq 0$

The results are given in Table 7.18 and as it can be seen the frequencies become smaller as the boundary conditions change from case (1) to case (4) for a given pair of circumferential and axial mode number, n and m. The effect of clamping ($\beta = 0$) can be seen by comparing the frequencies for the following two pairs of boundary conditions: C-F and SSAC-F, CNAC-F and SSNAC-F. The influence of axial constraint (u=0), in contrast to the effect of clamping, is significant throughout most of the region of interest as it can be seen by comparing results between cases (1) and (2) in one hand and (3) and (4) in the other hand. The results are shown graphically in Fig. 7.10.

The problem of clamped-free shells has received considerable attention by Sharma and Johns [89-90]. The vibration characteristics of cylindrical shells (with a wide range of geometries) clamped at one end and either free or stiffened by an elastic ring at the other end was dealt with. Flügge's thin shell theory was used but comparison with some other theories was made. The Rayleigh-Ritz technique was employed to obtain an approximate solution. Sharma and Johns proved that, for shells of large length/radius ratio, the assumption of zero hoop and shear strain does give considerable simplification without any significant loss of accuracy. To compare the present results with those in reference

[90], a clamped-free cylindrical shell with the following parameters was studied: $L/R = 9$, $R/h = 250$, $\nu = 0.3$ and the results are shown in Table 7.19. A sixteen element grid was used.

The present finite element solution always gives lower frequencies than those in reference [90]. Again, the main reasons for this is probably due to the simplification of the frequency determined equation in reference [90] and the introduction of shear deformation and rotary inertia in the present finite element representation. Some exact results were published in reference [90], by special communication from Forsberg, and are shown in Table 7.19 as well. Very good agreement with the present finite element solution can be seen.

7.3.2.3 Clamped-Clamped Cylindrical Shells

The boundary conditions for a circular cylindrical shell which is clamped at both ends are : $u = v = w = \beta = \alpha = 0$ at both ends.

For this problem many authors have used the exact method for obtaining the natural frequencies and mode shapes [92-93, 98-100]. However, partly because of the complexity of the exact procedure, some have used the finite difference, the finite element, or the Rayleigh-Ritz method or an equivalent [94, 101, 102].

For the present finite element solution, two clamped-clamped circular cylindrical shells of different configurations were solved; the first was very thin and had the dimensions: L = 12 in, R = 3 in, h = 0.01 in; the second was relatively thick and had the following dimensions: L = 15.65 in, R = 1.924 in, h = 0.101 in. The material properties for both shells were: $E = 29.6 \times 10^6$ psi, $\nu = 0.29$, $\rho = 0.733 \times 10^{-3}$ lb-sec^2/in^4.

First, we divided both shells into 12 elements with four types of element layouts as shown in Fig. 7.11. It is found that case (1), which has 12 equally spaced elements, gives better and more accurate results than the other three cases. Hence, the next step was to divide the shells into 16 equally spaced elements. Frequencies, for the first four radial modes having one to seven (two to six for the second example) circumferential waves are presented in Table 7.20.

For the first shell (R/h = 300) very accurate results have been achieved just with 16 elements. No error of the first frequency mode exceeds one-half of 1%; indeed, for $n \geq 5$ the first mode frequencies, obtained by the present element, are slightly lower than those obtained by exact methods [99,100]. For the higher mode frequencies ($m>1$) no error exceeds 4%.

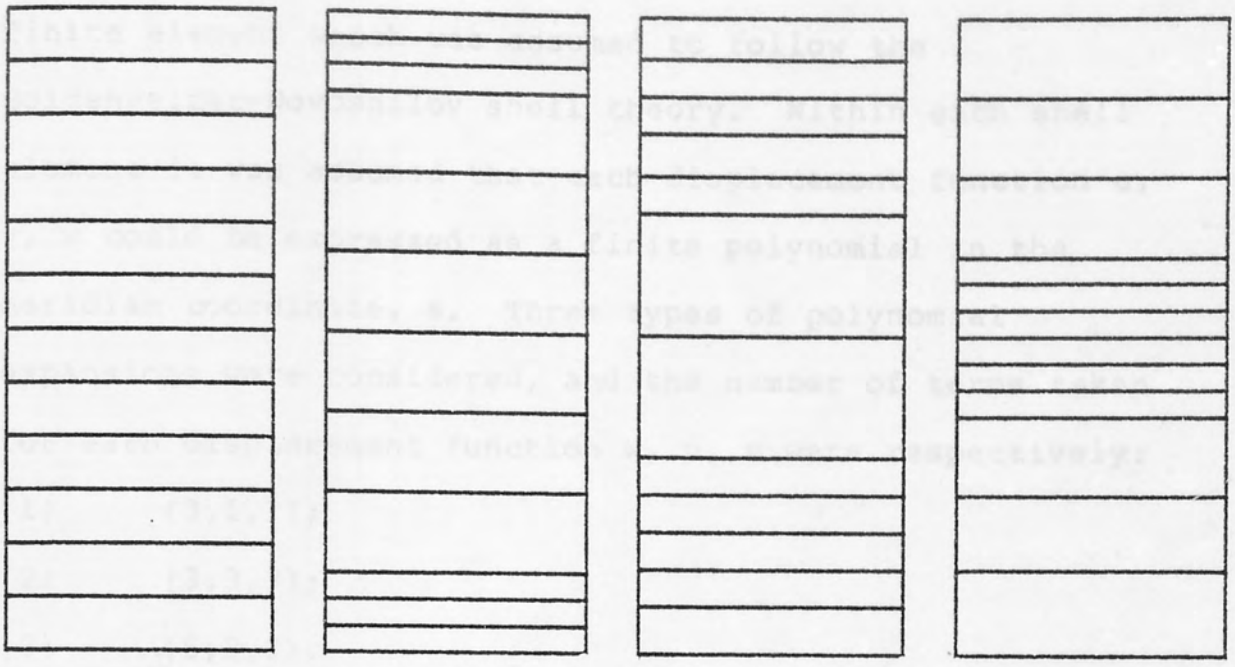

Fig. 7.11 different types of element layouts for a C–C cylindrical shell

The first shell was solved by Adelman and co-workers [102]. The element used in reference [102] was a ring finite element which was assumed to follow the Goldenveizer-Novoshilov shell theory. Within each shell element it was assumed that each displacement function u, v, w could be expressed as a finite polynomial in the meridian coordinate, s. Three types of polynomial expansions were considered, and the number of terms taken for each displacement function w, u, v were respectively:

(1) (3,1,1);

(2) (3,3,3);

(3) (5,3,3).

Ten equally spaced elements were considered in the solution and the results for (n=3, m=1) and for the three types of polynomial expansion 1, 2 and 3 were 1249, 1171, and 1156 Hz respectively, while the exact solution was 1154 Hz and the present finite element solutions is 1162 Hz. We mention this example to show the effectiveness of the present element in spite of its simplicity.

For the second shell (moderately thick) the effect of introducing the transverse shear and rotary inertia, in the present element, is evident. All the frequencies obtained by the present finite element are lower than those obtained by exact solution, were neither transverse shear nor rotary inertia was included in the analysis. The difference between the present results and the exact results range from 10 % (n=2) to 4% (n=6).

Results from the last two examples, and indeed from all the results presented so far, serve to provide full confidence in the present element.

TABLE 7.13 Comparison of natural frequencies (Hz) of simply supported cylindrical shells at both ends. $E = 2 \times 10^{11} N/m^2$, $\rho = 7850 Kg/m^3$, $\nu = 0.3$, $L = 6m$, $R = 1.5m$, $h = 0.075$.

Mode Shape		Exact Solution	Finite Element Solution		
n	m	Warburton [94]	Webster [58] 10 elements	Present 10 elements	Present 15 elements
0	V_1	260.80	262.00	-	-
0	1	398.84	400.45	400.2	398.68
0	2	521.21	523.32	522.57	521.82
0	V_2	521.811	530.50	-	-
0	3	532.13	534.76	533.32	532.59
0	4	538.45	542.40	543.19	540.00
1	1	144.30	145.50	145.89	145.12
1	2	322.12	327.20	331.66	325.63
1	V_1	332.18	332.20	332.07	333.11
1	3	428.70	436.40	444.67	435.19
1	4	481.40	490.20	500.4	489.56
1	V_2	498.70	500.00	501.87	498.58
2	1	68.20	69.20	68.88	68.40
2	2	187.80	193.40	195.77	191.11
2	3	297.70	309.20	319.57	306.78
2	4	380.00	396.20	419.00	396.03
2	5	441.20	460.40	507.80	466.56
2	6	492.20	513.45	633.60	535.33
3	1	73.70	73.70	73.14	72.97
3	2	134.60	139.30	139.87	136.36
3	3	220.50	232.80	241.70	228.39
3	4	303.90	324.30	252.19	321.88
3	5	378.30	405.00	470.70	410.98
3	6	445.86	476.90	633.42	502.45

TABLE 7.14 Comparison of natural frequencies (Hz) of simply supported cylindrical shells at both ends. $E = 2 \times 10^{11}$ N/m^2, $\rho = 7850$ Kg/m^3, $\nu = 0.3$, $L = 20m$, $R = 5m$, $h = 0.25m$.

Mode Shape		Exact Solution	Finite Element Solution		
n	m	Warburton [94]	Webster [58] 10 elements	Present 10 elements	Present 15 elements
0	v_1	78.20	78.60	-	-
	1	119.65	120.14	120.09	119.84
	2	156.36	157.00	156.76	156.44
	v_2	156.56	159.15	-	-
	3	159.64	160.43	159.95	159.63
	4	161.54	162.72	162.97	161.86
1	1	43.29	43.65	43.77	43.45
	2	96.636	98.15	99.50	97.53
	v_1	99.65	99.66	99.64	99.22
	3	128.612	130.91	133.40	130.52
	4	144.42	147.10	150.17	146.56
	v_2	149.62	150.00	157.13	149.36
2	1	20.5	20.77	20.66	20.52
	2	56.34	58.03	58.73	57.62
	3	89.3	92.75	95.87	91.66
	4	113.98	118.85	125.70	118.31
	5	132.37	138.13	152.34	138.94
	6	147.66	154.03	190.08	158.59
3	1	21.98	22.12	22.15	22.96
	2	40.39	41.78	42.00	41.42
	3	66.16	69.83	72.12	68.72
	4	91.18	97.28	103.18	96.09
	5	113.50	121.54	133.18	122.20
	6	133.76	143.06	167.98	148.25

TABLE 7.15 Comparison of natural frequencies (Hz) of simply supported cylindrical shells at both ends. $E = 2 \times 10^{11}$ N/m^2, $\rho = 7850$ Kg/m^3, $\nu = 0.3$, L = 15m, R = 3.75m, h = 0.1875m.

Mode Shape		Exact Solution	Finite Element Solution		
n	m	Warburton [94]	Webster [58] 10 elements	Present 10 elements	Present 15 elements
0	v_1	104.36	104.80	-	-
	1	159.53	160.18	160.11	159.59
	2	208.49	209.33	208.97	208.74
	v_2	208.75	212.20	-	-
	3	212.85	213.91	213.26	213.00
	4	215.39	216.96	217.24	216.11
1	1	57.72	58.20	58.22	57.99
	2	128.85	130.87	131.00	130.48
	v_1	132.86	132.88	133.31	132.64
	3	171.48	174.54	176.87	174.25
	4	192.55	196.08	200.01	195.99
	v_2	199.49	200.00	206.98	199.28
2	1	27.27	27.70	27.65	27.35
	2	75.12	77.37	77.49	76.44
	3	119.06	123.68	126.07	122.71
	4	151.98	158.48	165.00	158.41
	5	176.50	184.17	197.06	186.62
	6	196.88	205.38	229.98	214.13
3	1	29.31	29.49	29.27	29.19
	2	53.73	55.70	55.98	54.54
	3	88.21	93.11	96.17	91.35
	4	121.58	129.71	135.18	128.75
	5	151.33	162.05	175.00	164.39
	6	178.34	190.75	213.00	200.98

TABLE 7.16 Frequency parameters $\Delta^2(\times 10^2)$ for simply supported cylindrical shells at both ends with different L/R and R/h ratio.

R/h	L/R								
	1			5			10		
	n	m		n	m		n	m	
100	6	1	23.98	2	1	7.69	1	1	5.95
		2	54.57		2	24.49		2	19.05
		3	78.34		3	42.52		3	34.128
		4	100.12		4	57.83		4	48.97
		5	128.30		5	69.39		5	59.15
100	7	1	22.91	3	1	4.45	2	1	2.209
		2	49.78		2	14.00		2	7.84
		3	74.84		3	26.98		3	16.215
		4	98.93		4	40.53		4	26.23
		5	129.04		5	53.06		5	37.049
100	8	1	24.38	4	1	4.85	3	1	2.42
		2	47.17		2	9.68		2	4.52
		3	72.57		3	18.45		3	8.92
		4	98.42		4	29.17		4	15.11
		5	130.28		5	40.54		5	22.72
192	7	1	18.03	3	1	4.00	2	1	2.10
		2	44.84		2	13.83		2	7.807
		3	66.22		3	26.86		3	16.19
		4	82.04		4	40.41		4	26.19
		5	97.12		5	52.87		5	37.027
192	8	1	16.71	4	1	3.17	3	1	1.517
		2	39.91		2	8.84		2	4.077
		3	61.64		3	17.91		3	8.689
		4	78.80		4	28.70		4	14.947
		5	95.53		5	40.028		5	22.565
192	9	1	16.90	5	1	3.88	4	1	2.27
		2	36.40		2	6.835		2	3.205
		3	57.54		3	12.97		3	5.669
		4	76.03		4	21.227		4	9.568
		5	94.17		5	30.79		5	14.79

TABLE 7.17 Comparison of natural frequencies (Hz) for the thermal liner model with clamped-free boundary conditions.

Mode Shape		Exact Sol.	Finite Element Solutions			
n	m	CHUNG [95]	NASTRAN [97]	SAPIV [96]	Present 12 elements	Present 15 elements
1	1	855.10	856.3	-*	856.98	856.58
	2	2318.98	-	-	2339.00	2332.34
	3	3076.00	-	-	3090.94	3085.95
2	1	403.73	410.1	405.1	404.86	404.63
	2	1437.11	-	-	1456.21	1449.72
	3	2487.60	-	-	2543.69	2523.77
3	1	223.34	232.2	225	224.26	224.11
	2	928.28	943.2	-	943.84	938.55
	3	1834.82	-	-	1896.22	1874.28
4	1	171.77	180.5	174.3	173.34	173.28
	2	644.48	671.4	-	657.12	652.93
	3	1367.64	-	-	1424.25	1404.00
5	1	199.16	206.2	201.7	202.04	202.00
	2	494.69	529.3	505.8	505.28	502.09
	3	1057.12	-	-	1106.89	1089.27
6	1	268.86	275.5	272.0	273.19	273.20
	2	442.00	478.0	454.3	451.50	449.27
	3	864.82	-	-	907.90	893.07
7	1	361.92	370.1	366.2	367.90	367.88
	2	464.59	496.9	476.7	474.04	472.56
	3	767.65	-	-	804.74	792.68
8	1	472.54	483.5	478.4	480.34	480.33
	2	539.45	567.2	-	549.73	548.74
	3	750.67	-	-	782.78	773.39

* not calculated in these cases.

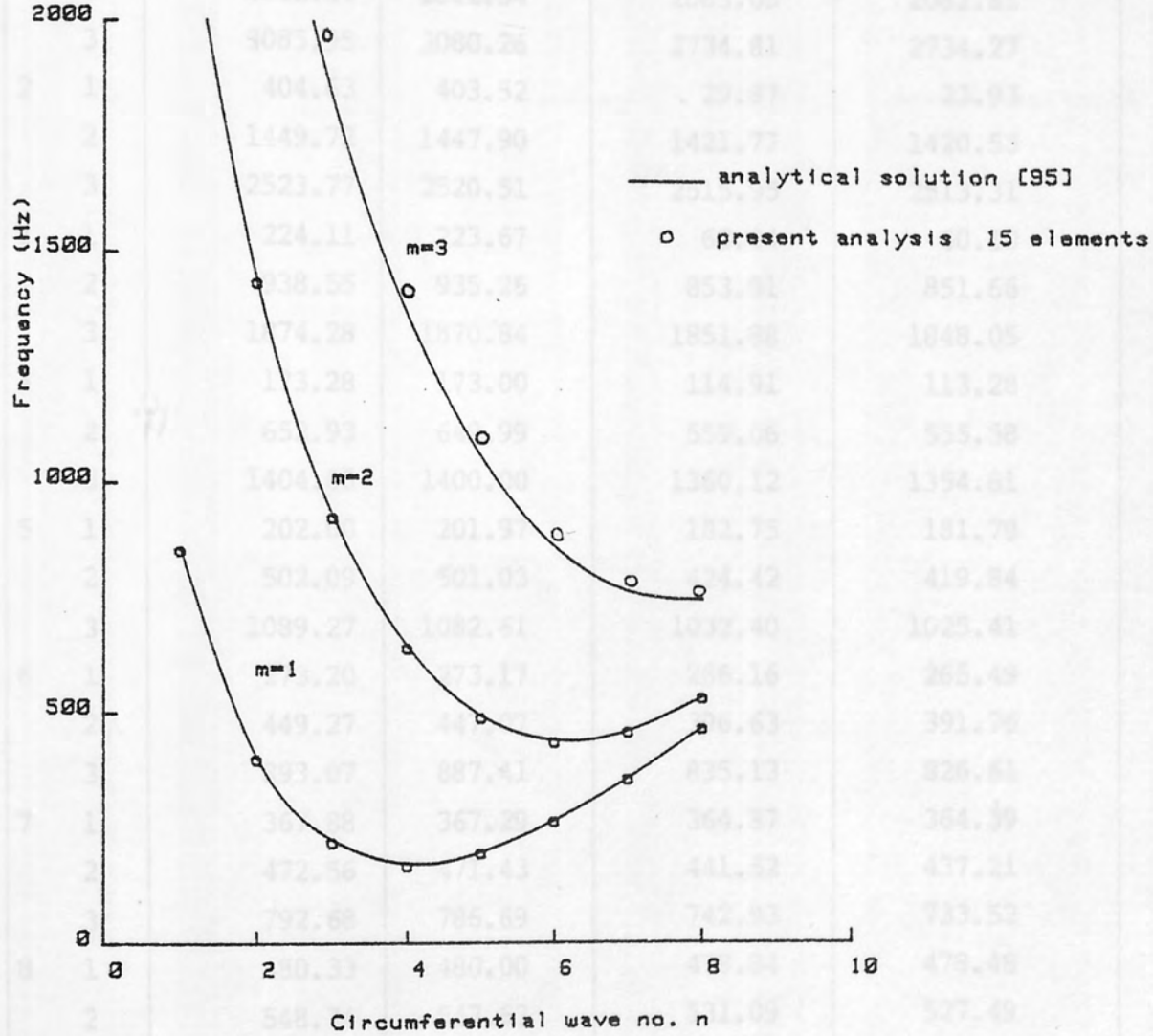

Fig. 7.9 natural frequencies of the thermal liner model (C-F)

(see table 7.17)

TABLE 7.18 Natural frequencies (Hz) of thermal liner model for various boundary conditions.

n	m	C-F	SSAC-F	CNAC-F	SSNAC-F
1	1	856.58	855.32	30.47	27.71
	2	2332.34	2332.34	2083.05	2082.81
	3	3085.95	3080.26	2734.81	2734.27
2	1	404.63	403.52	29.87	23.93
	2	1449.72	1447.90	1421.77	1420.53
	3	2523.77	2520.51	2515.95	2513.31
3	1	224.11	223.67	63.04	60.10
	2	938.55	935.26	853.91	851.66
	3	1874.28	1870.84	1851.88	1848.05
4	1	173.28	173.00	114.91	113.28
	2	652.93	649.99	559.06	555.58
	3	1404.00	1400.00	1360.12	1354.81
5	1	202.00	201.97	182.75	181.79
	2	502.09	501.03	424.42	419.84
	3	1089.27	1082.61	1032.40	1025.41
6	1	273.20	273.17	266.16	265.49
	2	449.27	447.07	396.63	391.76
	3	893.07	887.41	835.13	826.61
7	1	367.88	367.29	364.87	364.39
	2	472.56	471.43	441.52	437.21
	3	792.68	786.69	742.93	733.52
8	1	480.33	480.00	478.84	478.48
	2	548.74	547.63	531.09	527.49
	3	773.39	768.89	736.00	726.71

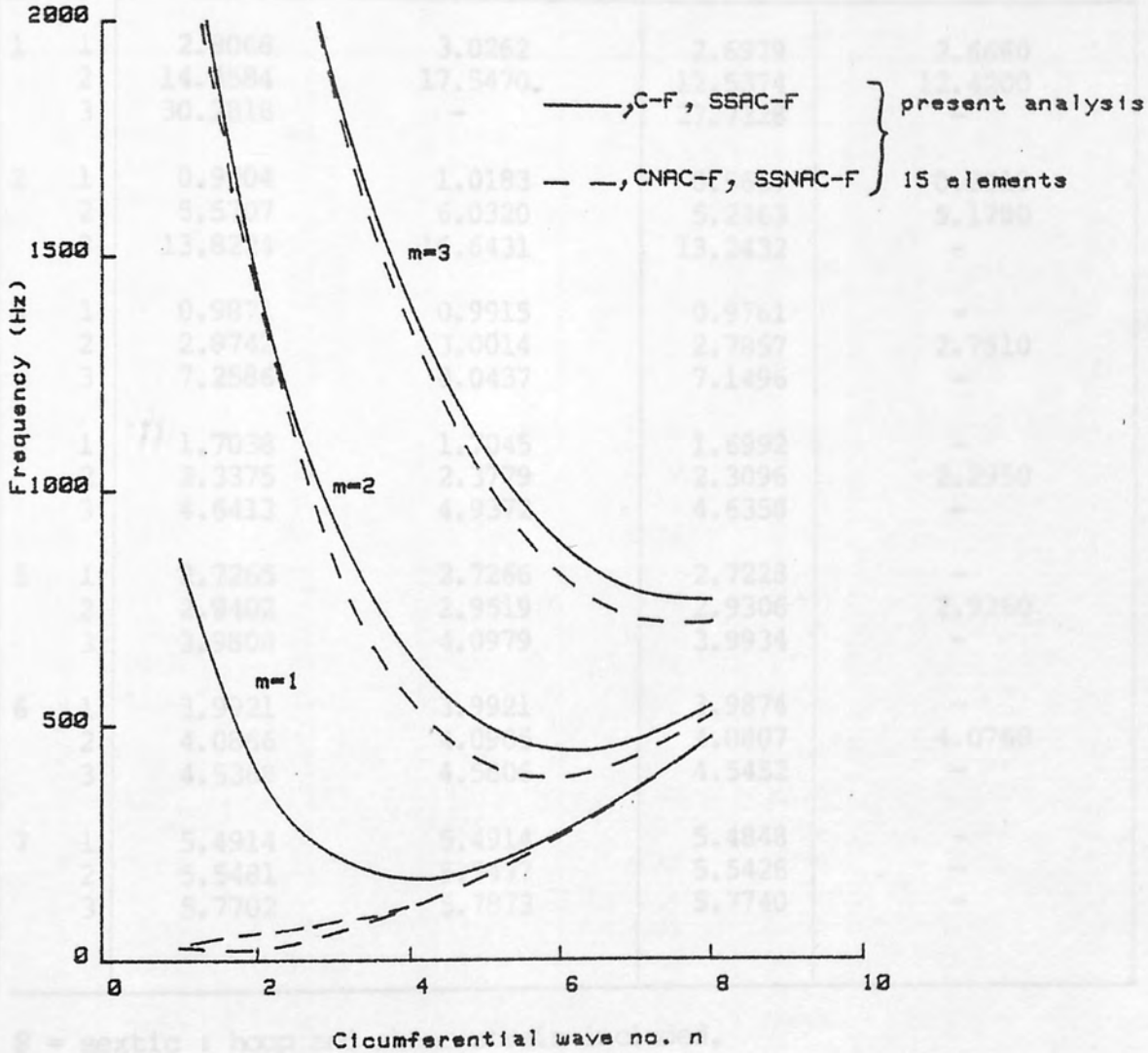

Fig. 7.10 natural frequencies of the thermal liner model for various boundary conditions (see table 7.18)

TABLE 7.19 Comparison of frequency parameter $\Delta^{\frac{1}{2}}(\times 10^2)$ for clamped-free cylindrical shells L/R = 9, R/h = 250, $\upsilon = 0.3$

Mode Shape		Energy Method [90]		Present analysis Ne = 16	Exact Forsberg from ref.[90]
n	m	S	Q		
1	1	2.8068	3.0262	2.6979	2.6660
	2	14.4584	17.5470	12.5374	12.4200
	3	30.2818	-	27.7328	-
2	1	0.9904	1.0183	0.9657	0.9510
	2	5.5707	6.0320	5.2463	5.1780
	3	13.8224	16.6431	13.2432	-
3	1	0.9871	0.9915	0.9761	-
	2	2.8742	3.0014	2.7857	2.7510
	3	7.2586	8.0437	7.1496	-
4	1	1.7038	1.7045	1.6992	-
	2	2.3375	2.3779	2.3096	2.2950
	3	4.6413	4.9372	4.6358	-
5	1	2.7265	2.7266	2.7228	-
	2	2.9402	2.9519	2.9306	2.9260
	3	3.9808	4.0979	3.9934	-
6	1	3.9921	3.9921	3.9874	-
	2	4.0866	4.0905	4.0807	4.0760
	3	4.5368	4.5806	4.5452	-
7	1	5.4914	5.4914	5.4848	-
	2	5.5481	5.5497	5.5426	-
	3	5.7702	5.7873	5.7740	-

S = sextic : hoop and shear strain included.

Q = Quadratic : zero hoop and shear strain.

TABLE 7.20 Comparison of natural frequencies (Hz) of a clamped-clamped circular cylindrical shell; $E=29.6\times10^{6}$ psi, $\rho = 0.733\times10^{-3}$ lb-sec^2/in^4, $\nu = 0.29$.

Mode Shape		L=12, R=3, h=0.01 in			L=15.65, R=1.924, h=0.101 in		
n	m	Exact [100]	Exact [99]	Present Ne = 16	Exact [100]	Exact [99]	Present Ne = 16
1	1	3423	3427	3438	-	-	-
	2	6412	6423	6484	-	-	-
	3	8493	-	8613	-	-	-
	4	9418	-	9532	-	-	-
2	1	1917	1918	1928	1432	1429	1286
	2	3902	3905	3966	2679	2682	2649
	3	5832	5844	5997	-	-	4428
	4	7299	7303	7551	-	-	6402
3	1	1154	1154	1162	2553	2336	2100
	2	2536	2538	2589	2770	2771	2564
	3	4051	4054	4198	3564	3570	3484
	4	5442	5447	5726	4634	4647	4780
4	1	765	765	769	4140	4142	3853
	2	1752	1753	1795	4332	4335	4053
	3	2918	2921	3047	4711	4717	4483
	4	4100	4104	4370	5298	5308	5212
5	1	581	581	580	6497	6500	6160
	2	1287	1287	1319	6640	6644	6303
	3	2190	2192	2299	6897	6903	6583
	4	3165	3168	3408	7287	7298	7055
6	1	539	538	534	9388	9400	8966
	2	1022	1022	1045	9518	9480	9093
	3	1719	1720	1808	9737	9630	9327
	4	2517	2516	2729	10059	9950	9704
7	1	599	597	590			
	2	908	907	920			
	3	1431	1431	1501			
	4	2076	2076	2258			

7.3.3 Free Vibration of Circular Conical Shells

The class of circular conical shells is a simple generalisation of circular cylindrical shells. Put in another way,the cylindrical shells are the special case arising when the vertex half-angle ϕ of the conical shell is zero. If the cone is bounded by two planes, then the surface is a frustum of a cone; otherwise, for a shell containing the vertex, i.e. having an apex, the term 'complete conical shell' is used. A cone frustrum has two ends: the small end is located at $s = s_1$; the large end is located at $s = s_2$. When $s_1 = 0$, the structure is known as a complete cone. Early interest in vibration of conical shells involved determination of the frequencies and mode shapes of vibration loudspeakers. Few research reports were available before the coming of the space era. At that time demand for knowledge about the strength and other dynamic characteristics of conical shells increased because conical shells were widely used in various parts of space vehicles. At the present time conical shells have obvious importance in ocean engineering, aeronautical engineering, civil engineering and other applications. A comprehensive review of conical shells by Leissa [27] is available.

The vast majority of numerical results for the free vibration of conical shells deal with frusta; that is, the conical surface is cut by two planes located at distances

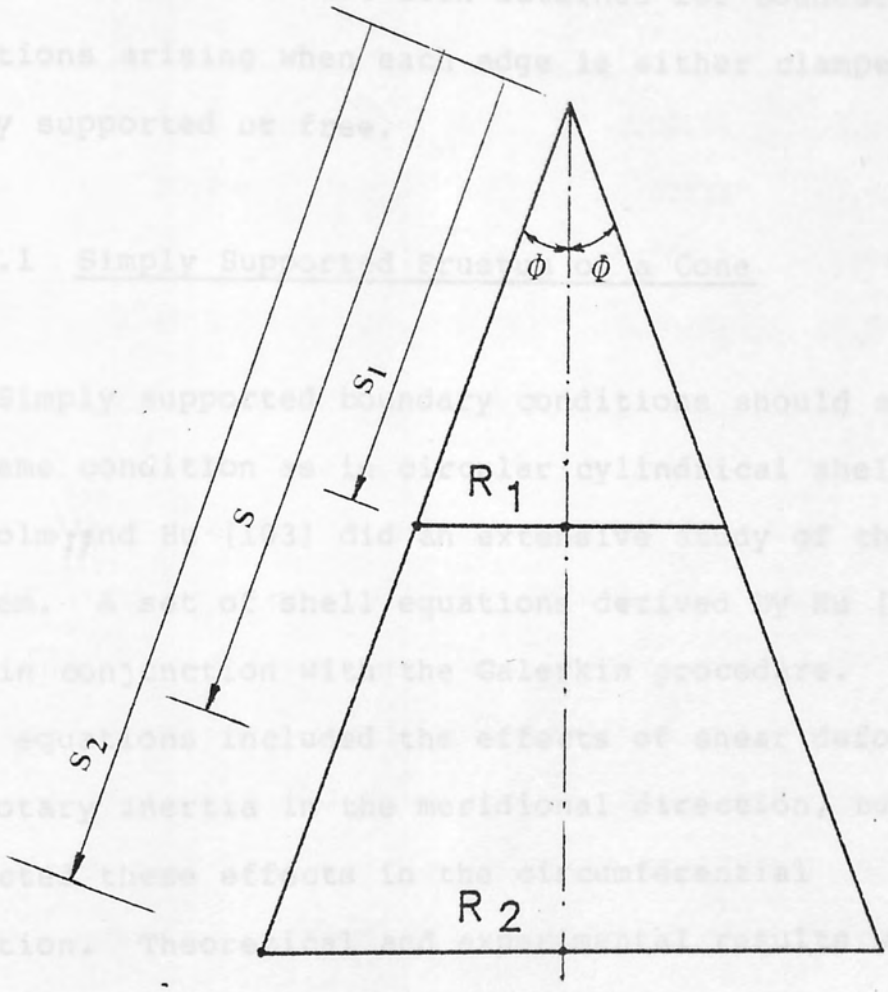

Fig. 7.12 Conical shell

s_1 and s_2 from the vertex with the associated radii of the bounding circles being R_1 and R_2 respectively, as shown in Fig. 7.12. As in the case of circular cylindrical shells, most of the results have been obtained for boundary conditions arising when each edge is either clamped, simply supported or free.

7.3.3.1 Simply Supported Frustum of a Cone

Simply supported boundary conditions should satisfy the same condition as in circular cylindrical shells. Lindholm and Hu [103] did an extensive study of the problem. A set of shell equations derived by Hu [104] was used in conjunction with the Galerkin procedure. The shell equations included the effects of shear deformation and rotary inertia in the meridional direction, but neglected these effects in the circumferential direction. Theoretical and experimental results were obtained in reference [103] for four models of steel and having the geometric parameters shown in Table 7.21.

TABLE 7.21 Geometric parameters for four conical shells

model number	ϕ, degrees	$\frac{s_2}{s_1}$	$\frac{h}{R_2}$	R_2, in
1	14.2	2.23	0.00166	6.07
2	30.2	2.27	0.00127	7.95
3	45.1	2.25	0.00112	8.96
4	60.5	2.25	0.00101	10.00

For the present solution, each of the four cones were divided into 14 elements. For models 1, 2 and 4 two sets of boundary conditions were considered; the first assumed that the cones were simply supported at both ends while the second assumed that the shells were simply supported with meridional constraints at their smaller ends and simply supported without any meridional constraint at their larger ends. We represent the first set of boundary conditions as SS-SS and second set as SSAC-SS. For the third model, five different boundary conditions were applied; these were: SS-SS, SSAC-SS, SSAC-SSAC, C-C and SSNTC-SS, simply supported with no tangential constraint-simply supported. It should be noted that, always the first of these boundary conditions represents the smaller ends while the second represents the larger ends. The purpose of these calculations was heuristic - it was desired to see how the frequency of these selected shells

changed when different boundary conditions were changed.

Lindholm and Hu [103] attempted to simply-support the conical shells at their ends, but by looking at the schematic diagram of the experimental apparatus [103, Fig. 2], and from the description of the boundary conditions which was stated : " the boundary condition is that used to simulate the simply supported edge condition. The right-angle groove in the circular plate supporting the lower end (smaller end) is machined to a close tolerance fit with the small radius R_1 of the shell. The upper circular plate (larger end) is positioned with a slight axial load to give a line support around the large radius R_2 of the shell. The only in-plane restraint is the slight friction between the shell and the support". We believe that it was likely that in practice the shells were inbetween the simply-supported and simply-supported with axial constraint condition at their smaller ends, but simply-supported at their larger ends.

The present finite element results, for models 1, 2 and 4, for two different boundary conditions, at their smaller ends, are shown in Table 7.22 while the results for model 3 with four different boundary conditions at both ends are shown in Table 7.23.

It can be seen from the results that the effect of clamping ($\beta = 0$) is not significant in contrast to the

effect of meridional constraint (u = 0). Meridional constraint effect decreases by the increase of the circumferential wave number. For model 4 the minimum frequency shifted from n = 10 when the boundary conditions are SS-SS, to n = 11 when the boundary conditions became SSAC-SS. Although the effect of the tangential restraint (v = 0) at the boundary is expected to be less significant, for low values of n it also has influence, since, for these modes, the spacing between the nodal points on the boundary is greater, thereby allowing greater circumferential displacements. To justify this argument, two different sets of boundary were considered; they were

(1) SSNTC-SS simply supported with no tangential constraint - simply supported;

(2) SS-SSNTC, simply supported - simply supported with no tangential constraint.

The first set represents tangential constraint on the smaller end and no tangential restraint at the larger end, while the second set represents an opposite case. Those results are shown in Table 7.24 and compared with the SS-SS case. From Table 7.24 we can see that when no tangential constraint is imposed at the larger end the frequencies are lower than those when no tangential constraint imposed at the smaller end.

Finally, Fig. 7.13 through Fig. 7.16 show, in graphical terms, the effect of meridional constraint for all the four models. Fig. 7.17 through Fig. 7.20 show a comparison between the present finite element solution and theoretical results obtained by Lindholm and Hu [103] for SS-SS boundary conditions. It can be seen from the graphs that very good agreement is found between the present work and the theoretical results.

Mode shapes were determined experimentally and theoretically in reference [103] for various modes and models. To investigate the performance of the present finite element in this respect many modes were drawn, after deflection normalisation, for different circumferential wave numbers. Very good agreement, with both experimental and theoretical, can be seen in Fig. 7.21 through to 7.24. The most striking feature of the axial mode shapes is their strong dependence on the circumferential wave numbers, n, for a given shell geometry. This is illustrated in Figs. 7.22 and 7.23 for m=1 and in Fig. 7.24 for m=2. In each case, the position of maximum displacement, or antinode, shifts towards the large diameter of the shell, $s = s_2$, with increasing circumferential wave number, n. For low values of n and in the neighbourhood of the minimum frequency, the displacement is relatively symmetric.

TABLE 7.22 Natural frequencies (Hz) for model 1, 2 and 4 under two different boundary conditions (14 conical elements)

		Model 1		Model 2		Model 4	
n	m	SS-SS	SSAC-SS	SS-SS	SSAC-SS	SS-SS	SSAC-SS
4	1	411.6	521.6				
	2	1427.5	1555.2				
	3	2617.9	2702.6				
	4	3688.5	3734.2				
	5	4507.5	4530				
	6	5078.2	5090				
5	1	299.9	373.6	675.6	783.8	751.3	782.5
	2	1007	1124.6	1941.7	2004.4	1427.9	1433.7
	3	1963	2063.4	2890.5	2913.5	1719.9	1724
	4	2960	3027.2	3434.6	3443.8	1978.7	1980.9
	5	3857	3896.2	3815.9	3822.4	2266.4	2268.6
	6	4579	4600.8	4212.5	4217.7	2610.9	2611.8
6	1	273.7	312.3	503	600	584	623.5
	2	764.5	861.2	1549	1626.8	1280.9	1292.3
	3	1515.7	1617.5	2506.7	2542	1627.6	1632.5
	4	2387.6	2469	3164.9	3180	1898.2	1900.9
	5	3266.7	3322	3606	3614.9	2195.7	2197.8
	6	4060.5	4094.8	4015	4021.9	2554.8	2555.7
7	1	299	311.9	406.6	485	470.7	512.9
	2	642.8	711.8	1257	1341.9	1135.9	1153.3
	3	1220.3	1313	2162	2208.9	1533	1539.4
	4	1958.5	2045.8	2880	2902.7	1821	1824.5
	5	2772.9	2840.5	3393	3405	2129.6	2132
	6	3576	3622.9	3827	3835.5	2503.8	2504.8
8	1	343.5	345.7	363.9	420	398.4	438
	2	612.5	650	1049.2	1131.5	1006.8	1029.4
	3	1042	1117.9	1874	1927	1437.6	1445.9
	4	1650.4	1735.6	2607.6	2634.8	1747.7	1752
	5	2379.6	2454.3	3179.9	3192	2068.8	2071.6
	6	3152.5	3210.7	3650.5	3656.7	2458.5	2459.8
9	1	394.5	394.6	359	393.9	356.8	390.6
	2	643.7	655	905	981.7	899.7	925.9
	3	963.6	1014.6	1636.6	1697.7	1345.6	1356.2
	4	1446.5	1522.4	2353	2391.2	1678.6	1684
	5	2081.3	2157.4	2961	2982.5	2013.4	2016.7
	6	2800	2865.6	3470	3484	2419	2420.5
10	1	450.4	450.3	380.9	397.4	341	366.4
	2	698.2	699.3	820	883.7	816.6	844.7
	3	968.4	990.8	1455	1517.8	1262	1274.8
	4	1338	1396.7	2135	2179.4	1614.6	1621.3
	5	1872.5	1943.6	2758.5	2785.2	1964	1968
	6	2521.7	1591	3301	3318.4	2385.5	2387.5

TABLE 7.22 Continued..

n	m	Model 1		Model 2		Model 4	
		SS-SS	SSAC-SS	SS-SS	SSAC-SS	SS-SS	SSAC-SS
11	1	512.4	511.7	415.7	421.8	343.7	360.6
	2	759.3	759.3	784.5	830.8	757.9	785.8
	3	1021.6	1025.5	1325	1384.4	1190.7	1205.4
	4	1319.7	1353	1954.7	2003	1557.3	1565.3
	5	1750.2	1809.5	2575.7	2607	1921.6	1926.3
	6	2318.3	2387	3142	3163	2358.6	2361
12	1	579.8	579.8	456.2	457.9	360.6	370
	2	827.7	827.8	788.8	816.6	723.2	748.5
	3	1089.4	1089.4	1243	1294.8	1134.4	1150
	4	1369.9	1379.6	1813.4	1863.4	1508.2	1517.7
	5	1714.9	1753.6	2417.2	2453	1886.5	1892.0
	6	2192.3	2254.2	2996.6	3021.5	2338.5	2341.4
13	1	653.5	653.3	500.2	500.4	385	389.4
	2	903.8	903.9	819.9	832.5	710.6	731.5
	3	1165.6	1165.7	1207.2	1247	1094.7	1110.8
	4	1448.6	1449.2	1712.8	1761.3	1469.6	1480.4
	5	1756.9	1771.7	2288.2	2326.7	1859.6	1865.9
	6	2148.6	2195.3	2869.4	2897.7	2325.5	2329
15	1			598.3	598.3	448.4	448.7
	2			915.3	916	738	747.9
	3			1245.9	1258	1068.4	1082
	4			1635.4	1669.8	1429.5	1441.8
	5			2127.6	2165.9	1834.2	1841.9
	6			2681.8	2716	2323.4	2328.2
18	1			773.5	773.6	564.4	564.4
	2			1095.2	1095	852.3	853.8
	3			1424.9	1424.9	1147.3	1152.2
	4			1769.5	1773.8	1475.4	1485.4
	5			2152.3	2169.8	1878	1886.7
	6			2613.7	2645	2385.8	2392.4

TABLE 7.23 Natural frequencies for a 45.1° conical shell under different boundary conditions (14 conical elements).

n	m	SS-SS	SSAC-SS	SSAC-SSAC	C-C
7	1	526.4	601	774.6	780
	2	1454	1497.7	1518.3	1527.6
	3	2141.4	2157.3	2180.8	2191
	4	2569.3	2576.8	2639.7	2650
	5	2936.9	2942.2	3029.2	3041
	6	3343.8	3347.5	3455.2	3472
8	1	441.4	507.3	665.9	671.4
	2	1247.7	1299.3	1333.2	1343.5
	3	1948.6	1970.5	1988.9	2001
	4	2428.5	2438.8	2490.4	2503
	5	2818.5	2825.4	2908.5	2923.7
	6	3238	3242.7	3350.9	3372.4
9	1	397.3	450.1	590.9	596
	2	1086.3	1141.9	1186.8	1197.5
	3	1770.9	1798.5	1817.2	1831.5
	4	2288.2	2301.7	2344.5	2360
	5	2705.8	2714	2791.6	2810
	6	3139.8	3145.6	3253.6	3279
10	1	384.8	422	545.2	548.5
	2	966.6	1022.5	1074.4	1083.4
	3	1615.5	1647.9	1669.8	1683
	4	2153.4	2170.5	2207.9	2222.9
	5	2598.2	2608.3	2680.3	2698
	6	3049.4	3056	3163.5	3188.9
12	1	420.6	432.3	525.6	528
	2	840.2	884.2	938.9	940.5
	3	1385.2	1422.7	1452.6	1460.5
	4	1920.2	1944.4	1978.8	1991
	5	2405.6	2419.9	2483.3	2496
	6	2893.4	2903.3	3007.5	3057
14	1	492.5	493.7	570.7	571
	2	838.4	860.4	908	910
	3	1270.8	1304.1	1338	1345
	4	1760.5	1789.2	1825.6	1840
	5	2257.8	2276.9	2336.3	2350.2
	6	2775.9	2789.6	2891	2932.7
15	1	533.3	533.5	605.9	605.9
	2	868.4	880.6	924.5	926.7
	3	1256.8	1284.2	1319.2	1328.8
	4	1714	1743	1781	1799.9
	5	2206.8	2227.7	2286.5	2315.3
	6	2734.5	2750	2850.7	2892.8

TABLE 7.24 Natural frequencies for model 3 (45.1°) under different boundary conditions with respect to the tangential displacement v, 14 conical elements

n	m	SS-SS	SSNTC-SS	SS-SSNTC
7	1	526	491.7	454.4
	2	1454	1317.8	1008.7
	3	2141	1996.2	1825
	4	2569	2455.4	2461
	5	2937	2816.4	2904
8	1	441	427.6	405
	2	1247.7	1163.5	930
	3	1948.6	1829	1625
	4	2428.5	2322.5	2279
	5	2818.5	2709	2767
12	1	420.6	421	413
	2	840	836	770
	3	1385	1361.6	1215
	4	1920	1877	1741
	5	2405.6	2348	2288
14	1	492	492.9	485
	2	838	839	797.3
	3	1270.8	1266	1167.4
	4	1760	1742.5	1620.7
	5	2257.8	2225	2140

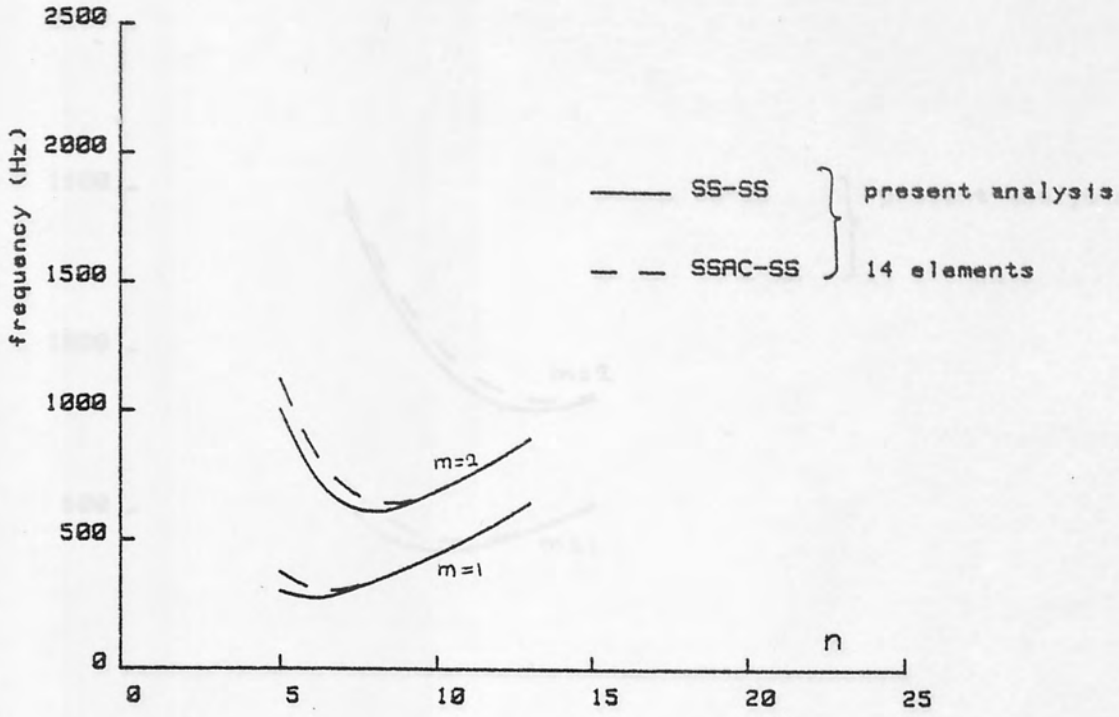

Fig. 7.13 frequency vs. circumferential wave number for 14.2° conical shell

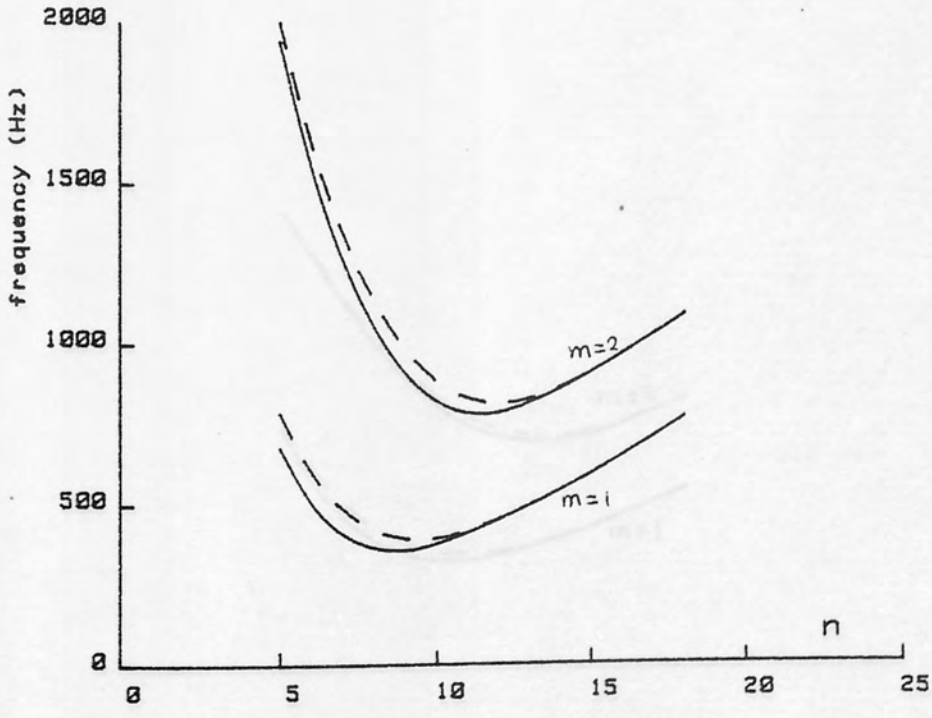

Fig. 7.14 frequency vs. circumferential wave number for 30.2° conical shell

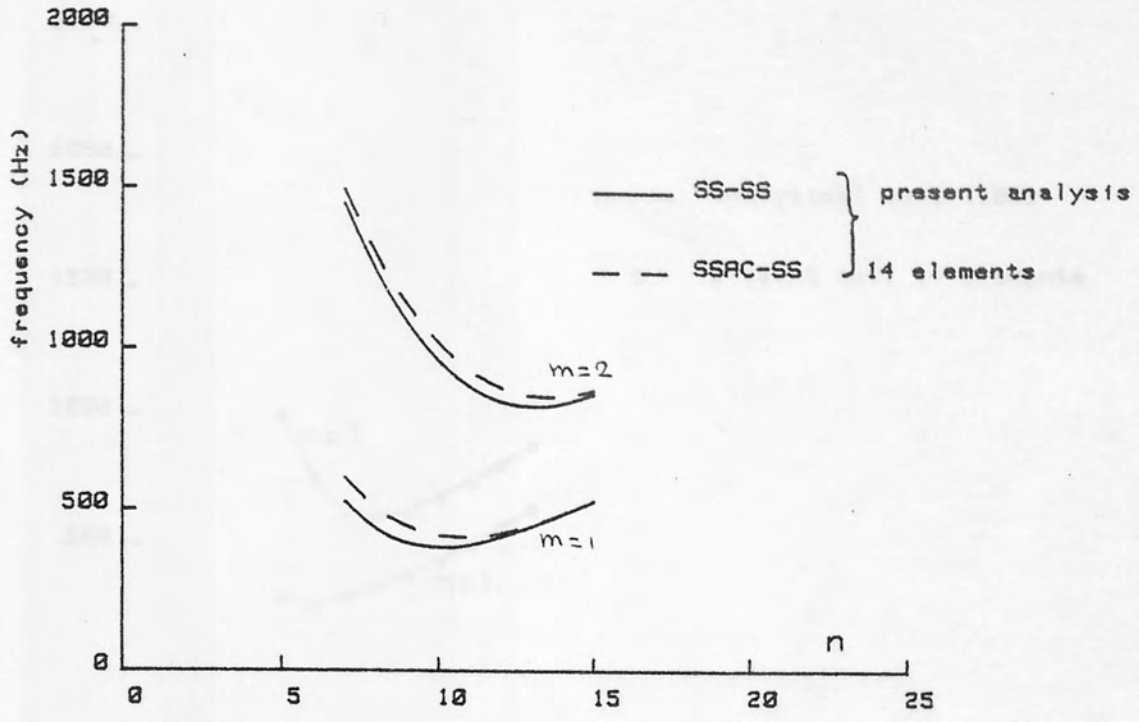

Fig. 7.15 frequency vs. circumferential wave number for 45.1° conical shell

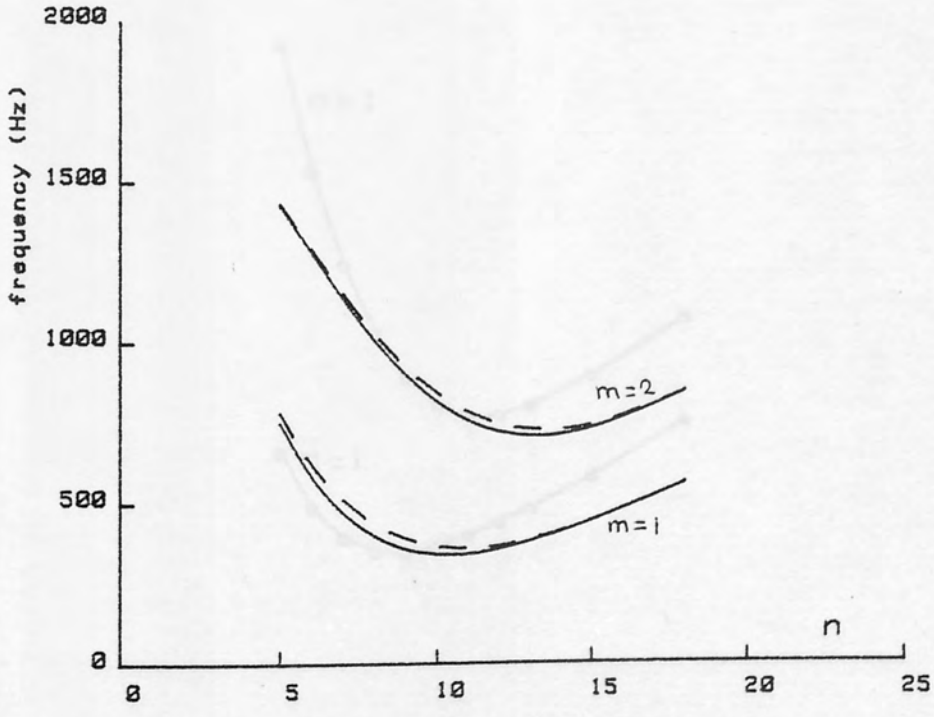

Fig. 7.16 frequency vs. circumferential wave number for 60.5° conical shell

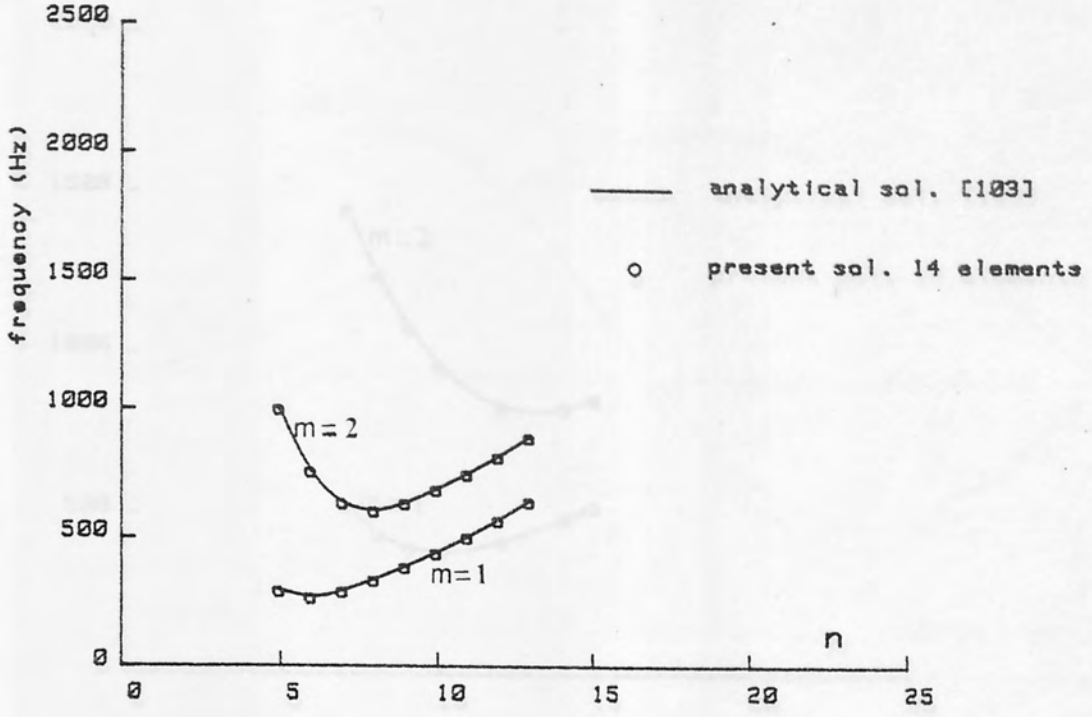

Fig. 7.17 Comparison of frequencies for a 14.2° SS-SS conical shell

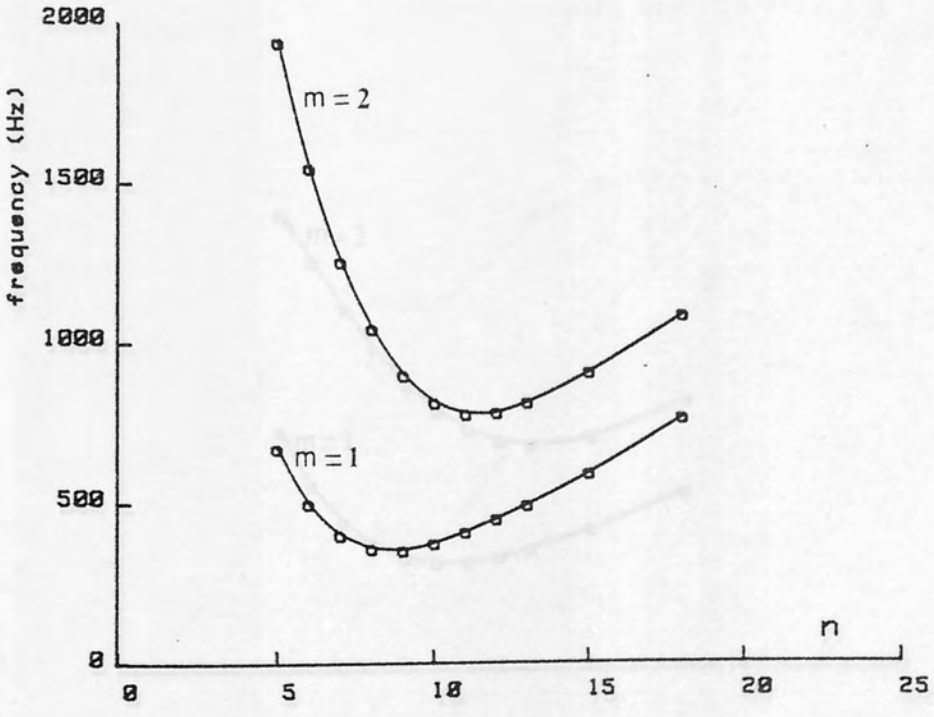

Fig. 7.18 Comparison of frequencies for a 30.2° SS-SS conical shell

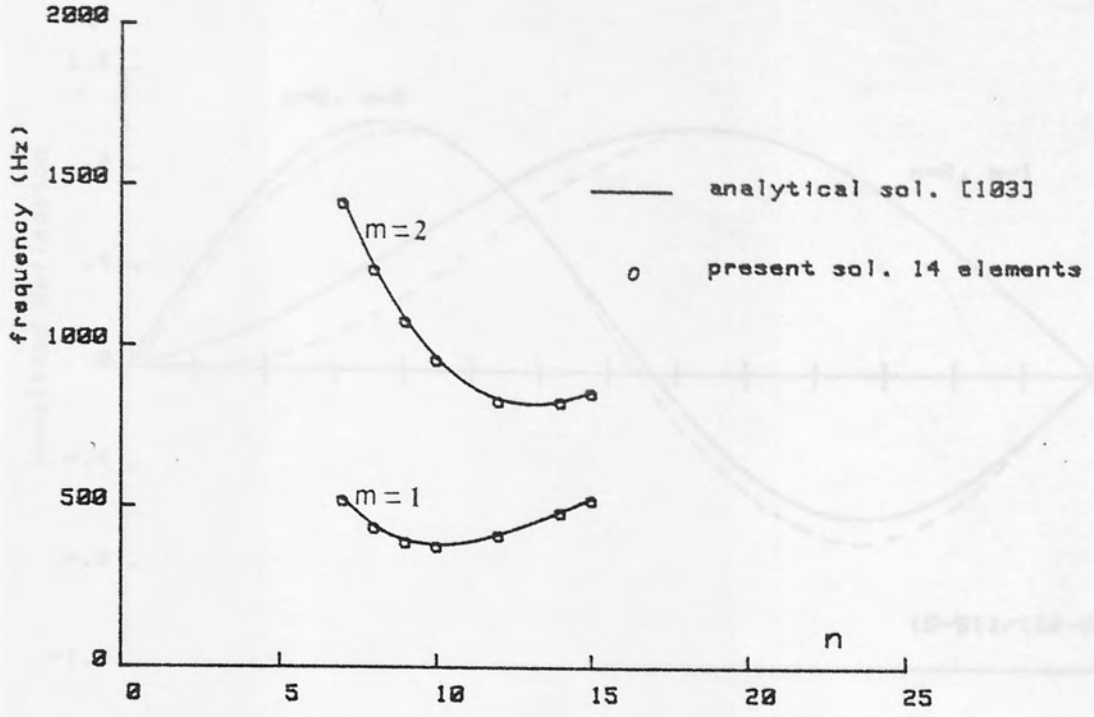

Fig. 7.19 Comparison of frequencies for a 45.1° SS-SS conical shell

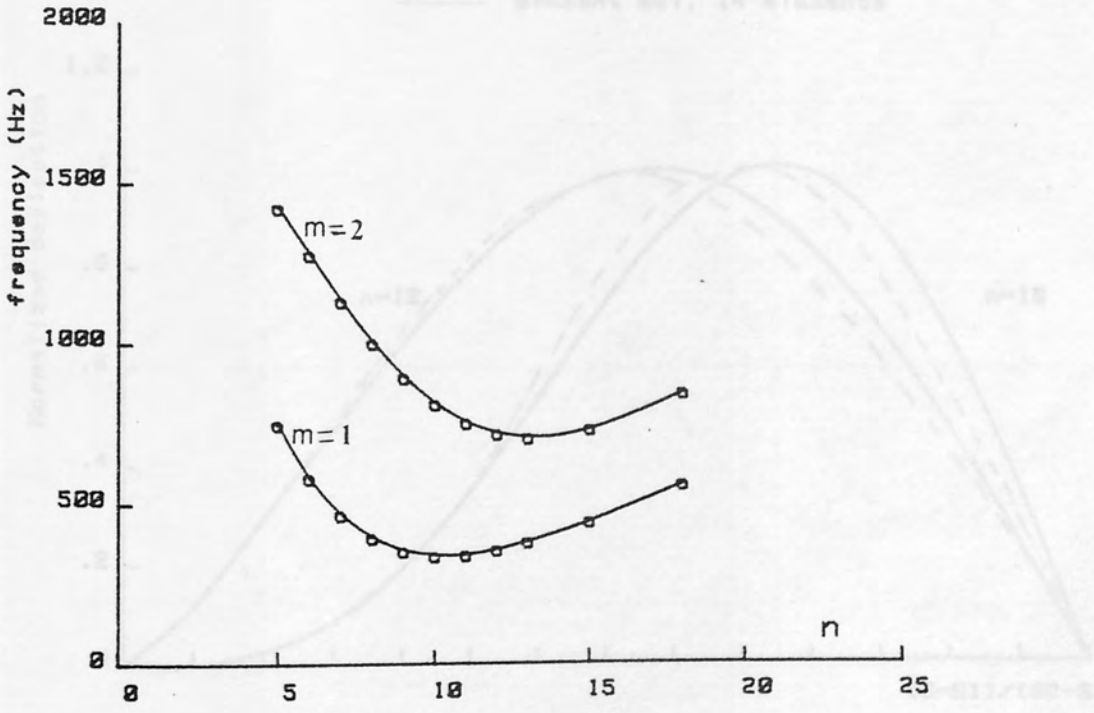

Fig. 7.20 Comparison of frequencies for a 60.5° SS-SS conical shell

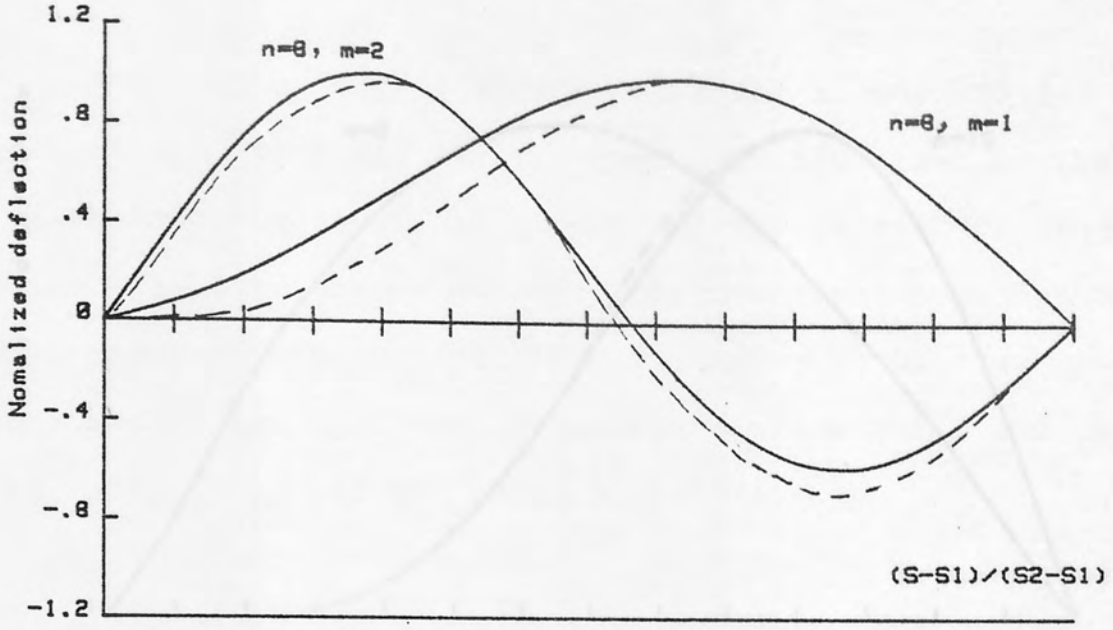

Fig. Transverse mode shape for SS-SS 14.2° cone

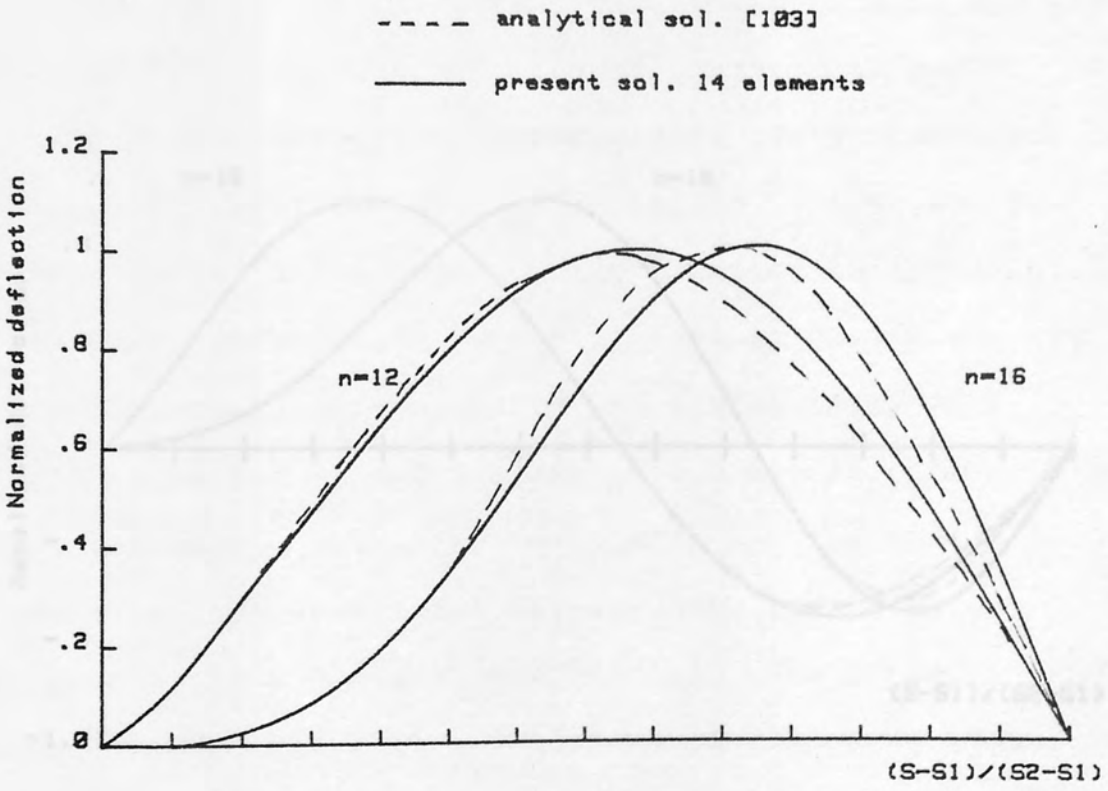

Fig. 7.22 Transverse mode shapes for SS-SS 45.1° cone

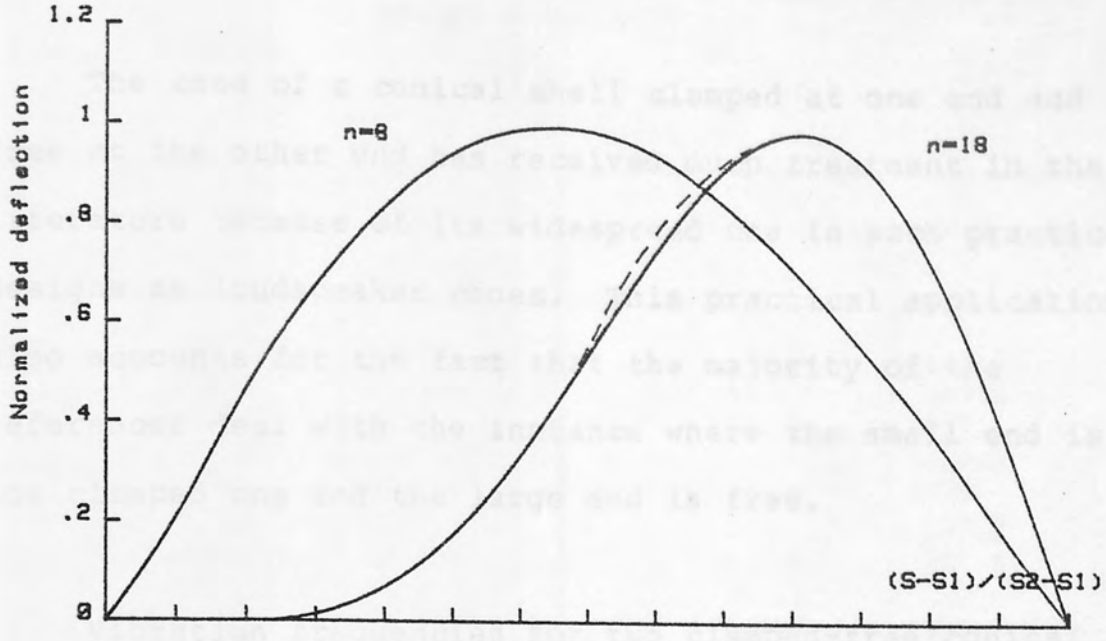

Fig. 7.23 Transverse mode shapes for SS-SS 45.1° cone

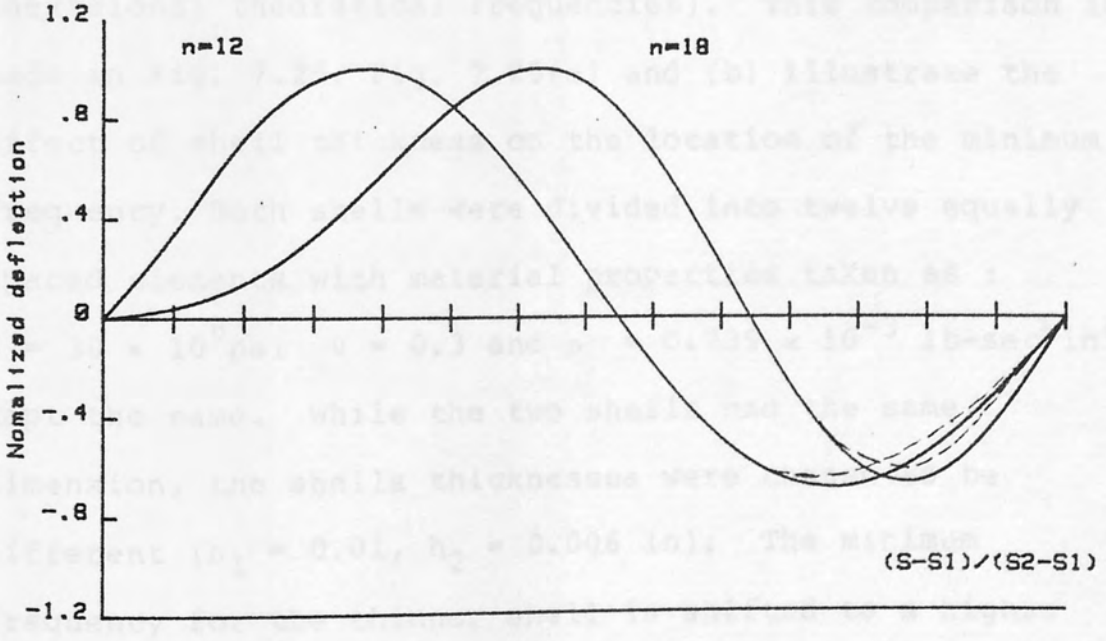

Fig. 7.24 Transverse mode shapes for SS-SS 45.1° cone

7.3.3.2 Clamped-Free Conical Shells

The case of a conical shell clamped at one end and free at the other end has received much treatment in the literature because of its widespread use in such practical designs as loudspeaker cones. This practical application also accounts for the fact that the majority of the references deal with the instance where the small end is the clamped one and the large end is free.

Vibration frequencies for two clamped-free conical shells are presented here and compared with those obtained by Platus [105]. (In ref. [105], frequencies obtained experimentally for the shells were compared with results derived from the superposition of extensional and inextsional theoretical frequencies). This comparison is made in Fig. 7.25. Fig. 7.25(a) and (b) illustrate the effect of shell thickness on the location of the minimum frequency. Both shells were divided into twelve equally spaced elements with material properties taken as : $E = 30 \times 10^6$ psi $\nu = 0.3$ and $\rho = 0.735 \times 10^{-3}$ lb-sec^2/in^4 kept the same. While the two shells had the same dimension, the shells thicknesses were chosen to be different ($h_1 = 0.01$, $h_2 = 0.006$ in). The minimum frequency for the thinner shell is shifted to a higher circumferential wave number n as can be seen from Fig. 7.25. The numerical results for both shells are given in Table 7.25.

TABLE 7.25 Natural frequencies for a 10.53° clamped-free conical shell with two different thicknesses, 12 conical elements

n	m	h=0.01 in	h=0.006 in	n	m	h=0.01 in	h=0.006 in
2	1	437.7	437.3	7	1	184.4	115.9
	2	2233	2232.4		2	433.1	384.4
	3	4417.7	4417		3	1041.3	1013
	4	5451.3	5450		4	1865	1842.3
	5	5875	5861.5		5	2803.4	2780
3	1	230.2	227.8	8	1	233	145.9
	2	1382.3	1380.8		2	425.4	338.6
	3	3140.3	3138.6		3	883.1	829.2
	4	4493.2	4491.2		4	1566.7	1527
	5	5339.5	5336.1		5	2403.9	2367
4	1	148.2	141	10	1	351.3	217
	2	916.5	913.2		2	522.6	349.8
	3	2262.3	2258.9		3	788.4	639.6
	4	3569.4	3565.6		4	1230.4	1122.2
	5	4621	4615.9		5	1864.6	1775.8
5	1	127.8	108.3	11	1	419.8	257
	2	651	642		2	596.9	387.9
	3	1681.8	1675		3	826	613.4
	4	2832.7	2825.6		4	1170.8	1005.7
	5	3916	3907.4		5	1706.5	1574
6	1	145.7	100.6				
	2	502.2	479.8				
	3	1295.9	1282.1				
	4	2276.6	2263.7				
	5	3305	3290.6				

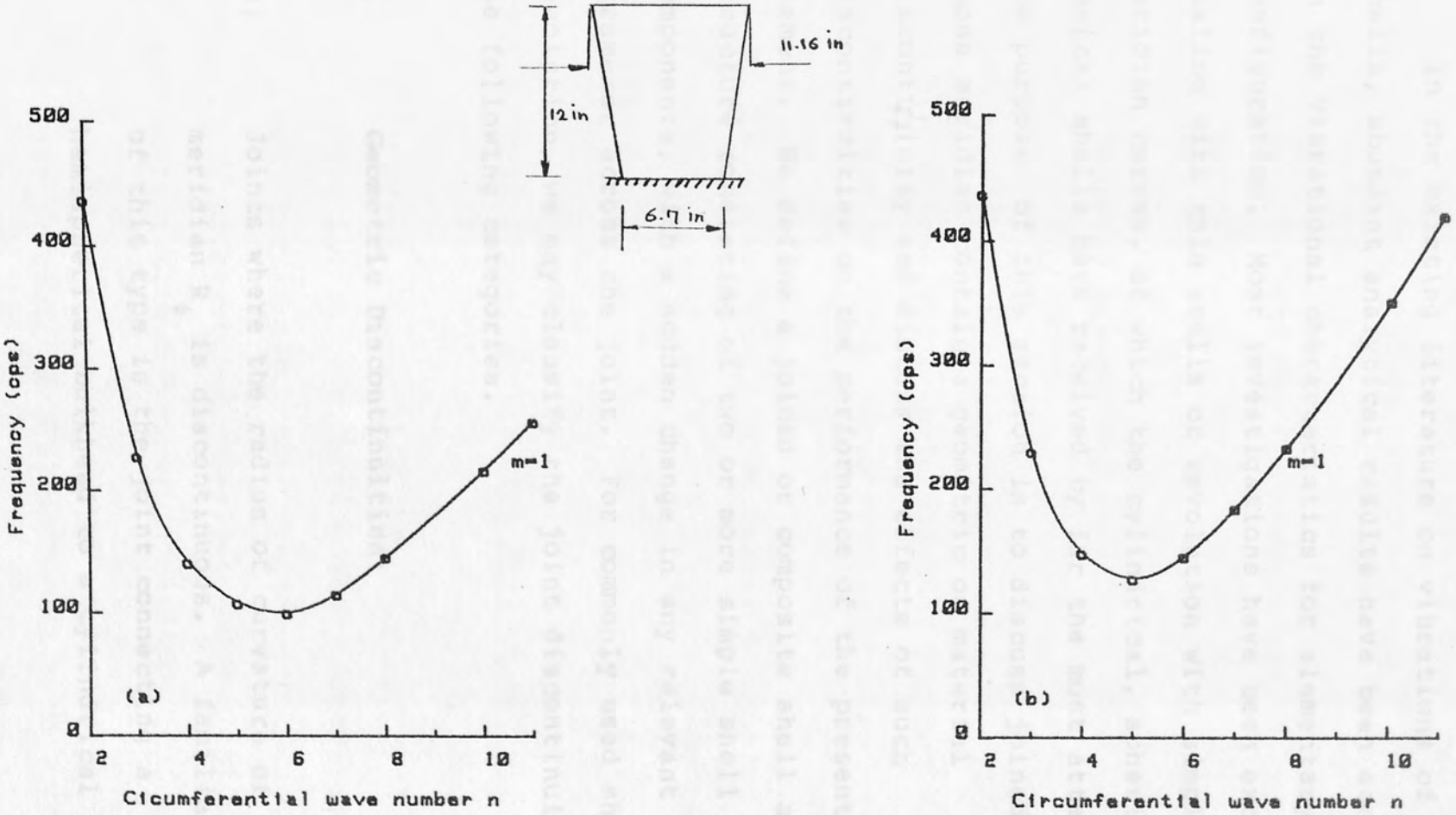

Fig. 7.25 comparison of frequencies for a 10.53 C-F conical shell

(a) h=0.006in (b) h=0.010in

——— analytical sol. [105]

o present sol. 12 elements

7.3.4 Free Vibration of Joined Shells

In the existing literature on vibrations of elastic shells, abundant analytical results have been accumulated on the vibrational characteristics for elementary shell configuration. Most investigations have been exclusively dealing with thin shells of revolution with simple meridian curves, of which the cylindrical, spherical, and conical shells have received by far the most attention. The purpose of this section is to discuss joined shells, whose meridian contain a geometric or material discontiniuity and discuss the effects of such discontinuities on the performance of the present element. We define a joined or composite shell as a structure consisting of two or more simple shell components, with a sudden change in any relevant shell parameter across the joint. For commonly used shells of revolution, we may classify the joint discontinuities into the following categories.

1. **Geometric Discontinuities:**

(a) Joints where the radius of curvature of the meridian R_ϕ is discontinuous. A familiar example of this type is the joint connecting a hemispherical bulkhead to a cylindrical shell.

(b) Joints where the second principal radius of

curvature R_θ is discontinuous. The joint connecting a conical shell to a cylindrical shell is an example. This type of joint has a much stronger discontinuity.

(c) Joints where the thickness h has an abrupt change.

2. **Material Discontinuities:**

Joints of two shell components made of different materials so that the elastic modulus, Poisson's ratio and the mass density change abruptly.

It is evident that, in an actual joint, two or more types of discontinuities listed previously may be present together.

7.3.4.1 Cylindrical Shells with Various End Closures

Cylindrical shells which are closed at their ends by shells of revolution (e.g. hemispheres, cones, etc.) are used in many industries. They are to be found, for instance, in submersibles, missiles and many structures in the Petro-chemical and nuclear industries.

In this section cylindrical shells with three different end closures are considered. The first end

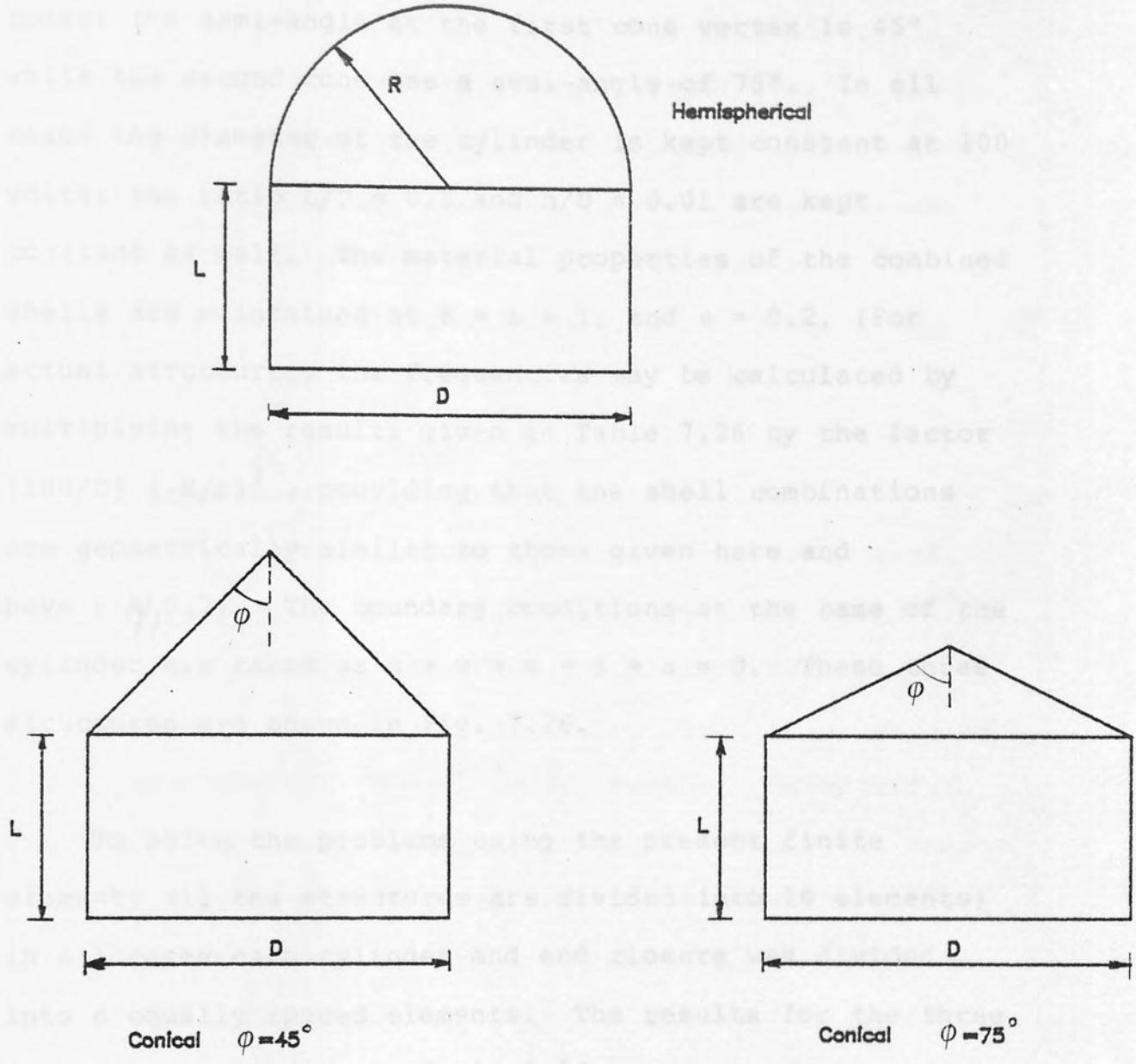

Fig. 7.26 Combinations of cylindrical shells with various end closures

closure is a hemisphere while the other two are complete cones; the semi-angle at the first cone vertex is 45° while the second cone has a semi-angle of 75°. In all cases the diameter of the cylinder is kept constant at 100 units; the ratio L/D = 0.5 and h/D = 0.01 are kept constant as well. The material properties of the combined shells are maintained at $E = \rho = 1$, and $\nu = 0.2$. (For actual structures, the frequencies may be calculated by multiplying the results given in Table 7.26 by the factor $(100/D)\ (E/\rho)^{\frac{1}{2}}$, providing that the shell combinations are geometrically similar to those given here and have $\nu = 0.2$). The boundary conditions at the base of the cylinder are taken as $u = v = w = \beta = \alpha = 0$. These three structures are shown in Fig. 7.26.

To solve the problems using the present finite element, all the structures are divided into 16 elements; in all cases each cylinder and end closure was divided into 8 equally spaced elements. The results for the three structures are shown in Table 7.26.

From Table 7.26 it can be seen that changing the shape of the end closure changes the four lowest natural frequencies to some extent. However, the maximum frequency, among the four lowest frequencies, given in Table 7.26 (1.126×10^{-3} Hz) is only 52.3% higher than the lowest (0.7394×10^{-3} Hz) and the four lowest natural frequencies of all the structures concerned lie between

these limits. The fundamental natural frequency occurred at n = 1, 2, 0 for the hemisphere, cone with 45° semi-angle, and cone with 75° semi-angle respectively. The change in the fundamental natural frequency is even less than that in the lowest four frequencies. The maximum fundamental frequency (0.9457×10^{-3} Hz) is only 30% higher than the lowest fundamental frequency (0.7394×10^{-3} Hz).

To show how the frequencies of vibration, particularly the fundamental frequency, can be changed, due to a change in the in-plane boundary conditions, calculations were repeated for the cylinder/hemisphere structure with the boundary conditions this time taken as $u = w = \beta = \alpha = 0$, $v \neq 0$, at the base of the cylinder. The natural frequencies versus circumferential wave number n, for the lowest three modes for the cylinder/hemisphere combination with two different boundary conditions at the base of the cylinder, are plotted in Fig. 7.27. As may be seen, the effect of not constraining v to be zero at the base of the cylinder is quite large for n=1 in the first mode - a 47% reduction in the value of the fundamental natural frequency.

The natural frequencies of vibration and mode shapes of the foregoing three structures were calculated by Galletly and Mistry [106]. The numerical methods employed in reference [106] are the variational finite-differences,

V.F.D., the finite elements and numerical integration.

The V.F.D. program used was the general purpose BOSOR3 which was written by Bushnell and his associates [107]. The finite element programs used were a special purpose one written at Liverpool University and known as MIST1, and another program written at Nottingham University and known as PAFEC; the elements used in both programs were axisymmetric elements but the displacement field and the order of the elements were different from those in the present finite element. The results obtained by a numerical integration scheme were by the programs known as KSHEL3 and STARS-2.

Comparison between the present results and those obtained in reference [106], using different methods, is made in Tables 7.27 and 7.28 and in Fig. 7.28. Very good agreement, as it can be seen between the present finite element representation and the other approximate results, is present.

Table 7.26 Natural frequencies (Hz $\times 10^{-3}$) of cylinder/hemisphere and cylinder/cones combinations [L/D = 0.5, h/D = 0.01, E = ρ = 1, ν = 0.2, D = 100, Ne = 16]

n	m	cylinder/hemisphere	cylinder/cone ϕ = 45°	cylinder/cone ϕ = 75°
0	1	2.0433	1.4964	0.7394
	2	2.6269	3.1129	1.8255
	3	3.0383	3.2473	2.908
	4	3.1873	3.4052	3.2056
1	1	0.9457	1.0785	0.9853
	2	2.5219	2.0396	1.3149
	3	2.7791	2.7438	1.9808
	4	3.1316	3.2848	2.7591
2	1	1.6353	0.9401	0.8384
	2	2.7086	1.9815	1.8344
	3	2.9901	2.4448	1.9933
	4	3.2107	3.0773	3.0346
3	1	1.3296	0.9613	0.9804
	2	2.5137	1.6060	1.6201
	3	3.0948	2.3156	2.2159
	4	3.2765	2.8445	2.8354
4	1	1.1204	1.1260	1.2552
	2	2.2945	1.3532	1.3638
	3	3.1208	2.4674	2.5634
	4	3.3467	2.6385	2.8024
5	1	1.0301	1.2062	1.2229
	2	2.1408	1.3993	1.6103
	3	3.1086	2.4915	2.4894
	4	3.4480	2.8169	3.3201
6	1	1.0586		
	2	2.0734		

TABLE 7.27 Comparison of natural frequencies (Hz $\times 10^{-3}$) for cylinder/hemisphere combinations [L/D = 0.5, h/D = 0.01, E = ρ = 1, ν = 0.2]

n	m	Present work	VFD* [106]	n	m	Present Work	VFD* [106]
0	1	2.0433	2.0589	6	1	1.0586	1.041
	2	2.6269	2.750		2	2.0734	2.060
	3	3.0383	3.100		3	3.1183	2.9330
1	1	0.9457	0.9435	7	1	1.1924	1.1872
	2	2.5219	2.5092		2	2.0981	2.0800
	3	2.7791	2.7000		3	3.1722	2.9800
2	1	1.6353	1.6222	8	1	1.4091	1.4050
	2	2.7086	2.7000		2	2.2116	2.200
	3	2.9901	2.8100		3	3.2797	3.080
3	1	1.3296	1.3100	9	1	1.6892	1.6800
	2	2.5137	2.4330		2	2.4054	2.3800
	3	3.0948	3.0700		3	3.4446	3.2415
4	1	1.1204	1.0978	10	1	2.0204	2.0200
	2	2.2945	2.2521		2	2.6688	2.6300
	3	3.1208	3.0140		3	3.6673	3.4637
5	1	1.0301	1.008				
	2	2.1408	2.103				
	3	3.1086	2.9230				

* Variational finite difference.

TABLE 7.28 Comparison of natural frequencies (Hz × 10^{-3}) of cylinder/complete cone combinations [L/D = 0.5, h/D = 0.01, E = ρ = 1, ν = 0.2, D = 100]

φ	n	m	Finite Element Method			Variational Finite-Difference		Numerical Integration	
			Present Work	Mist 1	PAFEC	BOSOR3 with round apex	BOSOR3 with hole at apex	STARS-2	KSHEL3
45°	0	1	1.4964	1.494	1.56	1.596	1.490	1.494	1.495
		2	3.1129	3.026	3.16	3.072	–	3.362	3.202
	1	1	1.0785	1.079	0.96	1.068	1.079	1.078	1.080
		2	2.0396	2.015	2.20	2.111	2.010	2.06	2.018
	2	1	0.9401	0.935	0.88	0.918	0.935	0.936	0.947
		2	1.9815	1.958	1.96	1.975	1.955	2.009	1.964
75°	0	1	0.7394	0.737	0.76	0.787	0.736	0.739	0.739
		2	1.8255	1.739	2.00	1.787	1.738	1.763	1.740
	1	1	0.9853	0.974	0.80	1.024	0.972	1.057	0.974
		2	1.3149	1.312	1.28	1.315	1.312	1.70	1.312
	2	1	0.8384	0.831	0.80	0.855	0.830	0.831	0.829
		2	1.8344	1.719	1.84	1.759	1.715	1.75	1.717

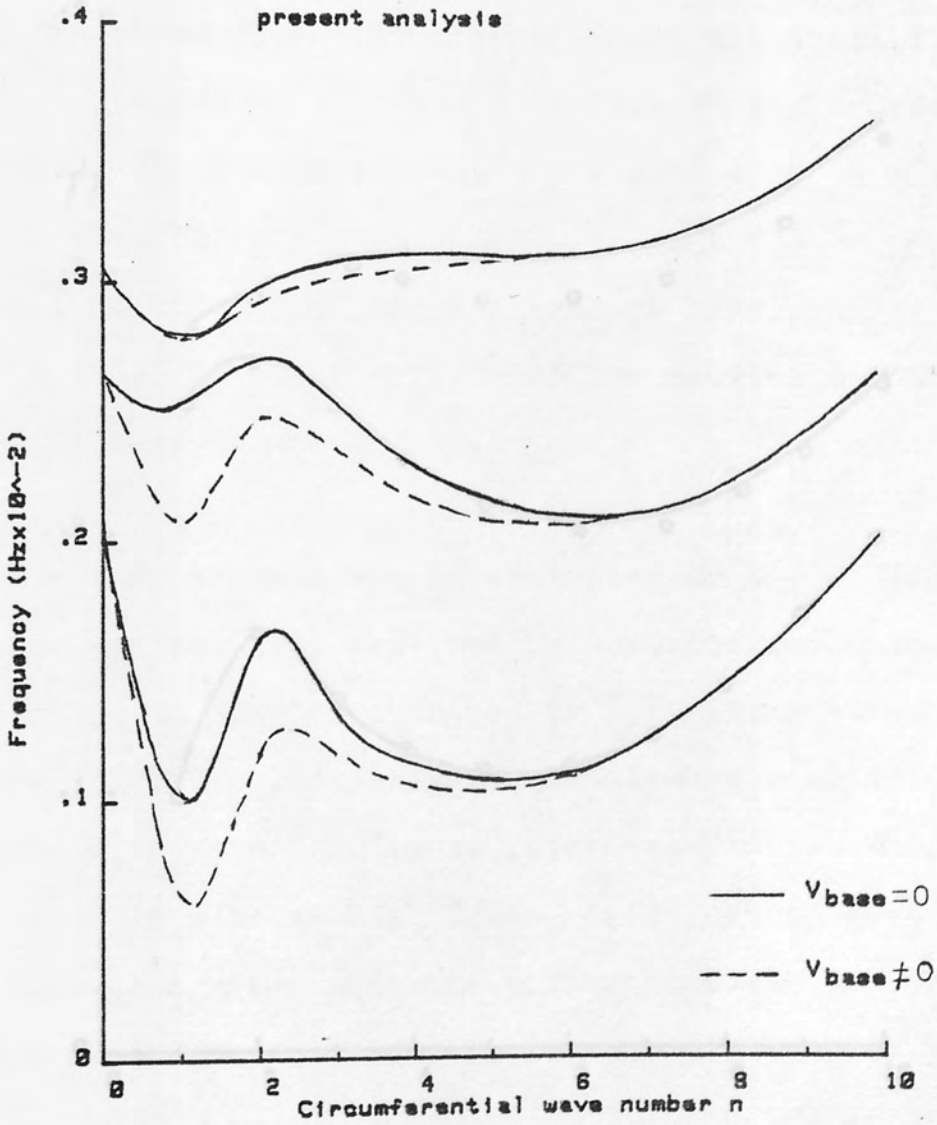

Fig. 7.27 natural frequencies for cylinder/hemisphere combination

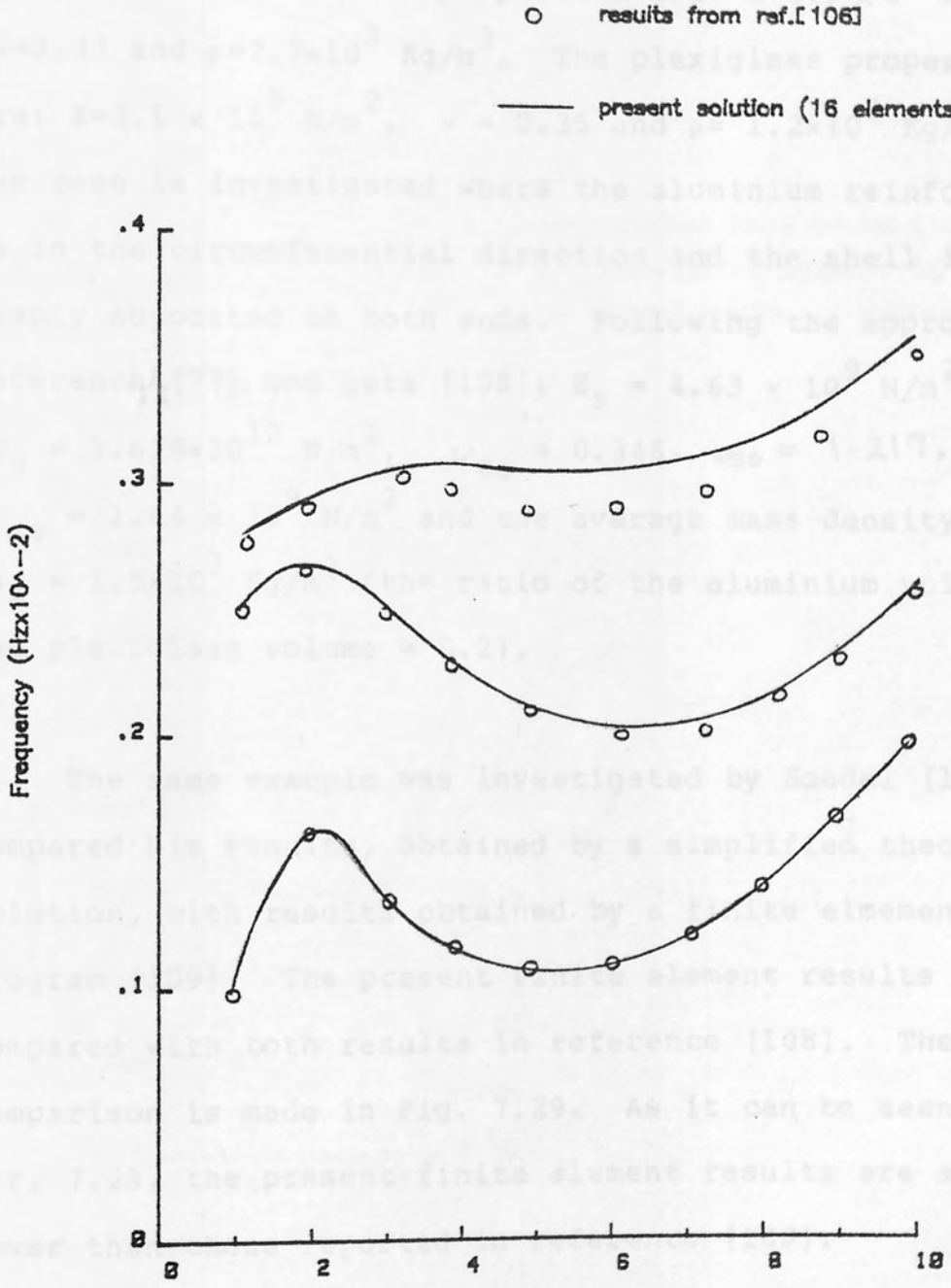

Fig. 7.28 comparison of natural frequencies for cylinder/hemisphere combination

7.3.5 Free Vibration of Orthotropic Shells

As a numerical example of orthotropic shells, a plexiglass cylindrical shell reinforced by aluminimum is considered. The dimensions are: L=3m, R=1.5m and h=0.02m. The aluminium properties are: $E=6.9 \times 0^{11} N/m^2$, $\nu=0.33$ and $\rho=2.7\times10^3$ Kg/m^3. The plexiglass properties are: $E=3.1 \times 10^9$ N/m^2, $\nu = 0.35$ and $\rho= 1.2\times10^3$ Kg/m^3. The case is investigated where the aluminium reinforcement is in the circumferential direction and the shell is simply supported at both ends. Following the approach of reference [77] one gets [108]: $E_s = 4.63 \times 10^9$ N/m^2, $E_\theta = 1.628\times10^{10}$ N/m^2, $\nu_{\theta s} = 0.346$, $\nu_{s\theta} = 1.217$, $G_{s\theta} = 1.64 \times 10^9$ N/m^2 and the average mass density $\rho_a = 1.5\times10^3$ Kg/m^3 (the ratio of the aluminium volume to the plexiglass volume = 0.2).

The same example was investigated by Soedel [108] who compared his results, obtained by a simplified theory solution, with results obtained by a finite elmement program [109]. The present finite element results are compared with both results in reference [108]. The comparison is made in Fig. 7.29. As it can be seen from Fir. 7.29, the present finite element results are always lower than those reported in reference [108].

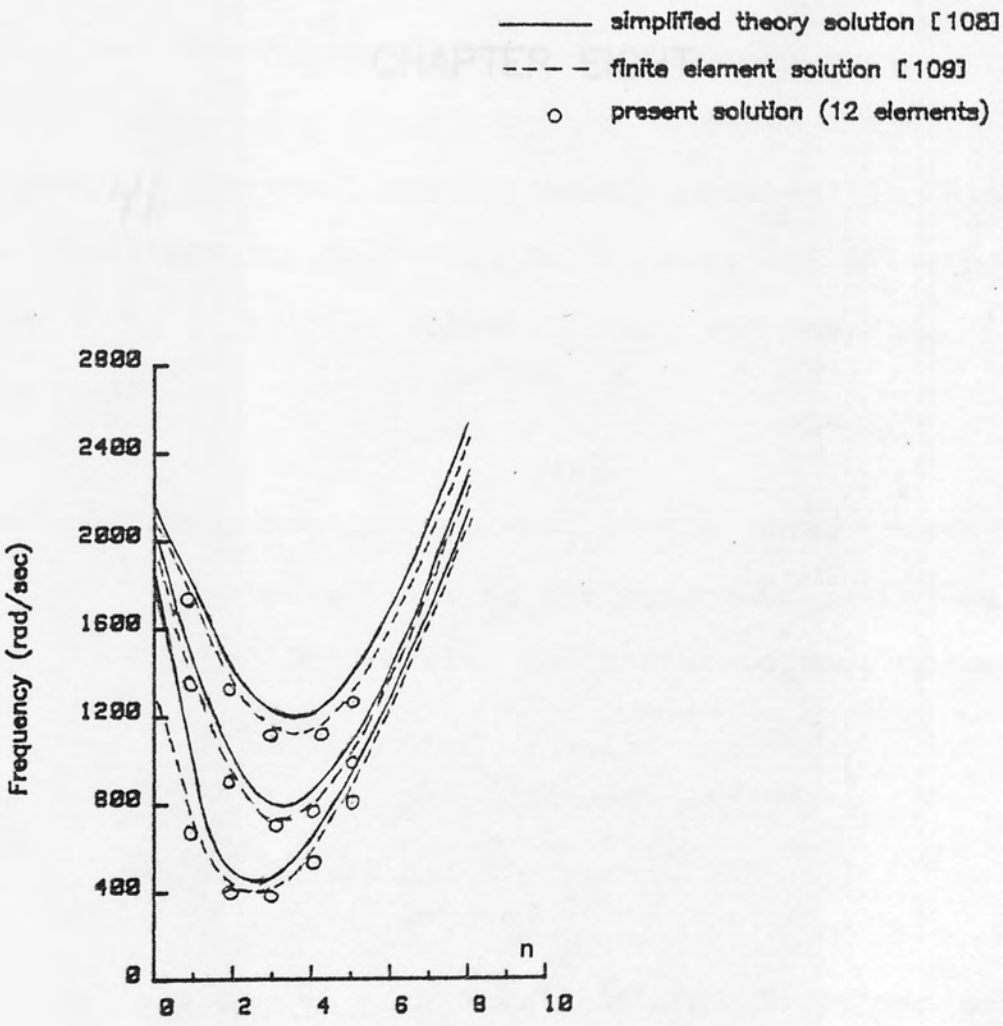

Fig. 7.29 Natural frequencies for orthotropic cylindrical shell, orthotropic reinforcement is in the circumferential direction

CHAPTER EIGHT

CHAPTER 8

DISCUSSION AND CONLUSIONS

In addition to the description of the development and formulation of the truncated cone element, another objective of the project was to develop a computer program in order to investigate the performance of the element in the solutions of axisymmetric shells. The element characteristic equations in discrete forms have been formulated and the overall system matrices obtained by an 'assembly' process. The information present in this thesis allows the following magnitudes, for axisymmetric shells, to be readily obtained using the computer programs:

1. Displacement components at the nodal points.
2. Stress resultants at the centre of the elements.
3. Natural frequencies and vibration mode shapes of the shells.

8.1 Static Analysis

Deflection and stress calculations have been carried out for circular and annular plates, cylindrical and conical shells. The response to different types of loadings were examined. It has been shown that acceptable accuracy can be obtained with a reasonable number of

elements. The thicker the shell is the less elements are needed. For the very thick plate, oscillation of results about the exact solution (see Table 7.1) is due to h/Le ratio.

Stress calculations have been carried out for a spherical cap loaded by a uniform external pressure. It is in this problem type that the conical element was thought to be deficient and was abandoned in favour of the curved element [56]. The present conical element provides good results with an assemblage of 16 elements. The accuracy of the solution could be increased when the elements are reduced in size.

8.2 Vibration Analysis

The applications have shown the efficiency and applicability of the truncated cone element to the dynamic analysis of:

1. One segmented axisymmetric shell (cylindrical shells, conical shells, annular plates).

2. Some combinations of axisymmetric shells (cylinder/hemisphere, cylinder/cone).

For annular plates, the results obtained indicate that the frequencies converge rapidly to the exact

solutions with an increasing number of elements and that only a few element for thick plates, are required to predict the modes with a small number of nodal diameters and nodal circles. Also, it can be observed from Table 7.3 throught to Table 7.9 that the difference between the results given by the present finite element and the classical theory decreases then increases with an increase in the radii ratio b/a. The present results become lower than the classical theory results when b/a >0.3. Less elements are needed with the increase of b/a ratio. More careful examination of the results in Table 7.3 through to 7.12 indicates that transverse shear and rotary inertia effects become significant as the ratio b/a increases or a/h decreases. One more point should be mentioned here, that is when the plates become very thick or when b/a large the finite element solution gives an inaccurate picture of the order of the modes.

Natural frequencies for cylindrical shells of different configurations, subjected to a variety of boundary conditions, have been computed using the truncated cone element. These results were compared with solutions obtained by analytical methods, the Rayleigh-Ritz method and with some other finite element solutions. This comparison shows that the natural frequencies are predicted more accurately by the present finite element than by the approximate energy method. In most cases the present finite element is superior to other

finite elements. For moderately thick cylinder shells the effects of transverse shear and rotary inertia is evident. All the frequencies obtained by the present finite element are lower than those obtained by analytical solutions, where transverse shear and rotary inertia were neglected in the analysis.

Natural frequencies and vibration modes for conical shells of different configurations have been computed. Very good agreement, was found, between the present work and the theoretical results reported in reference [103]. This good agreement is, probably, due to the inclusion of the effects of transverse shear deformation and rotary inertia in the meridional direction in the theoretical formulations of reference [103].

The natural frequencies of vibration of cylindrical shells clamped at one end and closed at the other by different types of shells of revolution (hemisphere, cones) have been determined using the present computer program based on the truncated cone element. The results were compared with those reported in reference [106] where different methods (the variational finite differences, the finite element method, numerical integration) were employed to obtain the results. The comparison indicates that the natural frequencies are predicted accurately using the present finite element. Very good agreement was found with the other approximate results.

The sensitivity of the natural frequencies, for cylindrical shells, conical shells and a cylinder/hemisphere structure, to changes in boundary conditions has been investigated using the present finite element. The results reported in this thesis show that the influence of constraining axial or tangential displacements (u=0, v=0), in contrast to the effect of clamping (β=0), is significant when the circumferential and axial mode numbers are small.

8.3 Conclusions

The conclusions of these results, obtained by using the truncated cone element, can be summarised as follows:

1. Although the element is a simple one, the accuracy of the solutions, with a maximum of 16 elements used in any problem, not only lends itself to concise and efficient computer implementation but also provides an efficient tool for analysing different types of axisymmetric shells.

2. As shells used in actual practice have appreciable thickness, studies based on classical thoery fail to predict satisfactory results. Hence it is important to include effects of inertia and shear deformation in order to predict their dynamic

behaviour with a fair amount of accuracy.

3. The great efficiency, in terms of computational cost and accuracy, which has been achieved by the truncated cone element, confirms that complete C_1 continuity does not necessarily correspond to an increase in efficiency.

4. For very thick shell situations, h/Le ratio should not exceeds 1.2.

5. If a shell problem were being studied in which the distributed loading or the radii of curvature varied considerably along the meridian, good accuracy could not be obtained with so few elements.

8.4 Further Improvements

The present work has demonstrated that the semi-analytic truncated cone element can predict the vibration characteristics of axisymmetric shells accurately. Further work can be done to find the natural frequencies and vibration mode shapes for more examples especially for joined and orthotropic axisymmetric shells.

As it was mentioned before, the computer program was designed to be modified or extended with little

difficulty. An extension to the program to investigate the performance of the element in forced vibrations can be an objective of further work. More work could be done by extending the program to include some other types of finite elements (triangular, quadrilateral) to enable the study of practical problems of axisymmetric shells like the one shown in Fig. 3.3.

REFERENCES

REFERENCES

1. Turner, M. J., Clough, R. W., Martin, H. C. and Topp, L. C., 'Stiffness and deflection analysis of complex structures', J. Aeronaut. Sci., Vol. 23, No. 9, 1956.

2. Clough, R. W., 'The finite element in plane stress analysis', Proc. 2nd A.S.C.E. Conf. on Electronic Computation, Pittsburg, Pa., September 1960.

3. Grafton, P. E. and Strome, D. R., 'Analysis of axisymmetrical shells by the direct stiffness method', A.I.A.A. Jnl., 1(10), pp. 2342-2347, 1963.

4. Percy, J. H., Pian, T. H. H., Klein, S. and Navaratna, D. R., 'Application of matrix displacement method to linear elastic anlaysis of shells of revolution', A.I.A.A. Jnl., 3(11), pp. 2135-2145, 1965.

5. Zienkiewicz, O. C., Bauer, J., Morgan, K. and Onate, E., 'A simple and efficient element for axisymmetric shells', Int. J. Num. Meth. Engng., 11, pp. 1545-1558, 1977.

6. Kumagai, N., 'A semi-analytic finite element method to the stress analysis of axisymmetric shells', M.Sc. Thesis, The University of Aston in Birmingham, 1981.

7. Archer, J. S., 'Consistent mass matrix for distributed mass system', Journal of the Structural Division, A.S.C.E., pp. 161-178, August, 1963.

8. Zienkiewicz, O. C. and Cheung, Y. K., 'The finite element method for analysis of elastic isotropic and orthotropic slabs', Proc. Inst. Cir. Eng., 28, 471, 1964.

9. Novozhilov, V. V., 'The theory of thin shells', D. Noordhoff Ltd., Groningen, The Netherlands, (Trans. P. G. Lowe), 1959.

10. Love, A. E. H., 'A treatise on the mathematical theory of elasticity', 1st Edn. Cambridge University Press (1892); 4th Edn. Dover Pub. Inc., New York, 1944.

11. Donnell, L. H., 'A discussion of thin shell theory', Proc. 5th Int. Cong. Appl. Mech., 1938.

12. Timoshenko, S., 'Theory of plates and shells', McGraw-Hill, New York, 1959.

13. Reissner, E., 'Stress strain relations in the theory of thin elastic shells', J. Math. Phy., 31, 109-119, 1952.

14. Naghdi, P. M., 'Foundations of elastic shell theory', Progress in solid mechanics (End., I. N., Sneddon and R. Hill), Vol. IV, Chapter 1, North-Holland, 1963.

15. Vlasov, V. Z., Obshchaya teoriya obolochek; Yeye prilozhniya v tekhnike. Gos. Izd. Tekh-Teor. Lit., Moscow-Leningrad (1949) (English translation: NASA TTF-99, 'General theory of shells and its applications in engineering', April 1964).

16. Flügge, W., 'Stresses in shells', Springer-Verlag, Berlin, 1962.

17. Goldenveizer, A. L., 'Theory of thin shells', Pergamon Press, New York, 1961.

18. Kraus, H., 'Thin elastic shells', New York, John Wiley & Sons, 1967.

19. Reissner, E., 'A new derivation of the equations for the deformation of elastic shells', American Journal of Mathematics, 63, pp. 177-184, 1941.

20. Timoshenko, S., 'On the correction for shear of the differential equations for transverse vibrations of prismatic bars', Philosophical Magazine, 41, pp. 742-748, 1927.

21. Mindlin, R. D., 'Influence of rotary inertia and shear on flexural motions of isotropic elastic plates', J. Applied Mechanics, 18, pp. 31-38, 1951.

22. Truesedell, C. nad Toupin, R. A., Encylopaedia of Physics, Vol. III/1, Springer-Verlag, 1960.

23. Gol'denveizer, A. L., 'Theory of elastic shells', (Trans. G. Herrman), Pergamon Press, Oxford, 1961.

24. Meirovitch, L., 'Analytical methods in vibration', McMillan Co., New York, 1967.

25. Lanczos, C., 'The variational principle of mechanics', University of Toronto press, Fourth Edition, 1970.

26. Soedel, W., 'On the vibration of shells with Timoshenko-Mindlin type shear deflections and rotary inertia', J. Sound and Vibration, 83 (1), pp. 67-79, 1982.

27. Leissa, A. W., 'Vibration of shells', NASA SP-288, 1973.

28. Zienkiewicz, O. C., 'The finite element method', 3rd Edition, McGraw-Hill, London, 1977.

29. Green, B. E., Strome, D. R., and Weikel, R. C., 'Application of the stiffness method to the analysis of shell structures', Proc. Aviation Conf. Amer. Soc. Mech. Eng., Los Angeles, March 1961.

30. Argyris, J. H., 'Matrix displacement analysis of anisotropic shells by triangular elements', J. Ray. Aero. Soc., 69, pp. 801-805, 1965.

31. Clough, R. W. and Johnson, C. P., 'A finite element approximation for the analysis of thin shells', J. Solids Struct., 4, pp. 43-60, 1968.

32. Zienkiewicz, O. C., and Cheung, Y. K., 'Finite element procedures in the solution of plate and shell problems', Chapter 8 of stress analysis (edn. Zienkiewicz and G. S. Holister), Wiley, 1965.

33. Utku, S., 'Stiffness matrices of thin triangular elements of non-zero Gaussian curvature', A.I.A.A. Jnl., 5, pp. 1659-1667, 1967.

34. Ashwell, D. G. and Gallager, R. H. (Eds.), 'Finite elements for thin shells and curved members', Wiley, London, 1976.

35. Strickland, G. E., and Loden, W. A., 'A doubly-curved triangular shell element', Proc. Conf. Matrix Meth. Struct. Mech., Wright-Patterson Airforce Base, Ohio, AFFDL-TR-68-150, pp. 641-666, 1968.

36. Green, B. E., Jones, R. E., Mclay, R. W. and Strome, D.R., 'Dynamic analysis of shells using doubly curved finite elements', Proc. Conf. Matrix Meth. Struct. Mech. Wright-Patterson Airforce Base, Ohio, AFFDL-TR-68-150, pp. 185-212, 1968.

37. Ahmad, S., Irons, B. M. and Zienkiewicz, O. C., 'Analysis of thick and thin shell structures by curved finite elements', Int. J. Num. Meth. Engng., 2, pp. 419-451, 1970.

38. Dunne, P., 'Complete polynomial displacement fields for the finite element method', The Aeronautical Journal, Vol. 72, March 1968.

39. Desai, C. S., and Abel, J. F., 'Introduction to the finite element method', VNR Company, 1972.

40. Anderheggen, E., 'A conforming triangular finite element plate bending solution', Int. J. Num. Meth. Engng., 2, pp. 259-264, 1970.

41. Thomas, G. R. and Gallagher, R. H., 'A triangular thin shell finite element: Linear analysis', NASA Contractor Report 2482, Washington DC, 1975.

42. Kikuchi, F. and Ando, Y., 'A new variational functional for the finite-element method and its application to plate and shell problems', Nucl. Eng. Design, 21, pp. 95-113, 1972.

43. Keg, S. W., 'A specialization of Jones' generalization of the direct-stiffnes method of structural analysis', AIAA Jnl., 9, pp. 984-985, 1971.

44. Haugeneder, E. and Many, H. A., 'Admissible and inadmissible simpifications of variational methods in finite element analysis', Proc. IUTAM Symp. on Variational Methods in the Mechanics of Solids, Evanston III, (S. Nemat-Nasser, Edn.), Pergamon Press, London, pp. 187-198, 1980.

45. Zienkiewicz, O. C., 'Constrained variational principles and penalty function methods in finite element analysis', Lect. Notes in Math., No. 363, Springer-Verlag, Berlin, pp. 207-214, 1974.

46. Bathe, K. J. and Wilson, E. L., 'Numerical methods in finite element analysis', Prentice-Hall Inc., Englewood Cliffs, New Jersey, 1976.

47. Wilkinson, J. H., 'The albegric eigenvalue problem' Oxford University Press Inc., London, 1965.

48. Peters, G. and Wilkinson, J. H., ' $Ax = \lambda Bx$ and the generalised eigenproblem', S.I.A.M., J.Numerical Analysis, Vol. 7, pp. 479-492, 1970.

49. Wilson, E. L., Farhoomand, I. and Bathe, K. J., 'Nonlinear dynamic analysis of complex structures', Int. J. of Earthquake Engng. and Structural Dynamics, Vol. 1, pp. 241-252, 1973.

50. Hitchings, D. and Dance, S. H., 'Response of nuclear structural systems to transient and random excitations, using both deterministic and probabilistic methods', Nucl. Eng. Design, 29, pp. 311-337, 1974.

51. Warburton, G. B., 'The dynamical behaviour of structure', 2nd Edn., Pergamon Press, 1976.

52. Wilson, E. L., and Penzien, J., 'Evaluation of orthogonal damping matrices', Int. J. Num. Meth. Engng., 4, pp. 5-10, 1972.

53. Clough, R. W. and Penzien, J., 'Dynamics of Structures', McGraw-Hill, 1975.

54. Thomson, H. T., Colkins, T. and Caravani, P., 'A numerical study of damping', Int. J. Earthquake Engng. Structural Dynamics, 3, pp. 97-103, 1074.

55. Popov, E. P., Penzien, J. and Lu, Z. A., 'Finite element solution for axisymmetric shells', Proc. A.S.C.E.E.M, pp. 119-145, 1964.

56. Jones, R. E. and Strome, D. R., 'Direct stiffness method of analysis of shells of revoution utilizing curved elements', A.I.A.A. Jnl., 4(9), pp. 1519-1525, 1966.

57. Stricklin, J. A., Navaratna, D. R. and Pain, T. H. H., 'Improvements on the analysis of shells of revolution by the matrix displacement method', A.I.A.A. Jnl., 4(11), pp. 2069-2072, 1966.

58. Webster, J. J., 'Free vibrations of shells of revolution using ring finite elements', Int. J. Mech. Sci., Vol. 9, pp. 559-570, 1967.

59. Fonder, G. A., 'A doubly curved quadrilateral element for thin elastic shells of revolution', Ph.D. dissertation, Department of Civil Engineering, University of California, Berkeley, 1972.

60. Bogner, F. K., Fox, R. L. and Schmit, C. A., 'A cylindrical shell discrete element', A.I.A.A. Jnl., 5, pp. 745-750, 1967.

61. Melosh, R. J., 'A flat triangular shell element stiffness matrix', Proc. Conf. Matrix. Meth. Struct. Mech., Airforce Institute of Technology, Wright-Patterson Airforce Base, Ohio, 1965.

62. Wempner, G. A., Oden, J. T. and Kross, D. A., 'Finite element analysis of thin shells', Proc. Am. Soc. Civ. Engng. EM6, pp. 1273-1294, 1968.

63. Wempner, G. A., 'Finite elements, finite rotations and small strains of flexible shells', Int. J. Solids Struct., 5, pp. 117-153, 1969.

64. Stricklin, J. A., Haïsler, W. E., Tisdale, P. R. and Ganderstom, R., 'A rapidly converging triangular plate element', A.I.A.A. Jnl., 7, pp. 180-181, 1969.

65. Martin, H. C., 'Stiffness matrix for triangular sandwich element in bending', TP-32-1158, Jet Propulsion Laboratory, Pasadena, California, 1968.

66. Keyand, S. W. and Beisinger, Z. E., 'The analysis of thin shells by the finite element method', Symposium on High Speed Computing for Elastic Structures, IUTAM, Leige, 1970.

67. Zienkiewicz, O. C., Taylor, R.L. and Too, J. M., 'Reduced integration technique in general analysis of plates and shells', Int. J. Num. Meth. Engng., 3, pp. 275-290, 1971.

68. Fried, I., 'Shear in C^0 and C^1 bending finite elements', Int. J. Solids Structures, Vol. 9., pp. 449-460, 1973.

69. Pawsey, S. F. and Clough, R. W., 'Improved numerical integration of thick shell finite elements', Int. J. Num. Meth. Engng., Vol. 3, pp. 575-586, 1971.

70. Ahmad, S., Irons, B. M. and Zienkiewicz, O. C., 'Curved thick shell and membrane elements with particular reference to axi-symmetric problem', Proc. Conf. Matrix Meth. Struct. Mech., Airforce Institute of Technology, Wright-Patterson Airforce Base, Ohio, 1965.

71. Hughes, T. J. R., Taylor, R. L. and Kanoknukulchai, W., 'A simple and efficient finite element for plate bending', Int. J. Num. Meth. Engng, Vol. 11, pp. 1529-1543, 1977.

72. Venkataramana, J. and Venkateswara Rao, G., 'Finite element analysis of moderately thick shells', Nucl. Engng. Des., 33, pp. 398-402, 1975.

73. Mohr, G. A., 'Application of penalty functions to a curved isoparametric axisymmetric thick shell element', Computers and Structures, 15(6), pp. 685-690, 1982.

74. Jennings, A., 'A compact storage scheme for the solution of symmetric linear simultaneous equations', The computer Jnl, Vol. 9(3), pp. 281-285, 1966.

75. Alnajafi, A. M. and Warburton, G. B., 'Free vibration of ring-stiffened cylindrical shells', J. Sound Vib., 13, pp. 9-25, 1970.

76. Diets, A. G. H., 'Composite engineering laminates', The MIT Press, Chapter 1, 1969.

77. Jones, R. M, 'Mechanics of composite materials', New York: McGraw-Hill Book Company, 1975.

78. Timoshenko, S., 'Strength of materials', Part II, Advanced Theory and Problems, 3rd Edn., McGraw-Hill, New York, pp. 100-101, 1956.

79. Reissner, E., 'On bending of elastic plates', Quart. Appl., Math. 5, pp. 55-68, 1947.

80. Richards, T. H. and Delves, B., 'A semi-analytic finite-element analysis of circular plate bending problems', J. Strain Analysis, Vol. 15(2), pp. 75-82, 1980.

81. Giannini, M. and Miles, G., 'A curved element approximation in the analysis of axi-symmetric thin shells', Int. J. Num. Meth. Engng., Vol. 2, pp. 459-476, 1970.

82. Delpak, R., 'Static analysis of thin rotational shells', Computers and structures, Vol. 11, pp. 305-325, 1980.

83. Leissa, A. W., 'Vibration of plates', NASA SP-160, 1969.

84. Vogel, S. M. and Skinner, D. W., 'Natural frequencies of transversely vibrating uniform annular plates', J. Applied Mechanics, 32, pp. 926-931, 1965.

85. Mota-Soares, C. A. and Petyt, M., 'Finite element dynamic analysis of practical discs', J. Sound Vib., 61(4), pp. 547-560, 1978.

86. Rao, S. S. and Prasad, A. S., 'Vibrations of annular plates including the effects of rotary inertia and transverse shear deformation', J. Sound Vib., 42(3), pp. 305-324, 1975.

87. Richards, T. H., 'Energy methods in stress analysis', Ellis Horwood Ltd., 1977.

88. Arnold, R. N. and Warburton, G. B., 'Flexural vibrations of the walls of thin cylindrical shells having freely supported ends', Proc. Royal Soc. (London) 197(A), pp. 238-256, 1949.

89. Sharma, C. B. and Johns, D. J., 'Vibration characteristics of clamped/free and clamped/ring stiffened circular cylindrical shells - a theoretical analysis', Loughborough University Technol. Rep. TT7001, January 1970.

90. Sharma, C. B. and Johns, D. J., 'Free vibration of cantilever circular cylindrical shells - a comparative study', J. Sound and Vib., 25(3), pp. 433-449, 1972.

91. Johns, D. J. and Allwood, R. J., 'Vibration studies of a ring-stiffened circular cylindrical shell', J. Sound and Vib., 8(1), pp. 147-155, 1968.

92. Forsberg, K., 'Influence of boundary conditions on the nodal characteristics of thin cylindrical shells', A.I.A.A. Jnl., 2, pp. 2150-2157, 1964.

93. Forsberg, K., 'Axisymmetric and beam-type vibration of thin cylindrical shells', A.I.A.A. Jnl., 7, pp. 221-227, 1969.

94. Warburton, G. B., 'Vibration of thin cylindrical shells', J. Mech. Engng. Sci., 7(4), pp. 339-407, 1965.

95. Chung, H., 'Free vibration analysis of circular cylindrical shells', J. Sound and Vib., 74(3), pp. 331-350, 1981.

96. Wilson, E. L., Bath, K. J., Peterson, F. E. and Dovey, H. H., 'SAP - a structural analysis program for linear systems', Nuclear Engng. Design, 25, pp. 257-274, 1973.

97. McCormick, C. W., The NASTRAN User's Manual (Level 15), NASA Publications, 1972.

98. Yu, Y. Y., 'Free vibrations of thin cylindrical shells having finite lengths with freely supported and clamped edges', J. Appl. Mech., Vol. 22(4), pp. 547-552, 1955.

99. Smith, B. L. and Haft, E. E., 'Natural frequencies of clamped cylindrical shells', A.I.A.A. Jnl., Vol. 6(4), pp. 720-721, 1968.

100. Vronay, D. F. and Smith, B. L., 'Free vibration of circular cylindrical shells of finite length', A.I.A.A. Jnl., Vol. 8 (3), pp. 601-603, 1970.

101. Forsberg, K., 'A review of analytical methods used to determine the nodal characteristics of cylindrical shells', NASA CR-613, September 1966.

102. Adelman, H. M., Catherines, D. S. and Walton, W. J. R., 'A geometrically exact finite element for thin shells of revolution', A.I.A.A. 7th Aerospace Sci. Meeting (New York), January 1969.

103. Lindholm, U. S. and Hu, W. C. L., 'Non-symmetric transverse vibrations of truncated conical shells', Int. J. Mech. Sci., Vol. 8, pp. 561-579, 1966.

104. Hu, W. C. L., 'Free vibrations of conical shells', NASA TN D-2666, Contract No. NASr-94(06), Southwest Research Institute, 1965.

105. Platus, D. H., 'Conical shell vibrations', NASA TN D-2767, April 1965.

106. Galletly, G. D. and Mistry, J., 'The free vibrations of cylindrical shells with various end closures', Nucl. Engineering and Design, 30, pp. 249-268, 1974.

107. Bushnell, D., 'Analysis of buckling and vibrations of ring stiffened, segmented shells of revolution', Int. J. Solids Struct., pp. 157-181, February 1970.

108. Soedel, W., 'Simplified equations and solutions for the vibration of orthotropic cylindrical shells', J. Sound and Vib. 87(4), pp. 555-566, 1983.

109. Hunckler, C. J., 'The dynamic behaviour of an automobile tyre', Ph.D. thesis, Purdue University, U.S.A., 1979.